The Effects of Maternal Obesity on the Innate Immune System

Developmental Programming of Kupffer Cells

Dissertation

zur

Erlangung des Doktorgrades (Dr. rer. nat.)

der

Mathematisch-Naturwissenschaftlichen Fakultät

der

Rheinischen Friedrich-Wilhelms-Universität Bonn

Vorgelegt von

Nóra Réka Balzer

aus

Budapest (Ungarn)

Bonn, 2022

Angefertigt mit Genehmigung der Mathematisch-Naturwissenschaftlichen Fakultät

der Rheinischen Friedrich-Wilhelms-Universität Bonn

1. Gutachterin: Prof. Elvira Mass
2. Gutachterin: Prof. Dagmar Wachten

Tag der Promotion: 27.01.2023

Erscheinungsjahr: 2023

Declaration

I hereby declare that the work presented in this thesis has not been submitted for any other degree or professional qualification and that it is the result of my own independent work.

Nóra Réka Balzer (Candidate)

Date

Abstract

The global epidemic of obesity has led to an increasing number of obese women in childbearing age. It is now understood that maternal obesity has harmful consequences on fetal and adult health. The underlying mechanism of metabolic programming via maternal obesity remains elusive. Macrophages are important metabolite-sensing cells and mediators of pathological conditions caused by overnutrition. Interestingly, most tissue-resident macrophages have a fetal origin, which places these cells in a unique position of sensing and responding to metaflammation during embryogenesis. Kupffer cells (KCs) are the tissue-resident macrophages of the liver, therefore key candidates for metabolic programming.

Here, a mouse model was used to show how maternal obesity induces metabolic programming of KCs. Non-alcoholic or metabolic steatohepatitis (NASH) develops in offspring liver upon maternal obesity if the offspring follows a healthy control diet. Myeloid cell dynamics are investigated via a flow cytometric approach, and transcriptional analysis reveals immunometabolic modulation of KCs. A metabolic shift of KCs was observed from oxidative phosphorylation to glycolysis. Genetic manipulation of macrophages targeting HIF-1α rescued maternal obese offspring from NASH. Ligand-receptor interactions were targeted between KCs and hepatocytes, comparing rescued versus NASH samples. Moreover, the multi-omics approach of hepatocyte transcriptome and liver lipidome shed light on apolipoproteins, cholesterol esters (CE), and triacylglycerols (TAG) as the causative chain of maternal obesity-induced developmental programming leading to NASH.

Thus, we conclude that maternal obesity induces developmental programming of KCs. It leads to a high accumulation of TAG and CE in the liver and overexpression of Apolipoproteins in KCs. Therefore, NASH is developed, and a pathological amount of cholesterol may be carried to the bloodstream, inducing a whole-body metabolic assessment. Developmental programming may lead to further chronic diseases, and KCs are causative to those pathological mechanisms further in the individual's life.

Acknowledgments

I would like to thank Elvira Mass and Dagmar Wachten for giving me the opportunity to work on this exciting project in their research groups and for their scientific and personal guidance, enthusiasm, and beneficial discussions at any time.

I am thankful to all professors at the LIMES Institute, especially Christoph Thiele, Andreas Schlitzer, Eva Kiermayer, Irmgard Förster, Joachim L. Schultze and Waldemar Kolanus, for their multidisciplinary support, interest, and scientific discussions at any time.

I am thankful to Natalio Garbi for chairing my first talk at an international conference and agreeing to become a member of my thesis committee.

Thanks to all members within the Institute of Innate Immunity, the LIMES Institute and Mass lab for their tremendous support, collaborative attitude and great friendship.

I could not convey this work without the financial and child-care support of the LIMES-WIS, the equal opportunity office at the University of Bonn and the Immunosensation cluster.

On a personal note, I am incredibly grateful to my family, Thomas and David, for their encouragement and excitement about my work.

Table of contents

List of figures

List of tables

Abbreviations

ABCA1	ATP-binding cassette transporter
ALB	Albumin
ALT	Alanine aminotransferase
APO*	Apolipoprotein*
AST	Aspartate aminotransferase
ATP	Adenosine triphosphate
BM	Bone marrow
BMI	Body mass index
CCL2	Chemokine (C-C motif) ligand 2
CCR2	C-C chemokine receptor type 2
CD	Control Diet
cDC	Classical Dendritic Cells
cDC1	Classical Dendritic Cells type 1
cDC2	Classical Dendritic Cells type 2
CE	Cholesterol esters
CMs	Capsular macrophages
CXCR	C-X-C motif chemokine receptor
DAMPs	Damage-associated molecular pattern
DCs	Dendritic cells
DEG	Differentially expressed gene
DPP4	Dipeptidyl-peptidase 4
EMP	Erythro-myeloid progenitor
ESPRESSO	Epidemiology Strengthened by histopathology Reports in Sweden
EWAT	Epididymal white adipose tissue
F3	Coagulation Factor III,
GO	Gene Ontology

GPIHBP1	Glycosylphosphatidylinositol Anchored High Density Lipoprotein Binding Protein 1
GSEA	Gene set enrichment analysis
HFD	High-fat diet
HIF-1α	Hypoxia-inducible factor 1 α
HSC	Hematopoietic stem cells
IFN-γ	Interferon gamma
IL-4	Interleukin 4
ITGAM	Integrin Subunit Alpha M
ITGB2	Integrin Subunit Beta 2
KCs	Kupffer cells
KEGG	Kyoto Encyclopedia of Genes and Genomes
LCM	Liver capsular macrophages
LDLR	Low-density lipoprotein receptor
LDTFs	lineage-determining transcription factors
LRP1	Low-density lipoprotein receptor related protein
LR	Ligand-receptor
M-CSF	Macrophage colony-stimulating factor
MAFB	MAF BZIP Transcription Factor B
MDMs	Monocyte-derived macrophages
MDP	Macrophage dendritic cell progenitor
MP	Macrophage progenitor
mt-ATP6	Mitochondrially encoded ATP synthase membrane subunit 6
mt-CO*	Mitochondrially Encoded Cytochrome C Oxidase
mt-CYB	Mitochondrially Encoded Cytochrome B
mt-ND1	Mitochondrial genome coding for the NADH-ubiquinone oxidoreductase chain 1

mt-ND4	Mitochondrial genome coding for the NADH-ubiquinone oxidoreductase chain 4
MYD88	Myeloid differentiation primary response 88
NAFLD	Non-alcoholic fatty liver disease
NASH	Non-alcoholic steatohepatitis
O2PLS	Two-way orthogonal partial least squares regression
ORO	Oil-red-o stain
oxLDL	Oxidized low-density lipoprotein
OXPHOS	Oxidative phosphorylation
PAMPs	Pathogen-associated molecular patterns
PC1	First principal component
PC2	Second principal component
PCA	Principal component analysis
pDC	Plasmacytoid dendritic cells
pMacs	Pre-macrophages
PRR	pattern recognition receptors
ROD	Range of distribution
S100A8	S100 calcium-binding protein A8
S100A9	S100 calcium-binding protein A9
SALL1	Spalt-like transcription factor 1
SAMs	Scar associated macrophages
SED	Standard error of difference
SCs	Scavenger receptors
TAG	Triacylglycerols
TCA	Tricarboxylic acid
TF	Transcription factor
TGF-ß	Transforming growth factor-beta

THR-β	thyroid hormone receptor β
TLR4	toll-like receptor 4
TNF	Tumor Necrosis Factor
TREM2	Triggering Receptor Expressed On Myeloid Cells 2
TRF	Transferrin
TRMs	Tissue resident macrophages
VLDLR	Very Low Density Lipoprotein Receptor
WAT	White adipose tissue
YS	Yolk-sac
ZEB2	Zinc Finger E-Box Binding Homeobox 2

Chapter 1: Introduction

1.1 Developmental origin of health and disease

The concept, developmental origin of health and disease (DOHaD), states that lifestyle-related diseases originate from the time of fertilization, pre-, and perinatal stages[1–3]. The trigger comes from the interrelation between genes and environmental factors such as nutrition or stress[2]. DOHaD is derived from developmental programming, defined as the ability of exposures during prenatal development to cause permanent changes to physiology, metabolism, and epigenome[4–9]. Therefore, developmental programming subsequently affects health and disease.

The Dutch hunger winter study is the most famous cohort related to developmental programming[10–12]. Longitudinal studies highlighted that famine during early pregnancy positively correlates with the prevalence of obesity, cardiovascular disorders, and metabolic diseases[13].

1.1.1 Maternal obesity and hepatic steatosis

Famine is not a common issue in western countries anymore. Overnutrition is the next big challenge of our healthcare system, with all its obesity-related comorbidities, such as diabetes type 2 and metabolic syndrome[14]. Maternal obesity syndrome is defined as a pathologic function where the pre-pregnancy body-mass index (BMI) is related to the weight gain during pregnancy[15]. Obesity during pregnancy shows an increasing tendency. In Germany, the ratio of obese pregnant women increased from 9.4% to 19.2% between 1995 and 2017[16]. A recent Australian study has shown that nearly half of the mothers were overweight or obese in 2019 (classified according to BMI)[17]. Maternal obese offspring have higher rates of pre-term birth, stillbirth, and neonatal death[18]. The long-term effects of maternal obesity remained elusive until recently. It has been linked to the development of cardiovascular diseases and diabetes in offspring[18].

Non-alcoholic fatty liver disease (NAFLD) or metabolic fatty liver disease is defined by hepatic steatosis. It can be diagnosed via imaging techniques (such as ultrasound) or liver biopsy in people who consume little or no alcohol and do not have any known causes for hepatic steatosis (such as autoimmune hepatitis,

Wilson's disease or viral hepatitis)[19–21]. NAFLD stages are steatosis (lipid accumulation), steatohepatitis (inflammation), fibrosis (scar tissue), and cirrhosis[22]. Only a few biomarkers are available for NAFLD, such as elevated serum alanine aminotransferase levels (ALT) or increased aspartate aminotransferase (AST) to ALT ratio[23,24].

The liver fat content of maternal obese newborns is higher than in maternal lean ones. Moreover, the mother's BMI positively correlates with newborn hepatic lipid content. Those facts from correlational studies proposed the early epigenetic influences as possible contributors to the development of NAFLD[25–27]. Recently, the ESPRESSO[28] cohort study proved that maternal obesity is a risk factor for NASH and linked maternal obesity with offspring hepatic steatosis[29,30]. Other longitudinal human studies found further associations between maternal diet and offspring hepatic steatosis[31,32]. The role of epigenetic factors in NAFLD upon maternal obesity, especially DNA methylation-related alterations, has been proposed with elusive causality[33]. Inflammation is a pathogenic response to various types of liver diseases, such as NAFLD. Innate immune cells initiate and maintain inflammation. The combined pathogenic response involves activation of Kupffer cells, recruiting macrophages and inflammatory cells to produce cytokines and chemokines, which leads to a long-term inflammation[34].

1.2 Liver development and structure

The liver is the main metabolic organ, controlling cholesterol levels and blood detoxification. It supports the hematopoietic and digestive systems. Early liver-development starts with the formation of the endoderm at embryonic day (E) 7.5, derived from inner cell mass precursors[35]. During embryonic development, the fetal liver is the main hematopoietic organ, having a pivotal role in the development of tissue-resident macrophages[36–39]. Hepatic progenitors interact with stromal compartments, which induce hepatic sinusoidal endothelial cells and hepatic stellate cells. The embryonic-derived liver-resident macrophages are known as Kupffer cells (KCs) and reside in the sinusoids as early as E10.25. At the age of E15.5, hepatoblasts differentiate into hepatocytes and biliary cells. The final maturation of the liver continues through the post-natal period. Hepatocytes account for 70% of the adult organ, and they communicate with endothelial cells, Kupffer cells and hepatic stellate cells as well[40].

The mature liver has its functional units, organized into lobules, surrounding the central vein, where hepatocyte cords radiate to the portal triads. Sinusoids are discontinuous vessels built from endothelial cells, where KCs reside as well. Stellate cells are in the space between hepatocyte cords and sinusoids called Disse.

Myeloid cells arise from the common myeloid progenitors and give rise to monocytes, dendritic cells (DCs), macrophages, and granulocytes. They are responsible for recognizing foreign materials and controlling inflammatory responses to keep balanced liver homeostasis[41]. Monocytes are BM-derived circulating cells that can locate into inflamed tissue and differentiate locally into other myeloid cell populations, such as macrophages or dendritic cells[41].

NASH-induced lipid accumulation in the liver leads to hepatocyte damage. This hepatocyte damage triggers an inflammatory signal, and myeloid cells accumulate in the liver. A unique inflammatory phenotype is characterized by the downregulation of inflammatory calprotectin S100a8 and S100a9 in both macrophages and DCs, dependent on the TLR4 signalling[42].

1.2.1 Macrophages in the liver

Today, the fetal origin of most tissue-resident macrophages (TRMs) is well recognized. Fate-mapping studies revealed that TRM development is independent of hematopoietic stem cells (HSC). TRM arises before the generation of HSC, and they are maintained independently of adult BM progenitors[43]. Erythro-myeloid progenitors (EMPs) were identified as the common origin of TRM[44]. EMPs develop in the yolk-sac (YS) at embryonic day (E)8.5, differentiate into pre-macrophages (pMacs) at E9.5, and seed their tissue of residence to give rise to TRM as early as E10.25[45]. Both EMPs and pMacs migrate from the YS to the embryo, where the fetal liver serves as their reservoir. The pMacs continuously differentiate from fetal liver EMPs until at least E16.5[46] leave the fetal liver and migrate to the respective tissue of residence. After migration, they mature and self-renew within their tissue of origin without further input from definitive HSC-dependent hematopoiesis[47–49]. TRMs are intimately adapted to their tissue of residence, raising whether this adaption is enforced locally or is already present within embryonic precursors.

Primary macrophage identity is determined by a transcriptomic core program, including the lineage determining factors Spi1 (PU.1), MafB, and Zeb2[45,50]. Tissue-resident adaptation of macrophages is reflected by the expression of tissue-specific transcriptional programs, which allow for an organ-specific functional specialization of TRM. For instance, in the brain, Sall1, in the liver, DNA-binding protein inhibitor (Id3) have been identified as essential factors for macrophage development and identity[45,51].

Kupffer cells (KCs) are the TRM of the liver, with a crucial role in hepatic metabolism[52]. Bulk transcriptomics has shown that KCs highly express genes associated with iron and lipid metabolism[53]. Hepatocytes are the primary iron storing cells, but KCs are responsible for the uptake, processing, and export of iron[53,54]. Moreover, all macrophages can process lipids from dying cells through phagocytosis, but KCs are also involved in cholesterol uptake and transport to hepatocytes[53]. Those KC-specific tasks suggest a strong interaction between KCs and hepatocytes for balanced metabolism. According to the recently published classification, a $CD31^+$, $CD206^+$, $ESAM^+$ KC subpopulation (KC2) is responsible for that metabolic features[63].

Contrary, MDMs are recruited from the BM when the homeostasis is disturbed and can differentiate either into short-lived MDMs, "temporary macrophages," or into long-lived resident macrophages[55]. MDMs have a specific role NAFLD and can be identified by their anatomic location and expression pattern. Scar-associated macrophages (SAMs) were found in cirrhotic livers of both mice and men. SAMs are located close to the fibrotic areas, showing high expression of TREM2 and CD9. Tissue-resident KCs undergo apoptosis during steatohepatitis, and the empty niche gets filled by MDMs, such as SAMs [56–58].

Capsular macrophages (CMs) are MDMs located in the hepatic capsule, phenotypically closer to dendritic cells, and are derived from blood monocytic precursors. CMs are responsible for the recruitment of neutrophils in response to bacterial infection[59].

Prior to the ontogenetic revolution, macrophages were considered highly plastic cells, switching their phenotype from one to another upon inflammation or resolution thereof ("M1-M2 continuum"). However, it is now well established that the concept of M1 and M2 macrophages exists only in a petri dish when

monocyte-derived macrophages are stimulated with IFN-γ or IL-4 respectively[60–62]. Instead, recruited monocytes are highly plastic cells. Upon inflammation, loss of TRM allows circulating monocytes to differentiate into tissue macrophages[63–65]. However, not all monocytes develop into long-lived TRM. Recently, a new concept of macrophage function was suggested under inflammatory conditions, summarizing this cell type as infMac. The ontogeny of those inflammation-imprinted macrophages is mixed, and they can transfer epigenetic memory of that inflammatory event[66]. However, it remains to be investigated whether MDMs recruited to inflamed tissues and occupying the TRM niche are indeed long-lived, especially when the inflammation is resolved. It is conceivable that the remaining pool of TRMs may have a proliferative advantage over MDMs. Certainly, MDMs differentiate into short-lived macrophages that are only present until the resolution phase[67].

1.3 The metabolic state of macrophages

Most cells produce ATP by oxidative phosphorylation through the mitochondria. Both phagocytic activity and activation by inflammatory stimuli induce an increased rate of glycolysis in macrophages[68]. Glycolysis takes place in the cytosol and it converts glucose to pyruvate. In this way, two ATP molecules are generated from one glucose unit. Upon inflammation, macrophages rely mainly on glycolysis and exhibit mitochondrial oxidative phosphorylation (OXPHOS). In tumor biology, this metabolic switch from OXPHOS to glycolysis is called Warburg or Pasteur effect. It is led by the hypoxia-inducible factor 1a (HIF-1α), which promotes a non-efficient ATP production by glycolisis[69].

The metabolic programming of macrophages got highlighted in various trained immunity studies. The concept of trained immunity states that functional reprogramming of innate immune cells leads to an altered response towards a secondary challenge after the return to a non-activated state. Trained immunity involves epigenetic and metabolic programming of the innate immune cells. Increased aerobic glycolysis is a hallmark of trained myeloid cells, which is mediated by rapamycin (mTOR) and hypoxia-inducible factor 1α (HIF-1α)[70]. Therefore, trained immunity is abrogated by the blockade of the mTOR-HIF-1α pathway. Nevertheless, OXPHOS upregulation has been reported as well upon inflammation, which indicates the possibility that upon different type of

stimulations, different type of metabolic programming takes place [71,72]. Trained immunity and developmental programming are two different concepts with distinct ways of immune challenge, timeframe and outcome[73]. In trained immunity studies, the primary challenge is induced at any time (independent of cellular development), which induces an increase in relative immune response. The immune response gets back to homeostasis shortly after the primary challenge. Once secondary challenge is induced, the relative innate immune response becomes even higher than at the primary challenge. Contrary, developmental programming takes place during embryonal development[74]. The cellular programming is induced by the environment, which is the mother during embryonic maturation. Developmental programming does not have a specific time point, but a time frame. The period of developmental programming is during pregnancy, when embryonic development takes place (Figure 1). A secondary challenge is not involved, as the innate immune response is not challenged, but permanent programmed[75,76].

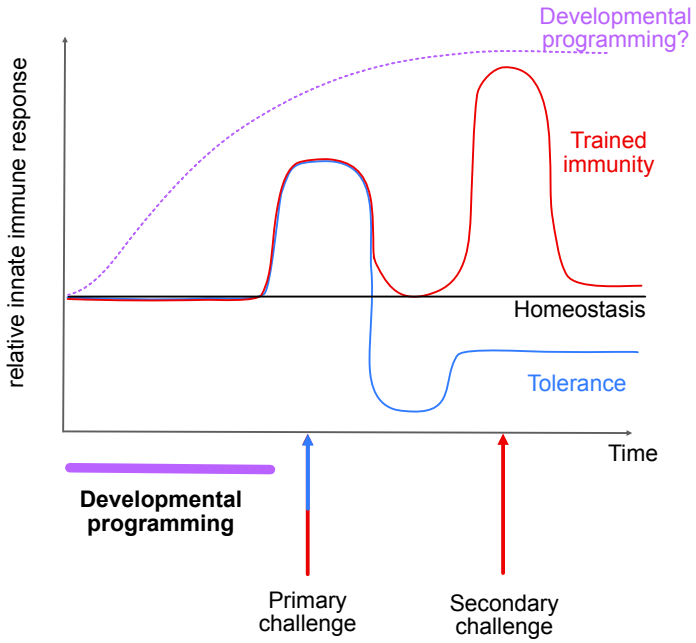

Figure 1. Trained immunity and developmental programming.
Infections or sterile triggers are used in trained immunity models to induce inflammation and immune response (primary challenge). Anti-inflammatory mechanisms are called to prevent overshooting inflammation and limit the inflammatory response in time. Trained immunity proves that innate immune cells can remember the primary stimuli. Upon secondary challenge, trained immune cells give a higher immune response. Developmental programming triggers immune cells during development. However, its short and long-term effects on immune metabolism and disease development remain elusive.

1.3.1 The role of HIF-1α in developmental programming

HIF-1α is considered as a main transcriptional regulator of cellular and developmental response to hypoxia. It belongs to the HIF-family, all of its members are heterodimers, made up of an alpha subunit with three members (HIF-1α, HIF-2α, HIF-3α) and a beta subunit (HIF-1β).

Oxygen-rich blood is crucial for cells to function and perform OXPHOS. In various diseases, such as cancer, heart diseases or NASH, the cellular oxygen balance is highly impaired and cells become hypoxic. Hypoxia activates the hypoxia signaling pathway, which is governed by HIF stabilization. Under normoxic conditions, HIF-prolyl hydroxylase domain proteins (PHD1-3) hydroxylate proline residues in cytoplasmic HIF-1α subunits in an oxygen-dependent manner. This allows recognition by the E3 ubiquitin ligase von-Hippel Lindau protein (VHL), leading to ubiquitination of HIF-1α and subsequent proteasomal degradation. PHD-mediated hydroxylation does not occur in hypoxia, allowing HIFα stabilization, translocation to the nucleus and dimerization with HIF-1β. Activated HIFs bind to hypoxia response elements in the promoters of target genes such as Ep300, leading to the transcription of genes required for adaptation to hypoxia (Figure 2).

Maternal obesity induces chronic fetal hypoxia and the upregulation of placental HIF-1α[77–80]. Fetal hypoxia may induce altered mitochondrial function, which is regulated by HIF-1α and may lead to NASH. Exposure to excess maternal fuels during fetal life uniquely alters hepatic fatty acid oxidation, tricarboxylic acid cycle activity, de novo lipogenesis, and mitochondrial health. These events promote increased oxidative stress and excess triglyceride storage. furthermore, they prime the fetal liver for NAFLD and might drive the risk for non-alcoholic steatohepatitis in the next generation[81,82].

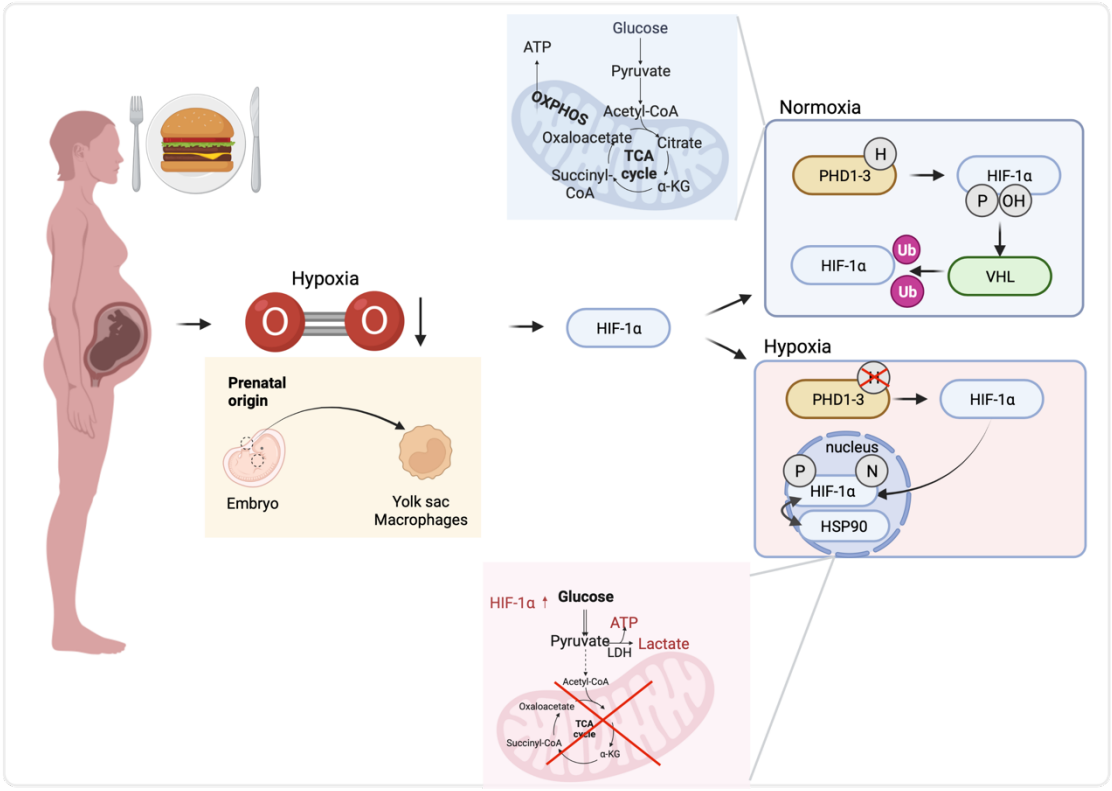

Figure 2. The role of HIF-1α in developmental programming caused metabolic shift
Obesity induces chronic hypoxia, which enables an altered environment for the developing embryo. Yolk sac derived macrophages have a prenatal origin, and the hypoxic environment may program them during development. This developmental programming affects the cellular metabolism. Under normoxic conditions (blue), PHD1-3 hydroxylate proline residues in cytoplasmic HIF-1α subunits, which enables the recognition by VHL. This process leads to ubiquitination of HIF-1α and to proteasomal degradation. In this case, pyruvate is produced from glucose through the glycolytic pathway. Pyruvate feeds the tricarboxylic acid (TCA) cycle in the form of Acetyl-CoA and subsequent oxidative phosphorylation (OXPHOS). TCA or Krebs cycle is a series of chemical reactions to release energy through the oxidation of Acetyl-CoA. This oxidation process involves (but is not restricted to) the formation of citrate, α-ketoglutarate (α-KG), Succinyl-CoA and Oxaloacetate. Under Hypoxic conditions (red), PHD-mediated hydroxylation does not take place, which stabilizes HIF-1α and leads to its translocation to the nucleus. Interaction between HIF-1α and HSP90 was shown to contribute to HIF-1α stabilization through the PI3K/Akt signaling pathway[83]. Under hypoxia, macrophage metabolism changes according to the Warburg effect (pink). In activated macrophages, pyruvate is produced only through glycolysis and subsequently metabolized into lactate. Upregulation of HIF-1α promotes the metabolic shift from OXPHOS to glycolisis[81,82,84]

Chapter 2: Aim of the Thesis

The aim of this thesis is to explore the long-term effects of maternal diet on the offspring's innate immune system until adulthood.

1. First, we prove the causality between maternal obesity and NASH through the developmental programming of KC.
2. Second, immunometabolic alterations of KC will be described using in-vivo maternal obesity models.
3. Furthermore, we aim to rescue offspring born to obese mothers suffering from NASH. For that purpose, we use macrophage-specific knock-out (KO) models. We target KC metabolic programming with the $HIF1a^{f/f}$ $Lysm^{cre}$ system and rescue the inflammatory phenotype with the Myd88 Tnsfrsf11a $(Rank)^{cre}$ model.

Chapter 3: Materials & Methods

3.1 Materials

3.1.1 Animal diet

Table 1 Product information - Control diet (CD)

Product	Source	Cat#
Meal/powder	Ssniff	E15748-00
10mm pellets, irradiated	Ssniff	E15748-047

Table 2 Product information - High-fat diet (HFD)

Product	Source	Cat#
10mm pellets, irradiated	ssniff	E15742-347

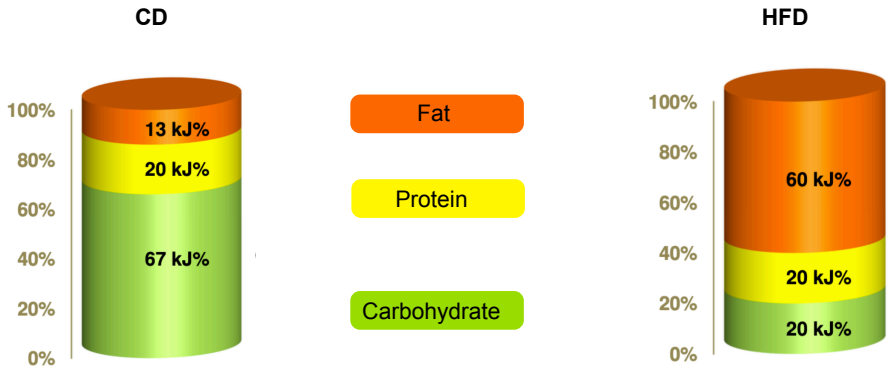

Figure 3. Fat, protein and carbohydrate content of the diets
Control diet (CD) food contains 13% fat, 20% protein and 67% carbohydrate. High-fat diet (HFD) food contains 60% fat, 20% protein and 20% carbohydrate. All mice were fed with those diets during all experiments.

Table 3 Mineral content of the diets

Minerals (%)	CD	HFD
Calcium	0.92	0.92
Phosphorus	0.63	0.64
Ca/P	1.46:1	1.44:1
Sodium	0.20	0.20
Magnesium	0.23	0.23
Potassium	0.97	0.97

Table 4 Fatty acid contents of the diets

Fatty acids (%)	CD	HFD
C 12:0	-	0.07
C 14:0	0.02	0.44
C 16:0	0.57	7.93
C 18:0	0.18	4.37
C 20:0	0.02	0.11
C 16:1	0.01	0.94
C 18:1	1.28	13.97
C 18:2	2.65	4.64
C 18:3	0.29	0.49

Table 5 Amino acid content of the diets

Amino acids (%)	CD	HFD
Lysine	1.52	2.02
Methionine	0.66	0.86
Cystine	0.33	0.45
Met+Cys	0.99	1.31
Threonine	0.80	1.07
Tryptophan	0.24	0.33
Arginine	0.71	0.95
Histidine	0.55	0.74
Valine	1.27	1.70
Isoleucine	1.02	1.38
Leucine	1.80	2.42
Phenylalanine	0.95	1.27
Phe+Tyr	1.90	2.56
Glycine	0.39	0.52
Glutamic acid	4.10	5.50
Aspartic Acid	1.35	1.82
Proline	2.09	2.80
Serine	1.09	1.46
Alanine	0.55	0.81

Table 6 Crude nutrient content of the diets

Crude nutrients (%)	CD	HFD
Crude protein	18.2	24.4
Crude fat	5.1	34.6
Crude fiber	7.0	6.0
Crude ash	5.3	5.3
Strach	37.3	0.1
Sugar	11.0	9.4
N free extracts	60.1	26.3

Table 7 Vitamin content of the diets

Vitamins per kg	CD	HFD
Vitamin A	15,000 IU	15,000 IU
Vitamin D3	1,500 IU	1,500 IU
Vitamin E	150 mg	150 mg
Vitamin K	20 mg	20 mg
Vitamin B1	25 mg	25 mg
Vitamin B2	16 mg	16 mg
Vitamin B6	16 mg	16 mg
Vitamin B12	30 µg	30 µg
Nicotinic acid	47 mg	47 mg
Pantothenic acid	55 mg	55 mg
Folic acid	16 mg	16 mg
Biotin	300 µg	300 µg
Choline	920 mg	1,140 mg

Table 8 Trace elements of the diets

Trace elements per kg	CD	HFD
Iron	168 mg	168 mg
Manganese	95 mg	95 mg
Zinc	65 mg	65 mg
Copper	13 mg	13 mg
Iodine	1.2 mg	1.2 mg
Selenium	0.2 mg	0.2 mg

3.1.2 Antibodies and secondary reagents

3.1.2.1 Antibodies - Flow cytometry - Liver myeloid cells

Table 9 Antibodies for the myeloid cell flow cytometry panel

Antigen	**Conjugate**	**Clone**	**Source**	**Cat#**
CD45	BUV805	30-F11	BD	748370
CD11b	PECy7	M1/70	BioLegend	101216
Tim4	AF647	RMT4-54	BioLegend	130008
F4/80	BV421	BM8	BioLegend	123132
NKp46	PE	29A1.4	BioLegend	137604
CD3	PE	145-2C11	BioLegend	100308
CD19	PE	1D3/CD19	BioLegend	152408
Ly6C	BV510	HK1.4	BioLegend	128033
Ly6G	PerCP/Cy5.5	1A8	BioLegend	127616
Cx3cr1	PE-Dazzle594	SA011F11	BioLegend	149014
CD11c	BV605	N418	BioLegend	117333
CD206	BV711	C068C2	BioLegend	141727
MHCII	AF700	M5/114.15.2	BioLegend	107622
CD172a	FITC	P84	BioLegend	144006
XCR1	APC-Cy7	ZET	BioLegend	148224
CD9	Biotin	MZ3	BioLegend	124804

3.1.2.2 Antibodies - Flow cytometry - HSC - BM

Table 10 Antibodies of the HSC flow cytometry panel

Antigen	Conjugate	Clone	Source	Cat#
CD11b	Biotin	M1/70	BioLegend	101204
NKp46	Biotin	29A1.4	BioLegend	137616
CD3	Biotin	145-2C11	BioLegend	100304
CD19	Biotin	6D5	BioLegend	115504
Gr1	Biotin	RB6-8C5	BioLegend	108404
Ter119	Biotin	TER-119	BioLegend	116204
Kit (CD117)	BV711	2B8	BioLegend	105835
Sca1	BV510	D7	BioLegend	108129
CD48	AF647	HM48-1	BioLegend	103416
CD150	PE-Cy7	TC15-12F12.2	BioLegend	115914
CD16/32	APC-Cy7	93	BioLegend	101328
CD34	BV421	MEC14.7	BioLegend	119321
CD135	PE	A2F10	BioLegend	135306
CD127	PerCP/Cy5.5	A7R34	BioLegend	135022

3.1.2.3 Antibodies - FACS for RNA-seq

Table 11 Antibodies for KC sorting

Antigen	Conjugate	Clone	Source	Cat#
CD45	APC-Cy7	30-F11	BioLegend	103116
CD11b	BV510	M1/70	BioLegend	101245
Tim4	BV786	21H12	BD	742778
F4/80	AF700	BM8	BioLegend	123130
NKp46	PE	29A1.4	BioLegend	137604
CD3	PE	145-2C11	BioLegend	100308
CD19	PE	1D3/CD19	BioLegend	152408
CD31	AF488	MEC13.3	BioLegend	102514
Lyve-1	APC	ALY7	eBioscience	50-0443-80
CD146	PerCP-Cy5.5	ME-9F1	BioLegend	134709
CD61	PECy7	2C9.G2	BioLegend	104317

3.1.2.4 Enzymes

Table 12 Enzymes

Name	Source	Cat#
Collagenase D	Miltenyi Biotec	11088882001
Dispase II	Fisher Scientific	115105036
DNAse (Deoxyribonuclease I) from bovine pancreas	Sigma Aldrich	DN25-1G

3.1.2.5 Chemicals

Table 13 Chemicals

Name	Source	Cat#
2-Propanol, 99.9%, LiChrosolv®, hypergrade for LC-MS, Supelco®	Merck Millipore	1027811000
BSA (Bovine Serum Albumin) heat shock fraction pH7	Sigma-Aldrich	A9647-500G
Chloroform, 99.0 - 00.4%, for analysis, Supelco®	Merck Millipore	1024421000
DAPI (4',6-Diamidino-2-Phenylindole, Dilactate	BioLegend	422801
EDTA (Ethylenediaminetetraacetic acid	Sigma-Aldrich	E9884-500G
Entellan® mounting medium	Merck Millipore	1079610100
Eosin Y solution, 0.5% in water, for microscopy	Carl Roth	X883.2
Ethanol, >= 99.8%, denatured, for histology	Carl Roth	K928.6
Hemalaun solution acidic acc. to Mayer, for microscopy	Carl Roth	T865.2
Kaiser's glycerol gelatine, phenol-free, for microscopy	Carl Roth	6474.1
Methanol, 99.9% LiChrosolc®, hypergrade for LC-MS, Superlco®	Merck Millipore	1060352500
Oil-Red-O, certified by the Biological Stain commission	Sigma-Aldrich	O0625-25G
Paraplast Plus® for histology	Carl Roth	X881.2
PBS (10x) without Ca^{++}, Mg^{++} , or phenol red	Biozym	882131
QIAzol Lysis Reagent	Qiagen	79306

Rat serum, with 0.1% sodium azide	Bio-Rad	C13SD
Sakura Finetek TM Tissue-Tek O.C.T. Compound	Fisher Scientific	12351753
Schiff's reagent for microscopy	Carl Roth	X900.2
Water for chromatography (LC-MS grade), Superlco® LiChrosolc®	Merck Millipore	115332500
Xylol (isomers), >98%, pure, for histology	Carl Roth	9713.3

3.1.3 Laboratory Equipment

Table 14 Equipment

Name	Description	Source
Axia Lab.A1	Microscope	Zeiss
CM3050	Cryostat	Leica
FACSAriaTM III	Cell Sorter	BD Biosciences
FACSymphony	Flow cytometer	BD Biosciences
Guava easyCyte	Flow Cytometer	Luminex
RM2245	Microtome	Leica
Thermo Q Exactive TM Plus	Mass spectrometer	Thermo Scientific
TP1020	Tissue processor	Leica

3.1.4 Consumables

Table 15 Consumables

Name	Source	Cat. #
TC-Platte 6 Well, Suspension, F	Sarstedt	83-3929.500
Strainer, 70µm or 100 µm	VWR	732-2758/9
Accu check Aviva strips	Roche	06114963
Blood collection microtube	Microvette	MCVTI100-EDTA
Syringe 10ml	Fisher Scientific	15879152

3.1.5 Buffers and standard solutions

Table 16 Buffers

Buffer	Components
FACS buffer	BSA 0.5% EDTA 2mM Diluted in 1x PBS
1X PBS	10X PBS Diluted with bides water (1:10)
Spray buffer	2-propanol:methanol:H_2O 8:5:1 Ammonium acetate 10 mM

Table 17 General solutions

Solution	Components
Digestion mix	Dispase 2.4 mg/ml EDTA 2mM Diluted in 1x PBS
1X PBS	10XPBS Diluted with bides water 1:10
FC block	Anti-mouse CD16/32 1:100 Rat serum 4% Diluted in FACS buffer

3.1.6 Softwares

- RStudio Desktop (renamed to Posit) with R 4.1.0
- Flowjo 10.8.1
- ImageJ 1.53s
- Biorender
- LipidXplorer 1.2.8

3.2 Mice

C57BL/6JRcc and C57BL/6JCrl mice were maintained under standard SPF conditions with a 12h dark/light cycle. Animal procedures were performed in adherence to our project licenses 2019.A146 and 2016.A221 issued by the "Landesamt für Natur, Umwelt und Verbraucherschutz" (LANUV).

3.2.1 Metabolic assessment of mothers

Three-week-old female mice are introduced to CD for 2 weeks, in order to get all mice on a comparable metabolic state. Subsequently, mice are separated into two groups and received either HFD or CD for eight weeks. The bodyweight of the mice is weighed and mice physiology is scored once a week. For metabolic assessment, the homeostatic model for insulin-resistance (HOMA-IR) is used, as described[85]. After six hours of fasting, blood was obtained from the facial vein. Blood sugar level was measured with the Accu-Check glucose meter (Aviva). The rest of the obtained blood was collected into serum tubes to gain serum (centrifuge 10.000G 5 min according to manufacturers instructions). Blood serum insulin levels areanalyzedd with the mouse serum Elisa kit, according to the manufacturers instructions. HOMA-IR is calculated using the formula below.

$$\mathrm{HOMA\_IR} = \frac{Glucose\ level\ (mg/ml)}{Insulin\ level\ (\mu U/ml)} / 405$$

Mice on HFD diet without metabolic assessment were excluded from the experiment. Those mice had no significant weight gain or higher HOMA-IR compared to CD-fed mice.

3.2.2 Breeding

Estrus cycle of females was visually addressed as described[86]. All females in proestrus and estrus phases were overnight mated with male mice fed with CD.

In every cage, one male was grouped with maximum two females. During breeding, all mice were on CD. Breeding always took place in a male's cage. On the following morning (between 8:00 am and 9:00 am), female mice were plug-checked and placed back into their original cage.

3.2.3 Offspring

When mice gave birth (post-mating 19-21 days), litter size was normalized to six, preferably male pups per mother. Further P0 pups were taken for further analysis. Offspring born to obese mothers were cross-fostered to CD mothers (HFD_MCD). Cross fostering took place also between mothers on the same diet in order to exclude the possible effects of cross-fostering from developmental programming. Gender was used to differentiate between own pups and fostered pups. Mothers tend to take foster pups if they can keep at least one of their own newborns. After three weeks of lactation at postnatal day (P)21, male offspring were weaned into their post-weaning cage (CD or HFD). Mice under 10g are not allowed to wean. Therefore, CD meal powder was placed in the cage in order to support the pups' weight gain. Mice born from different mothers were mixed into one cage in order to normalize possible microbiome-related effects (here, an ear tag identified the mice). During the post-weaning diet, bedding was weekly mixed between cages to reduce cage-specific effects related to the microbiome. During post-weaning, mice were weighed and scored once a week.

Based on the knowledge we gained from the WT model, we reduced the colony into 4 dietary groups. Those are CD_MCD_LCD, CD_MCD_LHFD, HFD_MCD_LCD and HFD_MHFD_LHFD. As lactational changes are excluded from those models, I continue to mark them as CD_MCD, CD_MHFD, HFD_MCD, and HFD_MHFD.

3.3 Methods

3.3.1 Genotyping

Tissues (ear tag or tail) are dissolved in 200µl of 50 mM NaOH for 1h at 95 °C at 900 RPM. After cooling the samples on ice, they are centrifuged for 5 min at max rpm. Afterward, 20µl of 1M TRIS HCl (pH8) is added and combined with an additional centrifugation step. 1µl of supernatant is taken for the subsequent polymerase chain reaction (PCR). The PCR was performed using the pipetting scheme (Table 19) and PCR program (Table 20-21) shown below.

Table 18 Primers for genotyping

Gene	Primer	Sequence
$Myd88^{f/f}$	Forward	5'GTT GTG TGT GTC CGA CCG T 3'
	Reverse	5´ GTC AGA AAC AAC CAC CAC CAT GC 3´
$Rank^{Cre}$	Forward	5' TGA AGG GTG ACA TCA TCG TGG T 3'
	Reverse	5' ACT TCT CCA TGG TAG CCT CCT CC 3'
	Reverse(mut)	5´ AAT AGG GGT GGG GTG ATA 3´
HIF-1α $^{f/f}$	Forward	GCA GTT AAG AGC ACT AGT TG
	Reverse	GGA GCT ATC TCT CTA GAC C
$LysM^{Cre}$	Forward	CCC AGA AAT GCC AGA TTA CG
	Reverse	CTT GGG CTG CCA GAA TTT CTC
	Reverse(mut)	TTA CAG TCG GCC AGG CTG AC

Table 19 Components for genotyping

Component	Volume (µl)
Forward primes	0.5
Reverse primer	0.5
DreamTaq ™ Green PCR Master-Mix (2x)	5
H_2O	3
Sample	1

Table 20 PCR program used for general genotyping.
Denaturation, primer annealing and elongation is to repeat for 35 cycles.

Step	Temperature	Time
Initial denaturation	95°C	3 min
Denaturation	95°C	30 sec
Primer annealing	60°C	30sec
Elongation	72°C	30sec
Final extension	72°C	5 min

Table 21 PCR program used for LysMCre genotyping
Denaturation, primer annealing and elongation is to repeat for 35 cycles.

Step	Temperature	Time
Initial denaturation	95°C	3 min
Denaturation	94°C	45 sec
Primer annealing	62°C	45 sec
Elongation	72°C	45 sec
Final extension	72°C	5 min

After amplification, samples were applied onto a 1.5% agarose gel in 1x TBE buffer and separated via electrophoresis at 12V for 30 min. The DNA was stained using Sybr safe/green and visualized via UV light.

3.3.2 Histological staining

3.3.2.1 Tissue preparation

Eleven weeks-old adult mice were narcotized with a mixture of Ketamine and Xylazine, diluted with NaCl (1:1:4). When mice achieve the deep narcotic phase, they are perfused with 1x PBS, and the liver is collected. Liver lobes and EWAT are collected in 4% paraformaldehyde (PFA) and agitated at 4°C for 48h. After fixation, the tissues were washed three times with 50ml 1X PBS for 10min at 4°C. For cryosections (ORO), the tissues are incubated in 30% sucrose for 3 days, carefully dried, and embedded in the Tissue-Tek compound, stored at -80°C. For paraffin sections, the tissues are processed with ascending alcohol series (70%, 80%, 90%, 95%, 100%) and xylol for 2h each step. Subsequently, dehydrated livers get embedded into paraffin.

3.3.2.2 Paraffin section staining

3.3.2.2.1 Hematoxylin-Eosin (HE) staining

Paraffin-embedded livers are cut at 5µm thickness. Prior to staining, sections are heated up for 1h at 65°C. Next, the sections get deparaffinized by two steps of xylol and a descending series of alcohol (100%, 95%, 90%, 80%, 70%) and rinsed in distilled water. The sections are stained with acidic hematoxylin solution for 1.5 min and neutralized by running tap water. Finally, the livers are dehydrated through an ascending series of alcohol and two steps of xylol before mounting with Entellan. Representative pictures are recorded using an Axio Lab.A1 microscope from Zeiss.

3.3.2.2.2 Periodic acid-Schiff (PAS) staining

Possible glycogen and other polysaccharide accumulation are detected via the PAS staining. Livers were prepared as described in section 3.3.2.2.1, and stained with periodic acid for 5 min, subsequently neutralized by running tap water and finally rinse with distilled water. Liver sections are stained with acidic hematoxylin solution for 3 min neutralized by running tap water. Finally, liver sections are dehydrated and mounted as described above (3.3.2.2.1). Representative pictures are recorded using an Axio Lab.A1 microscope from Zeiss and signal quantification is performed by ImageJ software.

3.3.3 Cryosection staining

3.3.3.1 Oil-red-O staining

Cryo blocks are cut at 10µm of thickness and dried at room temperature for 20 min. The sections were rinsed with distilled water and then with 60% isopropanol. To analyze lipid accumulation in the liver, the tissue sections were stained ORO working solution (prepared according to manufacturer's instructions) for 15 min. Sections are rinsed with 60% isopropanol and stained with acidic hematoxylin solution for 3 min. Lastly, liver sections are neutralized by tap water and mounted with Kaiser's glycerol gelatine (pre-heated at 65°C). Representative pictures are recorded using an Axio Lab.A1 microscope from Zeiss, and signal quantification is performed by ImageJ software.

3.3.4 Lipidomics

PBS-perfused livers were weighted, and 10µg of tissue was homogenized in 500µl LC-MS grade water, with the help of a drill. From the homogenate, 50µl was mixed with 500µl extraction mix containing LC-MS grade methanol, chloroform (5:1) and inhouse produced internal standard. This suspension was sonicated for 2 min in a bath sonicator. Sonicated samples were centrifuged for 2 min at 20.000G. The supernatant was collected and mixed with 200µl Chloroform and 750µl 1% Acetic acid in water. The purification solution got mixed manually and centrifuged for 3 min at 20.000G. Subsequently, the upper and intermediate aqueous phases were carefully aspirated and discarded to collect the entire lower chloroform phase, which contains the purified lipids. The solvent was evaporated in the speed vac at 45°C, for 20 min. The lipids got dissolved in 500 µl of spray buffer by sonication for 5 min. Liver samples got further diluted with spray buffer 1:5 and 50µl of the diluted extract got injected and recorded in the mass spectrometer.

The raw spectrum files (rsf) were converted into mzml files (an open, XML-based format for mass spectrometer output) and imported into Lipid Xplorer software. Internal standard contained the pre-defined lipid compositions.

Lipids and internal standards got identified, mass spectra got calibrated and annotated to discriminate different lipid species in the samples. The resulting

counts pro lipid class for each sample were transformed to picomole (pmol) and normalized to the injected volume.

3.4 Flow cytometric analysis

3.4.1 Flow cytometric analysis of myeloid cells in the liver

PBS perfused fresh livers were collected and 0.3g of tissue was placed in ice-cold 1X PBS in a 24-well plate. As soon as mouse preparation was finished, liver pieces were transferred into a 24-well plate filled with a pre-warmed digestion mix (Table 11). Livers were minced and separated into small pieces. Minced livers are digested for 30min at 37°C in a 500µl digestion mix. Single cell suspension was filtered through a 100µm strainer into 4 ml ice-cold FACS buffer (Table 10), and centrifuged 50G 3 min. Pellet contained the hepatocytes. Myeloid-cell containing supernatant was transferred into a fresh FACS tube and centrifuged at 400G 5min. The supernatant was removed and FC-block (Table 11) was added to the pellet for 5 min. Next, pellet volume was normalized to 200µl between different samples. 5µl of volume is separated for cell counting, and the rest of them are centrifuged 400G 5 min. We stained the pellet with 20µl antibody mix for 20 min. Stained cells were washed with 100µl FACS buffer and centrifuged 400G 5min. Supernatant got removed and pellet was diluted with 100µl FACS buffer. The single cell suspension was mixed with Hoechst (1:1) and cells were recorded with MS flow cytometer. Myeloid populations were analyzed by FlowJo flow cytometry analysis software.

3.4.2 Flow cytometric analysis HSC

Legs were collected from sacrificed mice, through disconnection the limbs from the body. Skin and muscle got removed. Femur got separated from tibia and the bones were cut. Bone marrow of both femur and tibia were flushed with 10ml RPMI (with 10% FBS) with a syringe, through a 70µm strainer into a 50ml falcon tube. We centrifuged the cell suspension 400g 10min and removed the supernatant. The pellet got resuspended with 50µl RS-block (2% rat serum in FACS buffer) for 10 min. Cells were diluted, aliquoted for cell counting, pelleted, stained and measured as described in 3.4.1.

3.5 Transcriptomic analysis of KC and Hepatocytes

Livers were harvested as described above (3.3.1.1). In order to protect the RNA-quality, we used 1ml double concentrated digestion mix and digested the liver at room temperature (RT). Stained cells were mixed with DAPI 1:1 directly before sorting. Single live cells were selected by excluding dead cells (DAPI, 1:10000), gating on side (SSC-A) and forward (FSC-A) scatter area. Doublet exclusion takes place through FSC-W FSC-A gating. KCs are identified gating on CD45+, CD31-, CD11b low, F4/80+, Tim4+ cells. Hepatocytes are identified based on their size and CD45- expression. 20,000 KCs and hepatocytes are sorted into 500µl Qiazol lysis buffer using the FACS ARIA^{TM} III cell sorter (BD Biosciences).

3.5.1 Library preparation and RNA sequencing

The SMART-Seq2 protocol[87] is used to construct the cDNA library for sequencing. The extracted mRNA is primed using poly-T oligonucleotides and converted into cDNA via SMART reverse transcription. Pre-amplification was performed by SMART ISPCR, followed by fragmentation using the Illumina Nextera XT kit, PCR amplification, and indexing. Library fragments were then selected by their size (300-400bp) and purified using SPRIBeads (Beckman-Coulter). The Agilent high sensitivity D5000 assay was used to measure the size distribution of cDNA libraries on a Tapestation 4200 system (Agilent). Quantification of cDNA libraries was performed using a Qubit high sensitivity dsDNA assay.

Sequencing was performed using a 75 bp single-end setup on the Illumina NextSeq500 system applying High Output v2.5 chemistry. Following the Illumina standard pipeline scripts (STAR version, bcl2fastq2 v.2.20) base calling, alignment to reference genome (Mus musculus, mm10, UCSC), and file conversion to fastq files were achieved. To quantify abundances of transcripts from the bulk RNA-seq data, Kallisto pseudo alignment was applied[88] .

3.5.2 DESeq2 pipeline for differential expression analysis

DESeq2[89] pipeline is followed to calculate normalized read counts and differential gene expression using the Kallisto read counts as an input. The read counts were stored in a DESeq Dataset (dds) and a minimal pre-filtering, excluding genes with less than 10 reads in total, was performed to reduce the memory size of the dds data object and to decrease computing time. Within the DESeq2 package[89], the standard differential expression analysis estimates the size factors and dispersion, performs the test for differential expression based on negative binomial distribution. Visual analysis of the data included PCA, Pearson correlation analysis Euclidean distance matrix between the samples, and functional classification of the recorded transcriptome.

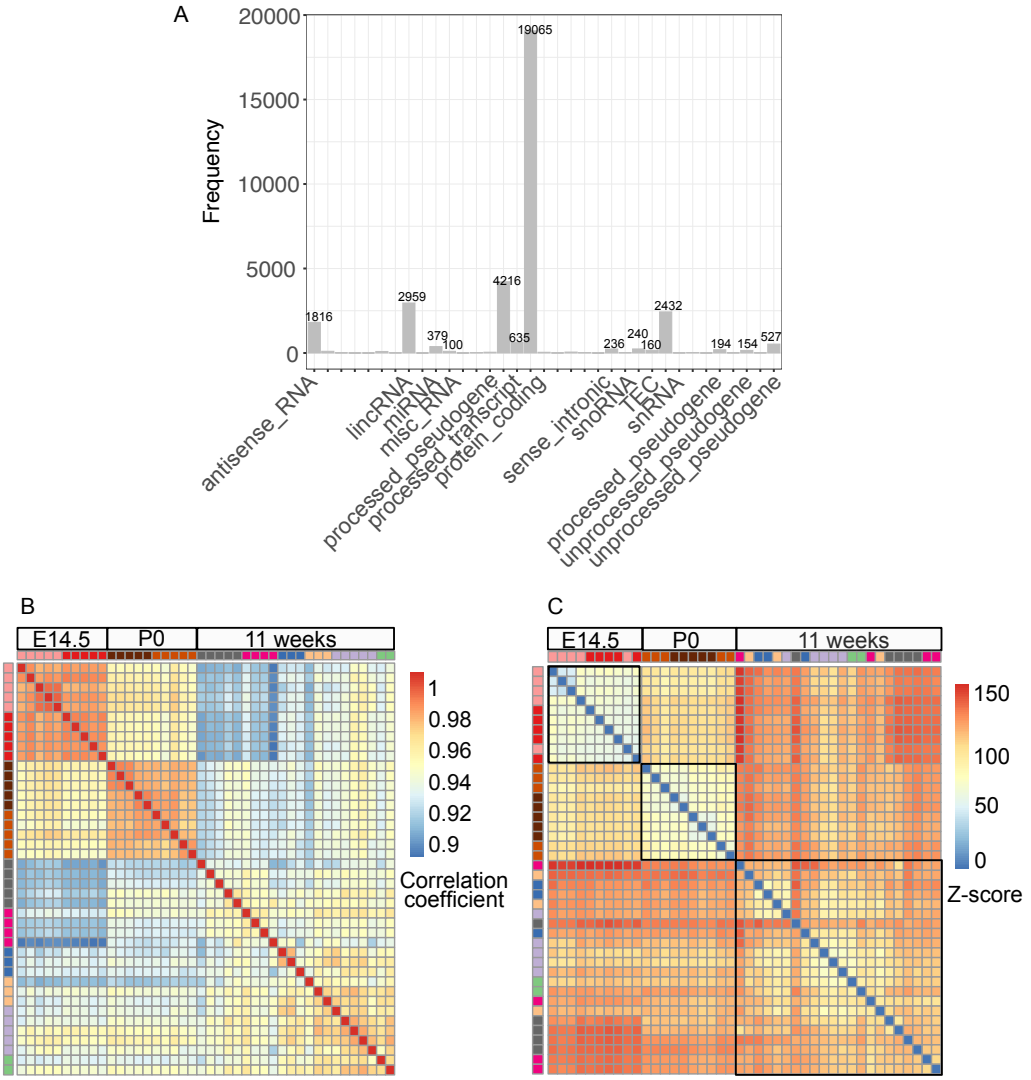

Figure 4. Quality assessment of transcriptomic datasets.
(A) Frequency of functional classes were assessed and concluded that protein coding transcripts are covered at highest. **(B)** Pearson correlation coefficient is calculated between every sample, which correlates to the age and dietary condition **(C)** Euclidean distance matrix shows the closest distances related to age and dietary condition. E14.5 sorted Kupffer cells are marked with rose (CD) and red (HFD), P0 sorted Kupffer cells are marked by dark-brown (CD) and light-brown (HFD). Eleven weeks old sorted Kupffer cells are classified into six dietary groups, with the following colour codes: Grey -

CD_MCD_LCD- mother is on control diet before and during pregnancy (Control Diet $_{Maternal}$), mother is on control diet during lactation (Control Diet $_{Lactational}$) and offspring is on control diet during post-weaning diet. Pink - CD_MCD_LHFD- mother is on control diet before and during pregnancy (Control Diet $_{Maternal}$), mother is on control diet during lactation (Control Diet $_{Lactational}$) and offspring is on High-fat diet during post-weaning diet. Blue - HFD_MCD_LCD- mother is on High-fat diet before and during pregnancy (High-fat Diet $_{Maternal}$), mother is on control diet during lactation (Control Diet $_{Lactational}$) and offspring is on control diet during post-weaning diet. Purple - HFD_MHFD_LCD- mother is on High-fat diet before and during pregnancy (High-fat Diet $_{Maternal}$), mother is on High-fat diet during lactation (High-fat Diet $_{Lactational}$) and offspring is on control diet during post-weaning diet. Yellow - HFD_MCD_LHFD- mother is on High-fat diet before and during pregnancy (High-fat Diet $_{Maternal}$), mother is on control diet during lactation (Control Diet $_{Lactational}$) and offspring is on High-fat diet during post-weaning diet. Green - HFD_MHFD_LHFD- mother is on High-fat diet before and during pregnancy (High-fat Diet $_{Maternal}$), mother is on High-fat diet during lactation (High-fat Diet $_{Lactational}$) and offspring is on High-fat diet during post-weaning diet.

Differentially expressed genes were calculated for the HIF-1α model, for every dietary condition WT vs. KO, with a significance limit of p=0.05, significant fold-change equals to 2, using independent hypothesis weighting (IHW). IHW compromises multiple testing methods in order to increase the detection power in genome-scale multiple testing[90].

3.5.3 Co-expression network analysis

Co-expression network analysis[91] (CO-CENA) was performed to analyze the effect of maternal, lactational or post-weaning obesity on KCs for all dietary groups and identify seven gene-sets, which follow a certain pattern between the conditions. Experimental date-related batch correction was applied via the Limma package[92], and the top 5000 most variable genes were used as an input for the CO-CENA pipeline. Pearson correlation analysis was applied with correlation significance p>0.05. The optimal correlation coefficient cut-off, 0.659 was calculated for the clustering. Gene set enrichment analysis (GSEA) was performed on each inter-condition gene-expression-related clusters using the clusterProfiler R package.

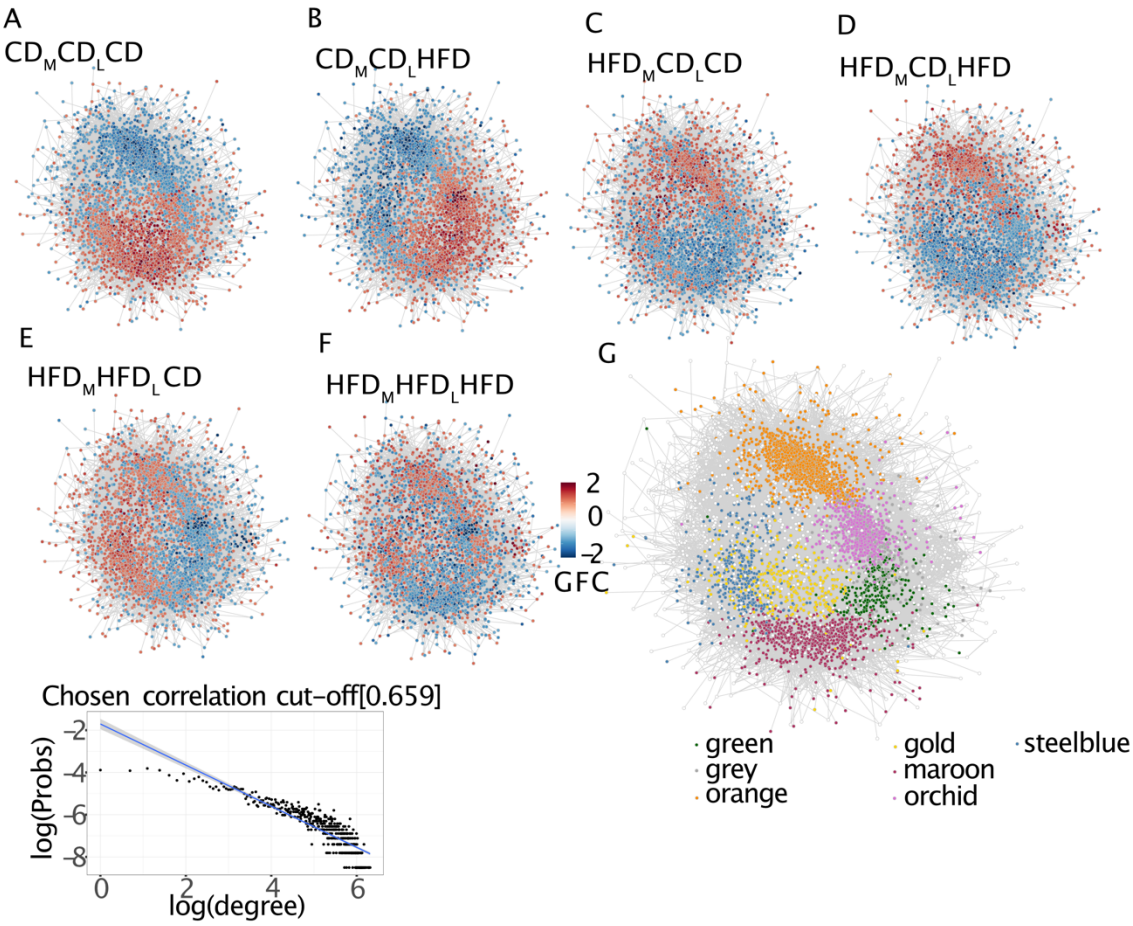

Figure 5. CO-CENA expression networks with gene fold change representation
Co-expression networks are visualized between the six adult dietary conditions. Every dot in the network represents a gene and its color-coded relative expression (gene fold change - GFC) between the different conditions. **(A)** Co-expression network of CD_MCD_LCD **(B)** Co-expression network of CD_MCD_LHFD **(C)** Co-expression network of HFD_MCD_LCD **(D)** Co-expression of HFD_MCD_LHFD **(E)** Co-expression network of HFD_MHFD_LCD **(F)** Co-expression network of HFD_MHFD_LHFD **(G)** CO-CENA network of the wild-type(WT) model. Based on cross-conditional expression patterns, genes are classified into seven clusters, marked by green, dakgrey, darkorange, gold, maroon, orchid and steelblue. In every cluster, genes have a specific expression pattern, discussed in detail in the results section. Correlation cutoff plot at chosen cut-off=0.659. GFC-Gene fold change, CD - control diet, HFD - High-fat diet, $_L$ - lactational phase (postnatal day 0-21), $_M$ - Maternal phase (from at least 8 weeks before pregnancy until birth)

3.6 Ligand-receptor analysis between KC and hepatocytes

3.6.1 Cell-talk DB

HFD_MCD $WT^{HIF\text{-}1\alpha}$ vs. $KO^{HIF\text{-}1\alpha}$ DEG were selected from KCs as possible ligands and from hepatocytes as possible receptors. Ligand receptor interactions were combined with CelltalkDB[93], a manually curated database of ligand-receptor (LR) interactions in human in mice containing 3398 human and 2033 mouse LR pairs. Every LR pair is annotated with references to backtrack the source of LR annotation. With this method, we found a small but specific group of LR pairs with 10 KC ligands and their DEG receptors in hepatocytes.

3.6.2 Nichenet

For an extensive analysis including all possible receptors, we used all $HFD_MCD\ WT^{HIF\text{-}1\alpha}$ vs. $KO^{HIF\text{-}1\alpha}$ DEG KC ligands and their predicted receptors. We did not filter on the gene-expression pattern in hepatocytes. On those Cell-talk DB-predicted LR pairs we performed regulatory potential prediction, based on the Nichenet pipeline.[94]

3.6.3 BRENDA - enzymatic activity analysis

The BRENDA[95] database and R-package were used to find the hepatocyte $HFD_MCD\ WT^{HIF\text{-}1\alpha}$ vs. $KO^{HIF\text{-}1\alpha}$ DEG receptors with enzymatic activity and prioritized them, as possible key enzymes in lipid synthesis. Those enzymes are the ones in hepatocytes that receive the maternal obese signal from KCs. Therefore, possible key regulators of maternal obesity-induced NASH.

3.7 O2PLS multi-omics analysis

OmicsPLS[96] package is used to combine lipidomics and hepatocyte transcriptomic data. OmicsPLS is based on the two-way orthogonal partial least square (O2PLS)[97] mathematical regression model, which is widely used in biomedical data analysis to integrate two highly dimensional datasets, visualize relationships between the features and inspect groupings across subjects. For that purpose, we imputed the shotgun lipidomics matrix with 439 lipid species and the hepatocyte RNA-seq count table with 11.382 transcripts and 29 joint samples between the two matrixes. Transcriptomic data was scaled down to the top 75% most variable transcripts. Mitochondrial transcripts were not excluded from the dataset, due to their possible role in metabolic programming. Data quality threshold was defined as at least 5.000.000 reads, and via visualization of genetypes. In the hepatocyte dataset, we found in total 17807 protein coding transcripts and 24 mitochondrial transcripts. Lipidomics and transcriptomics was joined through the shared host (datapoints are coming from the same mouse). Dimension reduction took place through cross validation to find the triplet (joint components, lipid specific components, and RNA-specific components) which enables the best prediction power. We found and used for the visualization one joint, 2 orthogonal to lipidome and 9 orthogonal components to the transcriptome. Joint predictional power was 0.83 for both transcriptome and lipidome.

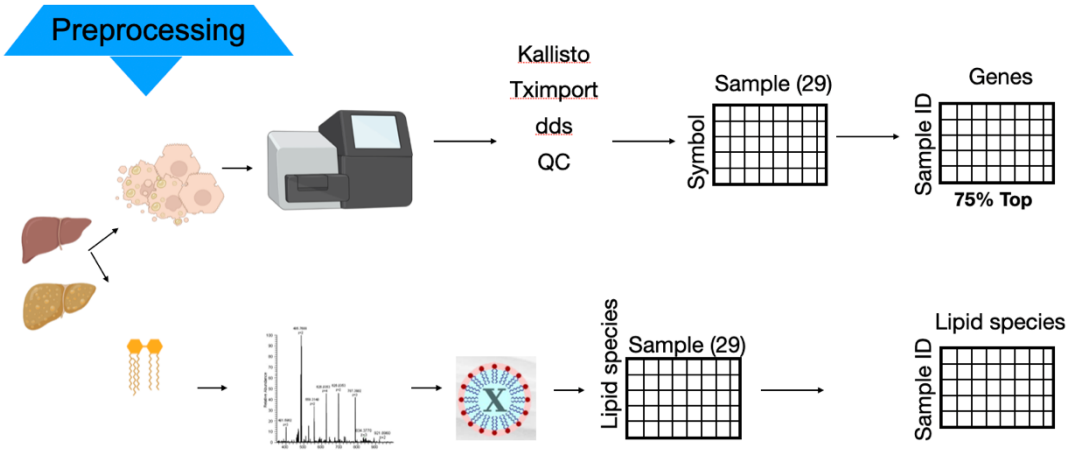

Figure 6. Prerpcessing steps of Omics-PLS
In order to analyse joint variants between hepatocyte transcriptomics and liver lipidomics, a multiomics analysis was performed. Liver samples were processed through bulk RNA-seq of hepatocytes and shotgun lipidomics of frozen liver pieces. After pre-processing, datasets were classified into matrices and joined through sample IDs. Matrices got transposed and jointly analyzed through the O2PLS (Two-way orthogonal partial least squares regression) machine learning method.

3.8 Statistical Analysis

R-studio and Prism were used for statistical assessment and visulaization. Statistical assessment was performed via one-way ANOVA - Turkey's multiple comparisons method. Thus, statistical significance was represented via the probalility (p-value) as follows: *= $p<0.05$, ** = $p<0.01$, ***=$p<0.001$.

4.1 Maternal obesity induces fatty liver disease and impaired glucose metabolism

A mouse model was established to study the impact of maternal obesity on the innate immune system. Diet-induced obesity was introduced to female mice, and their offspring were followed up to adulthood (11 weeks old). Five weeks old female mice followed either HFD or CD for eight weeks. After birth, offspring born to an obese mother were cross-fostered to a lean mother for lactation. With an additional dietary change at 3 weeks of age (at weaning), six dietary groups of offspring were analyzed (Figure 7).

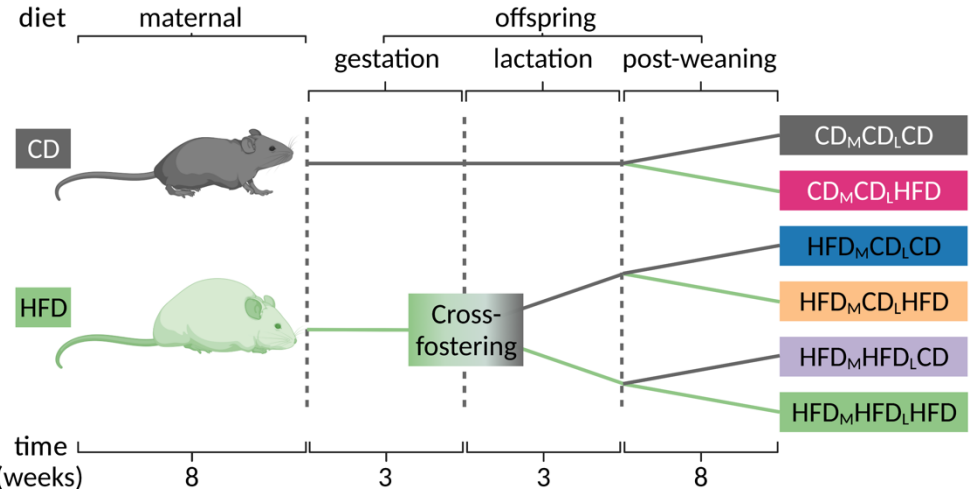

Figure 7. The maternal obesity wild-type model
Five-week-old mice were put on a control diet (CD) or high-fat diet (HFD) for eight weeks. After mating, females follow the same diet, $CD_{Maternal}$ (CD_M) or $HFD_{Maternal}$ (HFD_M). When mice gave birth, offspring were either kept with their mother on the same diet ($CD_MCD_{Lactational(L)}$ or HFD_MHFD_L) or offspring born to obese mother were cross-fostered to CD-mother for 21 days lactation (HFD_MCD_L). Post-weaning diet was either CD or HFD and lasted for eight additional weeks.
Grey - CD_MCD_LCD- mother is on control diet before and during pregnancy (Control Diet $_{Maternal}$), the mother is on a control diet during lactation (Control Diet $_{Lactational}$), and the offspring is on control diet during the post-weaning phase.
Pink - CD_MCD_LHFD- mother is on control diet before and during pregnancy (Control Diet $_{Maternal}$), the mother is on control diet during lactation (Control Diet $_{Lactational}$), and the offspring is on a high-fat diet during the post-weaning phase.
Green - HFD_MHFD_LHFD- mother is on a high-fat diet before and during pregnancy (High-fat Diet $_{Maternal}$), mother is on a high-fat diet during lactation (High-fat Diet $_{Lactational}$), and the offspring is on a high-fat diet during the post-weaning phase.
Purple - HFD_MHFD_LCD- mother is on a high-fat diet before and during pregnancy (High-fat Diet $_{Maternal}$), mother is on a high-fat diet during lactation (High-fat Diet $_{Lactational}$), and the offspring is on control diet during the post-weaning phase.
Yellow - HFD_MCD_LHFD- mother is on a high-fat diet before and during pregnancy (High-fat Diet $_{Maternal}$), mother is on control diet during lactation (Control Diet $_{Lactational}$), and the offspring is on a high-fat diet during the post-weaning phase.
Blue - HFD_MCD_LCD- mother is on a high-fat diet before and during pregnancy (High-fat Diet $_{Maternal}$), mother is on control diet during lactation (Control Diet $_{Lactational}$), and the offspring is on control diet during the post-weaning phase.

To target the effects of eight weeks high-fat diet (HFD) on the metabolism of female mice compared with the control diet (CD), a homeostatic model of insulin resistance (HOMA-IR) was calculated. After eight weeks of HFD, female mice have shown significantly higher HOMA-IR measures and body weight (Figure 8).

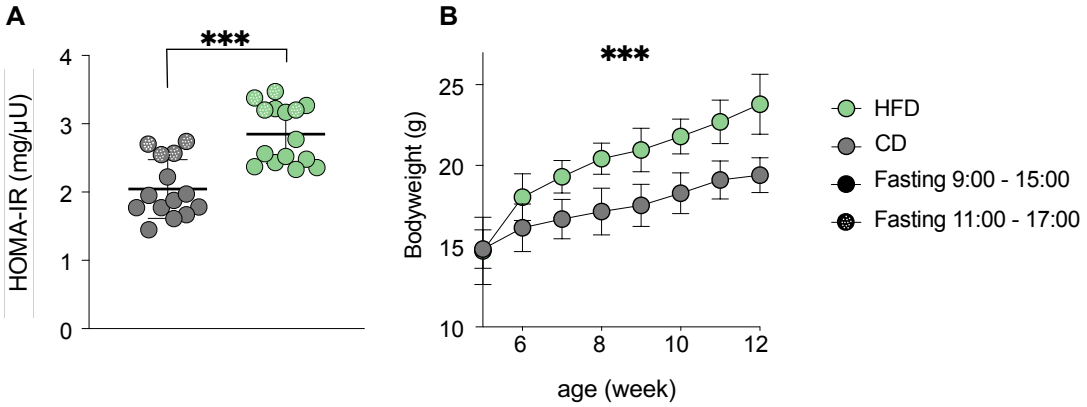

Figure 8. Metabolic assessment of mothers after eight weeks of diet
(A) Homeostatic model for insulin resistance (HOMA-IR) measurement of 13-week-old female mice after eight weeks of diet. Single mice are represented as circles, mice on control diet (CD) are marked with grey, high-fat diet (HFD) mice are marked with green. Prior to blood-withdrawal for HOMA-IR, six hours fasting took place either from 9:00 am (marked with colored circles) or from 11:00 am (marked with colored circles and white dots inside the circle). Samples size is n_{CD}=14 and n_{HFD}=15. Paired t-test was calculated and statistical significance is marked as *** - probability (p)-value <= 0.001. Data are represented as mean ± SED.
(B) Weight gain plot of female mice from 5 weeks to 12 weeks of age. The curve of weight gain for mice fed with CD (grey) or HFD (green). Samples size is n_{CD}=15 and n_{HFD}=15, mean value is represented as a circle for each week with error bars, representing the standard deviation of uncertainty. One-way analysis of variance (ANOVA) was used to address the statistical significance of variance between the body weight of mice on CD and on HFD. Analysis of variance was calculated and statistical significance is marked as *** - probability (p)-value <= 0.001. Data is represented as mean ± SED. SED - Standard error of difference.

Offspring's body weight was measured to address maternal diet related changes in offspring's body weight. HFD_MHFD and HFD_MCD have significant higher post-weaning (P21) body weight (BW) (Figure 9). HFD_MHFD responds clearly to maternal and lactational HFD and has an increased body weight (BW). Most of the HFD_MCD mice, respond to lactational CD and their P21-BW is comparable to CD_MCD mice.

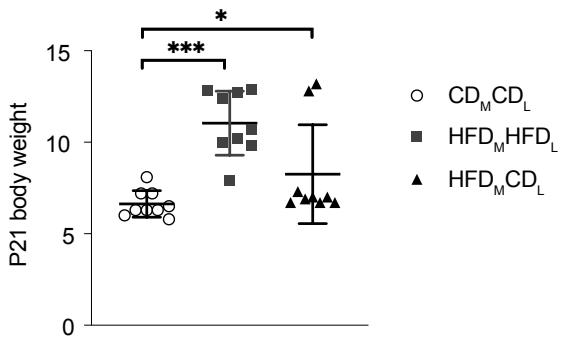

Figure 9. Post-weaning (P) body weight of P21 offspring.
Statistical assessment was performed via one-way ANOVA - Turkey's multiple comparisons method. P21 - post-weaning age 21 days, values are shown in gram. Circles, squares and triangles represent single male mice (n), from every group mice come at least from two different litters, with different mothers.
CD_MCD_L- Control diet $_{Maternal}$ Control diet $_{Lactational}$ n=9
HFD_MCD_L- High-fat diet $_{Maternal}$ Control diet $_{Lactational}$ n=9
HFD_MHFD_L- High-fat diet $_{Maternal}$ High-fat diet $_{Lactational}$ n=9
* - probability (p)-value <= 0.05, ** - p-value <= 0.01, *** - p-value <= 0.001
Data is represented as mean ± SED. SED - Standard error of difference.

There were two HFD_MCD non-responder, which mice did not respond to cross-foster-induced lactational dietary change. Their body weight got normalized until adulthood - postnatal 76 days of age (P76) (Figure 11-A)

Offspring's adult body weight and weight gain curve were increased upon HFD, but resistant to maternal diet (Figure 10-11A). The highest weaning weight (P21) and lowest post-weaning weight gain was noted in mice, where the mother was continuously on HFD, but offspring's diet got changed to CD (HFD_MHFD_LCD). That group reduced its adult body weight into the same range as CD_MCD_LCD and HFD_MCD_MCD.

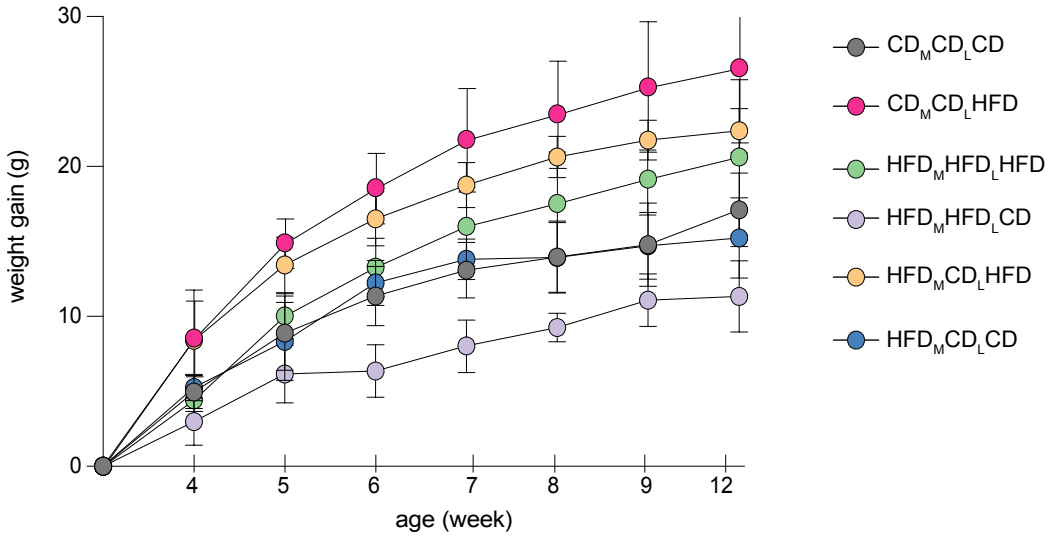

Figure 10 Offspring's weight gain curve during the post-weaning (PW) diet
Offspring's weight gain during the post-weaning phase from the age of 3 weeks to 12 weeks. The curve of weight gain for mice fed with CD (grey, purple, and blue) or HFD (pink, green and yellow). Mean weight gain value is represented as a circle for each week with error bars, representing the standard deviation of uncertainity. Colour code represents the different dietary pattern as following:
Grey - CD_MCD_LCD- mother is on control diet before and during pregnancy (Control Diet $_{Maternal}$), mother is on control diet during lactation (Control Diet $_{Lactational}$) and the offspring is on control diet during the post-weaning phase (n=8).
Pink - CD_MCD_LHFD- mother is on control diet before and during pregnancy (Control Diet $_{Maternal}$), mother is on control diet during lactation (Control Diet $_{Lactational}$) and the offspring is on a high-fat diet during the post-weaning phase (n=7).
Green - HFD_MHFD_LHFD- mother is on a high-fat diet before and during pregnancy (High-fat Diet $_{Maternal}$), mother is on a high-fat diet during lactation (High-fat Diet $_{Lactational}$) and the offspring is on a high-fat diet during the post-weaning phase (n=7).
Purple - HFD_MHFD_LCD- mother is on a high-fat diet before and during pregnancy (High-fat Diet $_{Maternal}$), mother is on a high-fat diet during lactation (High-fat Diet $_{Lactational}$) and the offspring is on control diet during the post-weaning phase (n=6).
Yellow - HFD_MCD_LHFD- mother is on a high-fat diet before and during pregnancy (High-fat Diet $_{Maternal}$), mother is on control diet during lactation (Control Diet $_{Lactational}$) and the offspring is on a high-fat diet during the post-weaning phase (n=7).
Blue - HFD_MCD_LCD- mother is on a high-fat diet before and during pregnancy (High-fat Diet $_{Maternal}$), mother is on control diet during lactation (Control Diet $_{Lactational}$) and the offspring is on control diet during the post-weaning phase (n=7). Data is represented as mean ± SED. SED - Standard error of difference.

To study the metabolic state of the liver, histological stains of neutral lipids (ORO) and glycogen (PAS) were performed (Figure 13). ORO quantification and shotgun lipidomics of the liver show that the maternal obese groups with post-weaning control diet (HFD_MCD_LCD & HFD_MHFD_LCD) have the highest lipid accumulation (Figure 11E, 12C and 13A). If the offspring follows the mother's

diet, the lipid accumulation is comparable with the obese group. HFD_MHFD_LHFD & HFD_MCD_LHFD groups show only a slight increase in liver lipid accumulation (ns).

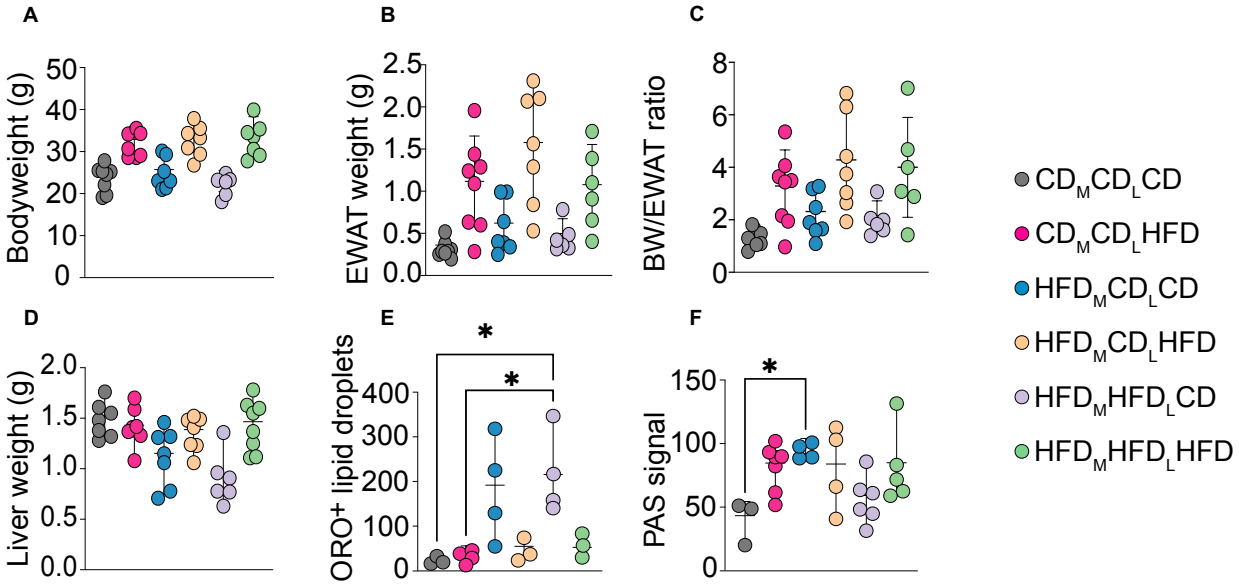

Figure 11 General physiology of 11-week-old adult offspring.
Physiological and histological measurements are quantified as dot plots, where the mean is represented as a middle line and range bars represent the highest and lowest measured value. Statistical assessment was performed via one-way ANOVA - Turkey's multiple comparisons method. Statistical significance is represented if maternal diet is the driving factor of the difference. Statistical significance is represented via the probability (p-value) as following: *= $p<0.05$, ** = $p<0.01$, ***=$p<0.001$. Data is represented as mean ± ROD. ROD - Range of distribution.
Each circle represents a single mouse, the color code identifies the dietary pattern as following:
Grey - CD_MCD_LCD- mother is on control diet before and during pregnancy (Control Diet $_{Maternal}$), mother is on control diet during lactation (Control Diet $_{Lactational}$) and the offspring is on control diet during the post-weaning phase.
Pink - CD_MCD_LHFD- mother is on control diet before and during pregnancy (Control Diet $_{Maternal}$), mother is on control diet during lactation (Control Diet $_{Lactational}$) and the offspring is on a high-fat diet during the post-weaning phase.
Green - HFD_MHFD_LHFD- mother is on a high-fat diet before and during pregnancy (High-fat Diet $_{Maternal}$), mother is on a high-fat diet during lactation (High-fat Diet $_{Lactational}$) and the offspring is on a high-fat diet during the post-weaning phase.
Purple - HFD_MHFD_LCD- mother is on a high-fat diet before and during pregnancy (High-fat Diet $_{Maternal}$), mother is on a high-fat diet during lactation (High-fat Diet $_{Lactational}$) and the offspring is on control diet during the post-weaning phase.
Yellow - HFD_MCD_LHFD- mother is on a high-fat diet before and during pregnancy (High-fat Diet $_{Maternal}$), mother is on control diet during lactation (Control Diet $_{Lactational}$) and the offspring is on a high-fat diet during the post-weaning phase.
Blue - HFD_MCD_LCD- mother is on a high-fat diet before and during pregnancy (High-fat Diet $_{Maternal}$), mother is on control diet during lactation (Control Diet $_{Lactational}$) and the offspring is on control diet during the post-weaning phase.
(A) Eleven weeks old adult offspring's body weight was measured and represented as dot plot in the measure of gram (g). **(B)** Epididymal white adipose tissue (EWAT) was measured and represented as dot plot in the measure of gram (g) of eleven weeks old adult offspring. **(C)** Body weight (BW) and Epididymal white adipose tissue (EWAT) ratio was calculated and represented as dot plot of eleven weeks old adult offspring. **(D)** Whole livers were measured and represented as dot plot in the measure of gram (g) of eleven weeks old adult offspring. **(E)** Oil-red-O (ORO) positive lipid droplets were quantified as µm2 red part of the stained liver records and represented as dot plot. **(F)** Periodic acid-Shiff (PAS) stained livers are quantified as intensity of PAS stain and represented as dot plot.

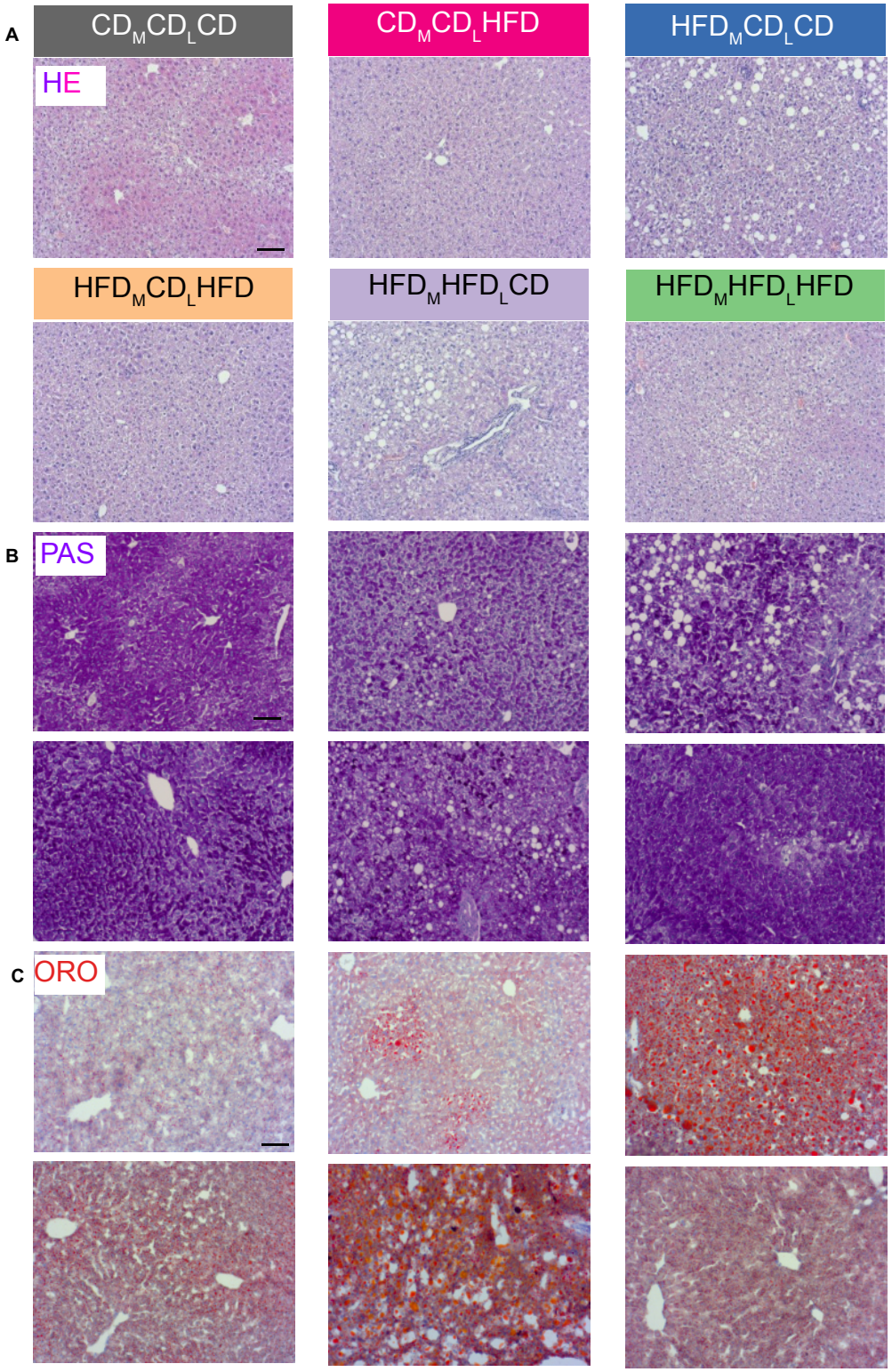

Figure 12 Histological assessment of maternal obese adult offspring.
(A) Representative stains for adult offspring's liver (11-weeks-old) HE - Hematoxylin-Eosin staining is a standard staining method in histology. Hematoxylin stains the cell nuclei blue and eosin stains the extracellular matrix and cytoplasm purple-pink. **(B)** PAS - Periodic acid Schiff staining aims to detect polysaccharides such as glycogens, glycoproteins and glycolipids. **(C)** ORO - Oil-red-O stains neutral triglycerides and lipids in the tissue red. The two groups, where maternal obesity was followed by post-weaning control diet (marked with blue and purple) show strong morphological differences. Paraffin stained HE and PAS shows white circles on the liver, which is a first sign of liver lipid accumulation. ORO confirms the fatty liver phenotype with the strong accumulation of neutral lipids. The six dietary groups are in the same order for every staining method. (Legend continues on the next page.)

Grey - CD_MCD_LCD- mother is on control diet before and during pregnancy (Control Diet $_{Maternal}$), mother is on control diet during lactation (Control Diet $_{Lactational}$) and the offspring is on control diet during the post-weaning phase.
Pink - CD_MCD_LHFD- mother is on control diet before and during pregnancy (Control Diet $_{Maternal}$), mother is on control diet during lactation (Control Diet $_{Lactational}$) and the offspring is on a high-fat diet during the post-weaning phase.
Blue - HFD_MCD_LCD- mother is on a high-fat diet before and during pregnancy (High-fat Diet $_{Maternal}$), mother is on control diet during lactation (Control Diet $_{Lactational}$) and the offspring is on control diet during the post-weaning phase.
Purple - HFD_MHFD_LCD- mother is on a high-fat diet before and during pregnancy (High-fat Diet $_{Maternal}$), mother is on a high-fat diet during lactation (High-fat Diet $_{Lactational}$) and the offspring is on control diet during the post-weaning phase.
Yellow - HFD_MCD_LHFD- mother is on a high-fat diet before and during pregnancy (High-fat Diet $_{Maternal}$), mother is on control diet during lactation (Control Diet $_{Lactational}$) and the offspring is on a high-fat diet during the post-weaning phase.
Green - HFD_MHFD_LHFD- mother is on a high-fat diet before and during pregnancy (High-fat Diet $_{Maternal}$), mother is on a high-fat diet during lactation (High-fat Diet $_{Lactational}$) and the offspring is on a high-fat diet during the post-weaning phase.

Relative distribution of lipid types in the liver shows that triacylglycerols (TAG) and cholesterol esters (CE) are accumulated in the liver, where the highest ORO signal was detected (HFD_MCD_LCD & HFD_MHFD_LCD), and phospholipids show a relatively low abundance in those groups (Figure 13B). Out of CE and TAG, cardiolipin, diacylglycerol, lipoprotein-lyso-phosphatidylcholine, lyso-phosphatidylcholine-O, lyso-phosphatidyl -ethanolamine, monoacylglycerol, phospholipids, sphingolipids were detected in the liver without any trend between the dietary subgroups (Figure 13B).

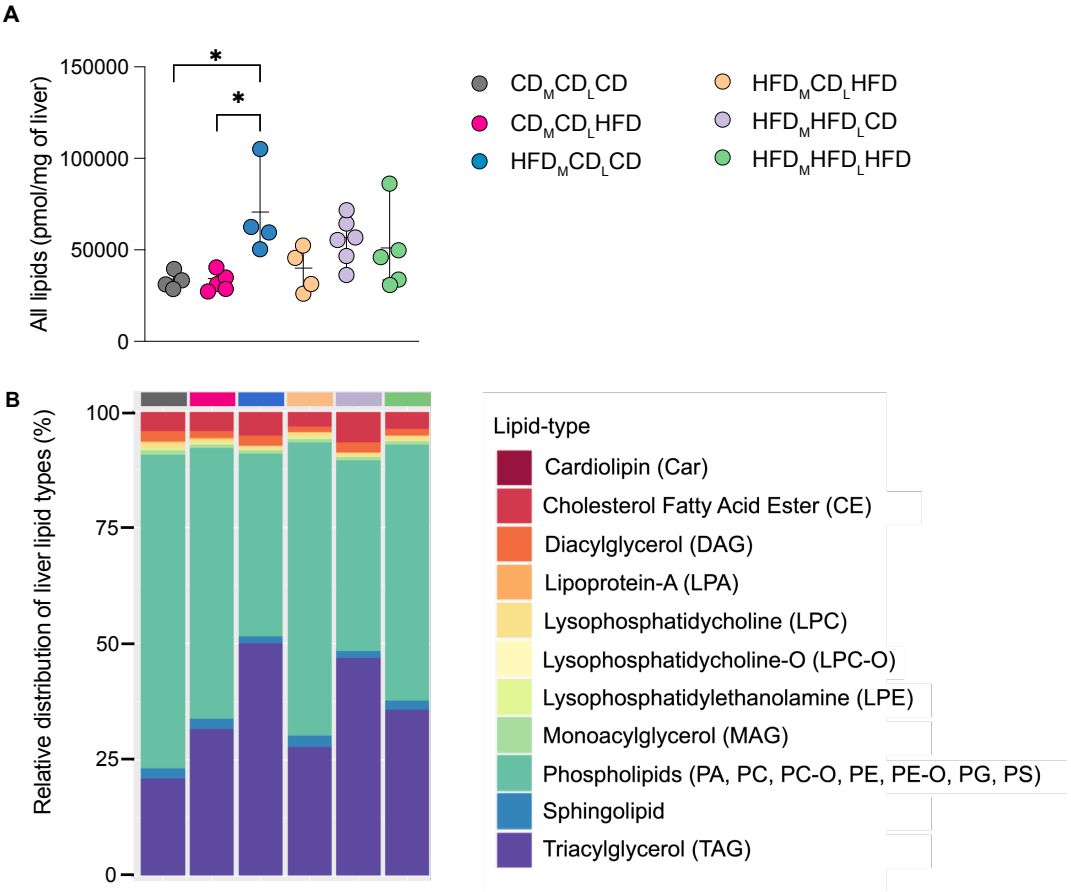

Figure 13. TAGs and CEs are accumulated upon maternal obesity
(A) Dot plot shows the accumulation of all lipids in 10 mg of liver species. Indentified lipids involve cardiolipins, cholesterol fatty acid esters, diacylglycerols, lipoprotein-a, lysophosphatidycholines, lysophosphatidylethanolamines, monoacylglycerols, phospholipids, sphingolipids and triacylglycerols (TAG). Every circle represents a single adult mouse liver and colors represent the dietary conditions. Statistical assessment was performed via one-way ANOVA - Turkey's multiple comparisons method. Statistical significance is represented via the probability (p-value) as following: * - $p<0.05$, ** - $p<0.01$. Data are represented as mean ± ROD. ROD - Range of distribution. (Legend continues on the next page.)

(B) Stack plot of liver lipid type relative distribution for every dietary condition. Merged dataset from at least three samples per condition from at least two different litters. Grey - CD_MCD_LCD- mother is on control diet before and during pregnancy (Control Diet $_{Maternal}$), mother is on control diet during lactation (Control Diet $_{Lactational}$) and the offspring is on control diet during the post-weaning phase (n=4). Pink - CD_MCD_LHFD- mother is on control diet before and during pregnancy (Control Diet $_{Maternal}$), mother is on control diet during lactation (Control Diet $_{Lactational}$) and the offspring is on a high-fat diet during the post-weaning phase (n=5). Blue - HFD_MCD_LCD- mother is on a high-fat diet before and during pregnancy (High-fat Diet $_{Maternal}$), mother is on control diet during lactation (Control Diet $_{Lactational}$) and the offspring is on control diet during the post-weaning phase (n=4). Purple - HFD_MHFD_LCD- mother is on a high-fat diet before and during pregnancy (High-fat Diet $_{Maternal}$), mother is on a high-fat diet during lactation (High-fat Diet $_{Lactational}$) and the offspring is on control diet during the post-weaning phase. Yellow - HFD_MCD_LHFD- mother is on a high-fat diet before and during pregnancy (High-fat Diet $_{Maternal}$), mother is on control diet during lactation (Control Diet $_{Lactational}$) and the offspring is on a high-fat diet during the post-weaning phase. Green - HFD_MHFD_LHFD- mother is on a high-fat diet before and during pregnancy (High-fat Diet $_{Maternal}$), mother is on a high-fat diet during lactation (High-fat Diet $_{Lactational}$) and the offspring is on a high-fat diet during the post-weaning phase. Phospholipids are defined as the combination of PA - Phosphatidic acid, PC - Phosphatidylcholine, PE - Phosphatidylethanolamine, PG - Phosphatidylglycerol, PS - Phosphatidylserine.

In summary, those results show that maternal obesity induces a high lipid accumulation in the offspring's liver. Hepatic lipid accumulation was confirmed with oil-red-o histological staining and shotgun lipidomics via mass spectrometry. Statistical significant lipid accumulation was found in those maternal obese groups, where the post-weaning diet was a control diet (HFD_MCD_LCD and HFD_MHFD_LCD). The relative distribution of liver lipid types shows that CE and TAG species are accumulated in those two groups. Moreover, HFD_MCD_LCD group shows a significantly increased PAS signal, which may indicate impaired glucose metabolism upon maternal obesity.

4.2 Impact of maternal obesity on the immune cell dynamics

In order to see the effects of maternal obesity-induced steatohepatitis on the myeloid cell dynamics, KC, LCM, monocyte, granulocyte and cDC populations were quantified via flow cytometry (Figure 14). Inflammation in the liver requires the recruitment of monocytes, granulocytes and possibly other myeloid cells as well. Liver myeloid cell dynamics are represented via uniform manifold approximation (UMAP) and compared between the six dietary conditions (Figure 16A). Higher amounts of KCs were observed in all maternal obese conditions, which is the highest in the cross-fostered offspring (HFD_MCD_LHFD & HFD_MCD_LCD, $p<0.05$). LCM show a high accumulation in the most affected dietary group (HFD_MCD_LCD, $p<0.01$). Monocytes, granulocytes, cDC1, and cDC2 cell numbers are significantly accumulated ($p<0.05$) in HFD_MCD_LCD compared to CD_MCD_LCD (Figure 14B). Flow cytometric analysis of adult bone marrow confirmed the upregulation of common myeloid progenitors (CD_MCD_LCD vs. HFD_MCD_LCD, $p<0.05$), while a relatively low distribution of common lymphoid progenitors in maternal obese conditions (Figure 14C).

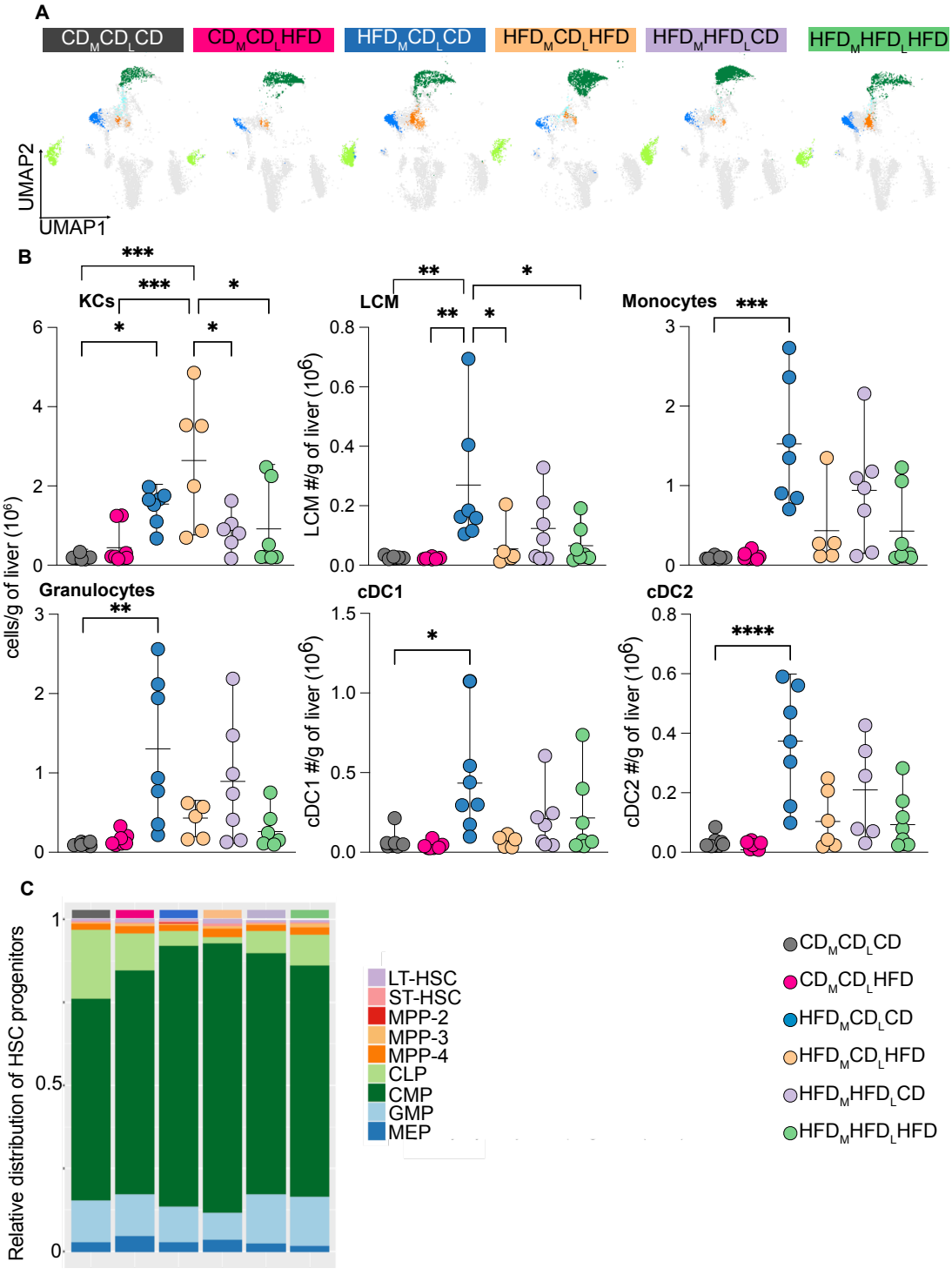

Figure 14. Myeloid cell dynamics upon maternal obesity
(A) Uniform manifold ***approximation*** (UMAP) dimension reduction and visualization of myeloid cells in the liver. ***For every*** dietary conditions**,** the most representative UMAP plot is shown. Every dot on the UMAP plot represents a cell, and all recorded samples got downsampled to 10.000 cells. Dark-green population represents Kupffer cells (KCs), light-blue shows liver capsular macrophages (LCM), monocytes are dark-blue, granulocytes are light-green, conventional dendritic cell type 1 (cDC1) are light-orange, and conventional dendritic cell type 2 (cDC2) are marked by dark-orange. (B) Myeloid cell number quantification normalized to gram of liver tissue. Quantification includes KCs, LCM, monocytes, granulocytes, cDC1, and cDC2 populations. Every circle represents a single adult mouse and colors represent the dietary conditions. (Legend continues on the next page.)

Statistical assessment was performed via one-way ANOVA - Turkey's multiple comparisons method. Statistical significance is represented via the probability (p-value) as following: * - p<0.05, ** - p<0.01, ** - p<0.001. Data is represented as mean ± ROD. ROD - Range of distribution. **(C)** Stack plot representing the relative distribution of HSC progenitors for the six adult dietary conditions. LT-HSC - long-term hematopoietic stem cell, ST-HSC - short-term hematopoietic stem cell, MPP-2 - multipotent progenitor type 2 , MPP-3 - multipotent progenitor type 3, MPP-4 - multipotent progenitor type 4, CLP - common lymphoid progenitor, CMP-common myeloid progenitor, GMP - granulocyte-monocyte progenitor, MEP - megakaryocyte-erythroid progenitor.
Samples are color coded as follows:
Grey - CD_MCD_LCD- mother is on control diet before and during pregnancy (Control Diet $_{Maternal}$), mother is on control diet during lactation (Control Diet $_{Lactational}$) and the offspring is on control diet during the post-weaning phase (n=6).
Pink - CD_MCD_LHFD- mother is on control diet before and during pregnancy (Control Diet $_{Maternal}$), mother is on control diet during lactation (Control Diet $_{Lactational}$) and the offspring is on a high-fat diet during the post-weaning phase (n=6).
Blue - HFD_MCD_LCD- mother is on a high-fat diet before and during pregnancy (High-fat Diet $_{Maternal}$), mother is on control diet during lactation (Control Diet $_{Lactational}$) and the offspring is on control diet during the post-weaning phase (n=7).
Purple - HFD_MHFD_LCD- mother is on a high-fat diet before and during pregnancy (High-fat Diet $_{Maternal}$), mother is on a high-fat diet during lactation (High-fat Diet $_{Lactational}$) and the offspring is on control diet during the post-weaning phase (n=7).
Yellow - HFD_MCD_LHFD- mother is on a high-fat diet before and during pregnancy (High-fat Diet $_{Maternal}$), mother is on control diet during lactation (Control Diet $_{Lactational}$) and the offspring is on a high-fat diet during the post-weaning phase (n=5).
Green - HFD_MHFD_LHFD- mother is on a high-fat diet before and during pregnancy (High-fat Diet $_{Maternal}$), mother is on a high-fat diet during lactation (High-fat Diet $_{Lactational}$) and the offspring is on a high-fat diet during the post-weaning phase (n=7).

In summary, flow cytometric analysis of the myeloid cells in the liver shows myeloid recruitment upon maternal obesity. All myeloid populations have significantly higher cell numbers in the HFD_MCD_LCD group. KC numbers were also significantly high in the HFD_MCD_LHFD group. Flow cytometric analysis of the bone marrow confirmed that common myeloid progenitors are significantly higher represented upon maternal obesity. Those results indicate a maternal obesity-induced inflammatory process, which leads to the recruitment of myeloid cells and local accumulation of KC.

4.3 Maternal obesity leads to developmental programming of KC

In order to analyze how Kupffer cells are programmed upon maternal obesity, bulk RNA-sequencing was performed on sorted KCs in three developmental stages; at the embryonic day 14.5 (E14.5), directly after birth on postnatal (P) day 0 (P0), and at eleven weeks of age at P76. Principal component analysis (PCA) shows that KCs classify primary based on age (PC1: Adult vs. pre-, and perinatal cells). However, the second principal component separates the adult KC based on the mother's diet. This developmental programming is not visible at the E14.5 and P0 samples (Figure 15A).

To find the driving forces for the adult KC classification, we analyzed the genes which relate to the PC2. Those genes are aimed to show the driving mechanisms behind adult KC classification based on the maternal diet. According to GSEA, those genes are primarily related to inflammation, oxidative phosphorylation, and glycolysis (Figure 15B). Inflammation-related genes are upregulated upon maternal obesity. Oxidative phosphorylation-related genes are upregulated in the

obese condition (CD_MCD_LHFD) and downregulated in all maternal obese groups. Glycolysis related transcripts are upregulated in the maternal obese dietary conditions.

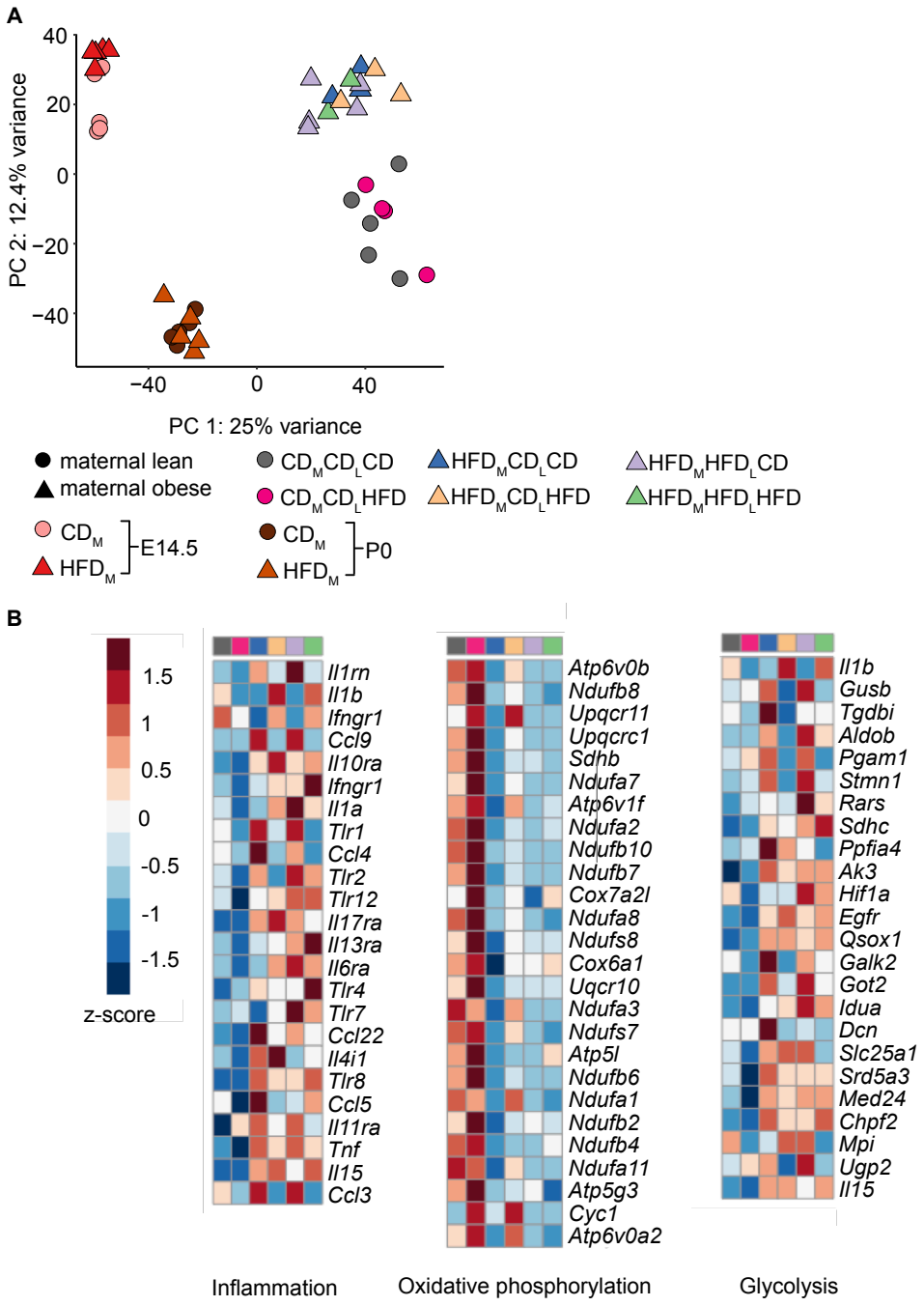

Figure 15. Transcriptomic analysis of developmental programmed Kupffer cells.
(A) Principal component analysis (PCA) of sorted KC. Principal component 1 (PC1) and principal component 2 (PC2) classify the samples based on the age of the host and maternal diet, respectively. Every shape represents a mouse born to either obese (represented as a triangle) or lean (represented as circle) mother. **(B)** Heatmap of adult samples containing genes related to GO:inflammatory response (GO:0006954), GO:oxidative phosphorylation (GO:0006119) and GO:glycolysis (GO:0006096). Inflammation-related genes are upregulated in all maternal obese KCs. Oxidative phosphorylation-related genes are downregulated in maternal obese conditions compared to maternal lean. Glycolysis related genes are upregulated in maternal obese conditions compared to maternal lean KCs. Expression pattern of genes is represented as a row-scaled Z-score between every sample. Every column represents the condition-specific mean expression of the sorted Kupffer cell (KC) expression profile.
Grey - CD_MCD_LCD- mother is on control diet before and during pregnancy (Control Diet $_{Maternal}$), mother is on control diet during lactation (Control Diet $_{Lactational}$) and the offspring is on control diet during the post-weaning phase (n=5). (Legend continues on the next page.)

Pink - CD_MCD_LHFD- mother is on control diet before and during pregnancy (Control Diet $_{Maternal}$), mother is on control diet during lactation (Control Diet $_{Lactational}$) and the offspring is on a high-fat diet during the post-weaning phase (n=4).
Blue - HFD_MCD_LCD- mother is on a high-fat diet before and during pregnancy (High-fat Diet $_{Maternal}$), mother is on control diet during lactation (Control Diet $_{Lactational}$) and the offspring is on control diet during the post-weaning phase (n=3).
Purple - HFD_MHFD_LCD- mother is on a high-fat diet before and during pregnancy (High-fat Diet $_{Maternal}$), mother is on a high-fat diet during lactation (High-fat Diet $_{Lactational}$) and the offspring is on control diet during the post-weaning phase (n=5).
Yellow - HFD_MCD_LHFD- mother is on a high-fat diet before and during pregnancy (High-fat Diet $_{Maternal}$), mother is on control diet during lactation (Control Diet $_{Lactational}$) and the offspring is on a high-fat diet during the post-weaning phase (n=3).
Green - HFD_MHFD_LHFD- mother is on a high-fat diet before and during pregnancy (High-fat Diet $_{Maternal}$), mother is on a high-fat diet during lactation (High-fat Diet $_{Lactational}$) and the offspring is on a high-fat diet during the post-weaning phase (n=2).
Rose - sample was taken at embryonic (E) day 14.5 from embryo of mother on control diet (CD) (n=5)
Red - sample was taken at embryonic (E) day 14.5 from embryo of mother on a high-fat diet (HFD) (n=5)
Dark-brown - sample was taken at postnatal (P) day 0 from offspring born to mother on control diet (CD) (n=5)
Light-brown- sample was taken at postnatal (P) day 0 from offspring born to mother on a high-fat diet (HFD) (n=5)

The 5000 most variant genes were classified into seven clusters based on their cross-condition expression profile (Figure 16A). The orange cluster contains 1454 genes, which all get upregulated in the maternal obesity groups. Gene set enrichment analysis referred to those genes involved in glycolysis and inflammatory response. Furthermore, HIF-1α signaling pathway, and TNF signaling pathway. Non-alcoholic fatty liver disease-related genes are programmed to be upregulated upon maternal obesity. Gene set enrichment confirmed the upregulation of inflammation and glycolysis-related mechanisms, especially Toll-like receptor and TNF-α-related cytokine production. Moreover, neurodegeneration-related pathways gave us hints into possible mechanistic insights and further impacts of developmental programming, respectively. Reactome enrichment sheds light on further possible mechanisms related to maternal obesity, such as "Myd88 dependent cascade initiated on endosome" and "Signaling by Interleukins"-related genes are upregulated in the maternal obese conditions. Disease enrichment highlighted arteriosclerosis, benign neoplasm, dementia, rheumatoid arthritis, and tauopathy, which diagnoses may have the trigger already during development. Epigenetic modifications may play a key role in maternal-fetal crosstalk as well. GO-enrichment gathered those possible epigenetic modifiers under the term "regulation of chromatin organization" and "chromatin organization involved in the regulation of transcription". Maternal obesity-induced upregulation of genes related to inflammation are mainly Toll-like receptors, Interlekunis, other cytokines, and their receptors. Other upregulated genes from the orange cluster are related to the glycolytic mechanism (Figure 16B, Appendix C).

The green cluster contains the genes, which become downregulated in KC upon maternal obesity. This cluster reveals the differences between obese and

maternal obese conditions. Oxidative phosphorylation becomes upregulated upon HFD, as higher caloric intake triggers a higher glucose production. However, in maternal obese conditions, oxidative phosphorylation-related genes are silenced (Figure 16B, Appendix A). Developmental programming induces a metabolic shift in KC from oxidative phosphorylation to glycolysis. GSEA refers to other mechanisms that are silenced by developmental programming. These include heme metabolism, thermogenesis, protein processing in the endoplasmatic reticulum, mitochondrial translation, TCA-cycle transport, and mRNA processing. The grey cluster collects genes that are upregulated in obesity and transgenerational obesity. Those 272 genes are related to "MYC Targets V1" and "DNA repair" which mechanisms are associated with cancer. "Pleural cancer" was also enriched, which may give a hint to obesity-associated cancer (Appendix B). The gold and maroon clusters collect genes that are downregulated in obesity and silenced in maternal obese conditions. Genes in the gold cluster are involved in apoptotic, lipid and atherosclerosis, foam cell and cellular stress-related mechanisms (Appendix D). The enriched mechanisms in cluster maroon involve oocyte meiosis, mRNA stability, chromosome organization and histone methylation (Appendix E). Genes are collected in cluster orchid, which are upregulated upon obesity. Furthermore, those genes are differently regulated upon lactational diet in the maternal obesity groups. GSEA shows that those genes are involved in adipogenesis, fatty acid metabolism, thermogenesis and non-alcoholic fatty liver disease (Appendix F).

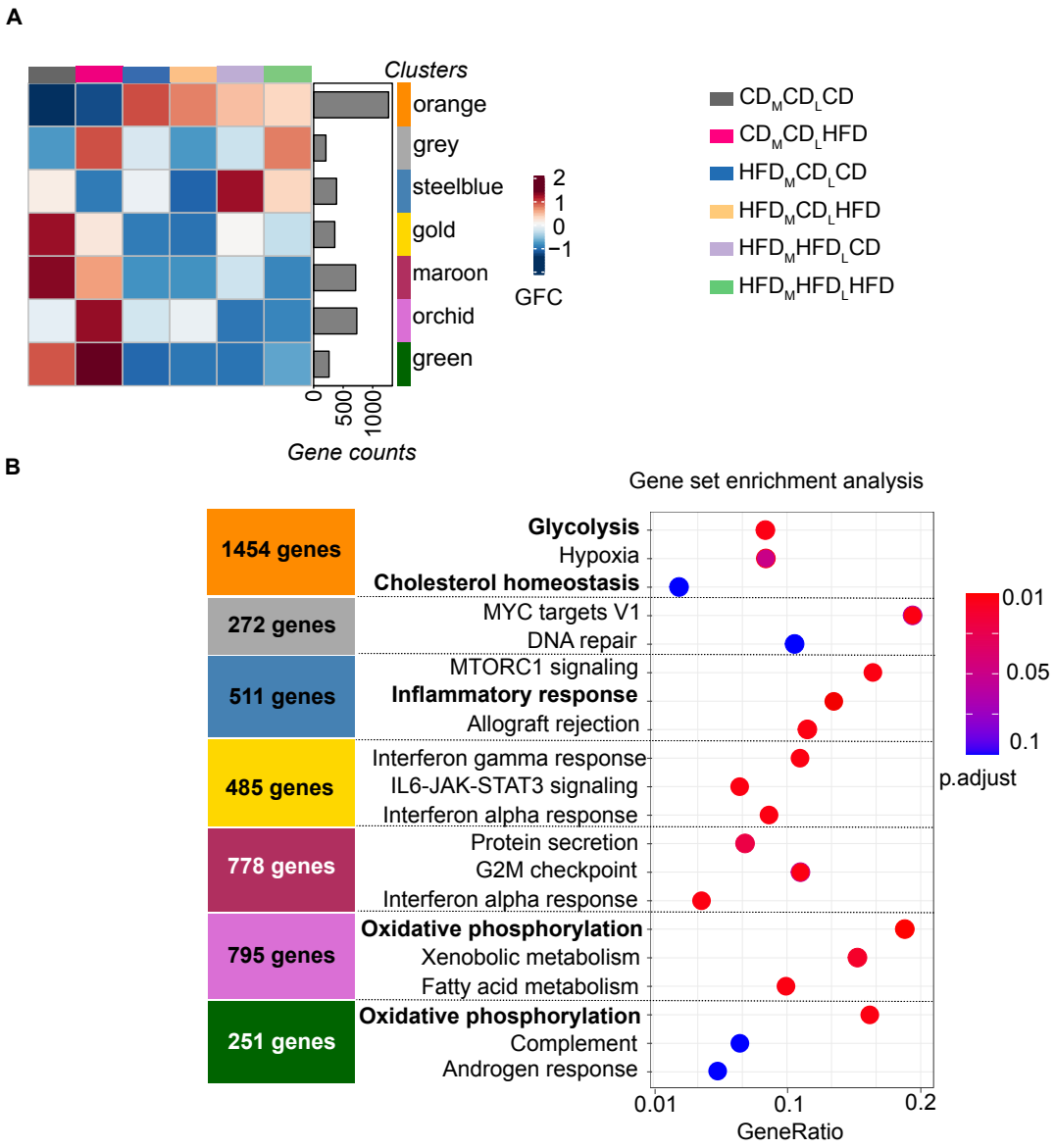

Figure 16. Gene set enrichment analysis of co-expression network analysis (CO-CENA) clusters

(A) Co-expression network analysis (CO-CENA) based on Pearson correlation and gene fold change pattern between the six adult dietary conditions. Every column represents a dietary condition color-coded as following:

Grey - CD_MCD_LCD- mother is on control diet before and during pregnancy (Control Diet $_{Maternal}$), mother is on control diet during lactation (Control Diet $_{Lactational}$) and the offspring is on control diet during the post-weaning phase (n=5).

Pink - CD_MCD_LHFD- mother is on control diet before and during pregnancy (Control Diet $_{Maternal}$), mother is on control diet during lactation (Control Diet $_{Lactational}$) and the offspring is on a high-fat diet during the post-weaning phase (n=4).

Blue - HFD_MCD_LCD- mother is on a high-fat diet before and during pregnancy (High-fat Diet $_{Maternal}$), mother is on control diet during lactation (Control Diet $_{Lactational}$) and the offspring is on control diet during the post-weaning phase (n=3).

Purple - HFD_MHFD_LCD- mother is on a high-fat diet before and during pregnancy (High-fat Diet $_{Maternal}$), mother is on a high-fat diet during lactation (High-fat Diet $_{Lactational}$) and the offspring is on control diet during the post-weaning phase (n=5).

Yellow - HFD_MCD_LHFD- mother is on a high-fat diet before and during pregnancy (High-fat Diet $_{Maternal}$), mother is on control diet during lactation (Control Diet $_{Lactational}$) and the offspring is on a high-fat diet during the post-weaning phase (n=3).

Green - HFD_MHFD_LHFD- mother is on a high-fat diet before and during pregnancy (High-fat Diet $_{Maternal}$), mother is on a high-fat diet during lactation (High-fat Diet $_{Lactational}$) and the offspring is on a high-fat diet during the post-weaning phase (n=2).

Rows represent gene clusters, where genes are classified based on their relative expression pattern between the dietary conditions. Gene counts show the number of genes grouped into the gene cluster. The top 5000 most variable genes are grouped into seven different gene clusters, which are marked by different colors: orange, grey, steelblue, gold, maroon, orchid and green. Relative gene expression pattern is represented as gene fold change (GFC).

(B) Gene set enrichment analysis (GSEA) representation of the CO-CENA gene clusters. All significantly enriched mechanisms are available in Appendix A-G. The seven gene clusters were enriched for GO, Hallmark, KEGG, Reactome and Disease databases. Two to three most representative mechanisms are manually selected and represented, where adjusted p-value is represented by color coding from blue to red.

In summary, RNA-seq analysis of sorted KC revealed the metabolic shift from oxidative phosphorylation to glycolysis upon maternal obesity. The metabolic shift was accompanied by a Myd88-related inflammatory signature. According to the PCA, maternal diet has the strongest effect on the adult KC signature. According to the CO-CENA results, various mechanisms are involved in lactational and post-weaning dietary changes as well.

4.4 Macrophage-specific KO models to reverse the effects of maternal obesity

In order to strengthen the causative role of KCs in maternal obesity-induced NASH and to reverse its adverse effects, we introduced two macrophage-specific KO-models to maternal obesity (Figure 17). Macrophage-specific KO of HIF-1α ($KO^{HIF\text{-}1\alpha}$) aims to reverse the metabolic shift of KCs, which was induced by maternal obesity. Furthermore, as Myd88-signalling pathway-related inflammatory genes were upregulated in maternal obese KC, we aimed to rescue the inflammatory phenotype with the macrophage-specific Myd88 KO model (KO^{Myd88}).

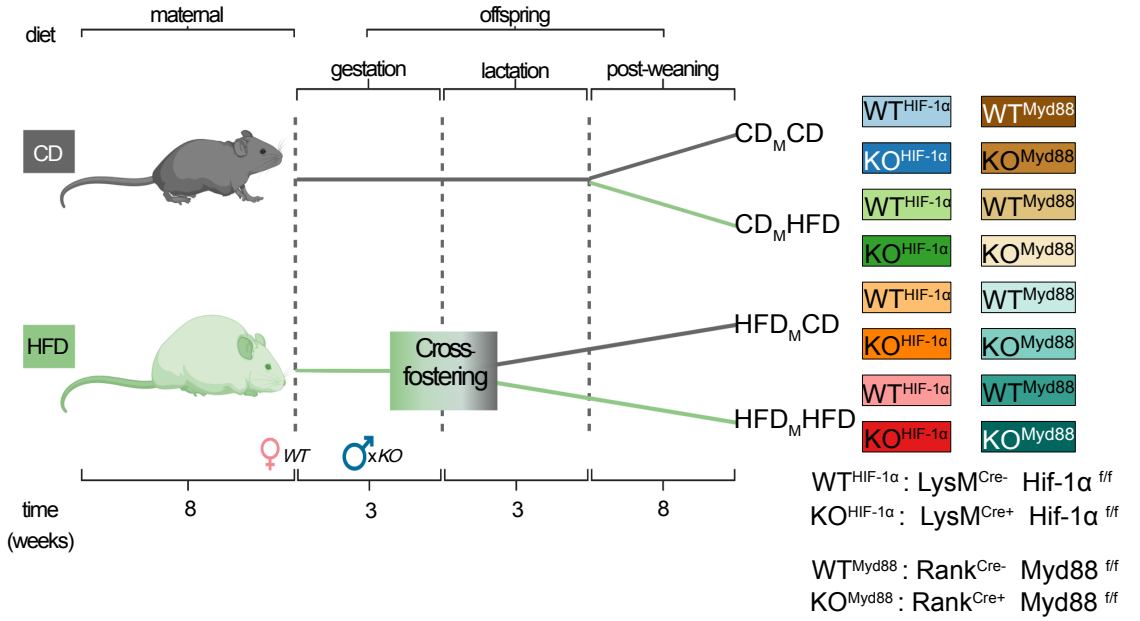

Figure 17. Genetic-modified models of maternal obesity
Five-week-old female mice (f/f Cre/- wild types-WT) were put on control diet (CD) or high-fat diet (HFD) for eight weeks. After overnight-mating with f/f Cre/+ genetic modified males (KO), females follow the same diet, $CD_{Maternal}$ (CD_M) or $HFD_{Maternal}$ (HFD_M). When mice gave birth, offspring were either kept with their mother on the same diet (CD_MCD_L or HFD_MHFD_L) or offspring born to obese mother were cross-fostered to CD-mother for 21 days lactation (HFD_MCD_L). Post-weaning diet was either CD or HFD.

4.4.1 The lack of Myd88 in macrophages worsens the effects of maternal obesity

In order to analyze, if Myd88 deficiency can resolve inflammation triggered by NAFLD, a Myd88 macrophage-specific KO model was established. Body weights of adult offspring keep constant between the genetic conditions. The Myd88 model represents the same pattern as we have seen in the previous models; only a post-weaning diet has an effect on body weight. The maternal and lactational diets have no significant effect on the body weight of adult offspring (Figure 18). An increasing trend is present in the body weight of the HFD_MHFD KO^{Myd88} group (Figure 18A). The liver weight of adult offspring is constant between dietary groups and genotypes (Figure 18B). Total lipid content and TAGs are slightly increased in the HFD_MCD groups with no difference between WT^{Myd88} and KO^{Myd88} (Figure 18C-D). There is no rescue of phenotype present in Myd88 macrophage-specific KO model, based on physiological phenotyping.

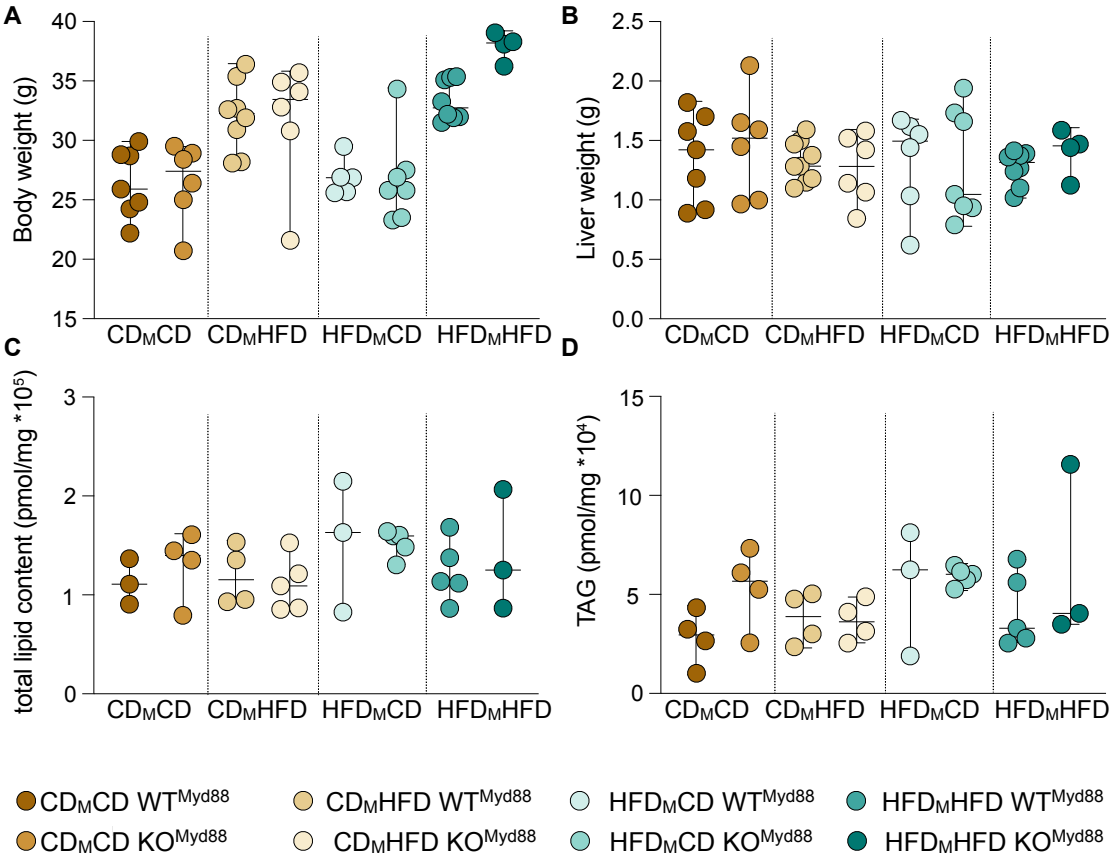

Figure 18. Physiological assessment of Myd88 maternal obesity model
Samples were sacrificed and measured at 11 weeks of age. Circles represent single offspring, and colors represent dietary groups and genotypes. Statistical assessment was performed via one-way ANOVA - Turkey´s multiple comparisons method. Statistical significance is represented only for genotype-specific differences. Data are represented as mean ± ROD. ROD - Range of distribution.
Dark-brown - CD_MCD WT^{Myd88}- mother is on control diet before and during pregnancy (Control Diet $_{Maternal}$), mother is on control diet during lactation and the offspring is on control diet during the post-weaning phase. Offspring´s genotype is $MYD88^{f/f}$ $RANK^{+/+}$ (n=3-7). (Legend continues on the next page.)

Light-brown - $CD_MCD\ KO^{Myd88}$- mother is on control diet before and during pregnancy (Control Diet $_{Maternal}$), mother is on control diet during lactation and the offspring is on control diet during the post-weaning phase. Offspring´s genotype is $MYD88^{f/f}\ RANK^{Cre/+}$(n=4-6).
Dark-yellow - $CD_MHFD\ WT^{Myd88}$- mother is on control diet before and during pregnancy (Control Diet $_{Maternal}$), mother is on control diet during lactation and the offspring is on a high-fat diet during the post-weaning phase. Offspring´s genotype is $MYD88^{f/f}\ RANK^{+/+}$(n=4-8).
Light-yellow - $CD_MHFD\ KO^{Myd88}$- mother is on control diet before and during pregnancy (Control Diet $_{Maternal}$), mother is on control diet during lactation and the offspring is on a high-fat diet during the post-weaning phase. Offspring´s genotype is $MYD88^{f/f}\ RANK^{Cre/+}$(n=5-6).
Light-blue - $HFD_MCD\ WT^{Myd88}$- mother is on a high-fat diet before and during pregnancy High-fat Diet $_{Maternal}$), mother is on control diet during lactation and the offspring is on control diet during the post-weaning phase. Offspring´s genotype is $MYD88^{f/f}\ RANK^{+/+}$(n=3-5).
Dark-blue - $HFD_MCD\ KO^{Myd88}$- mother is on a high-fat diet before and during pregnancy High-fat Diet $_{Maternal}$), mother is on control diet during lactation and the offspring is on control diet during the post-weaning phase. Offspring´s genotype is $MYD88^{f/f}\ RANK^{Cre/+}$(n=5-7).
Light-green - $HFD_MHFD\ WT^{Myd88}$- mother is on a high-fat diet before and during pregnancy High-fat Diet $_{Maternal}$), mother is on a high-fat diet during lactation and the offspring is on control diet during the post-weaning phase. Offspring´s genotype is $MYD88^{f/f}\ RANK^{+/+}$(n=5-8).
Dark-green - $HFD_MHFD\ KO^{Myd88}$- mother is on a high-fat diet before and during pregnancy High-fat Diet $_{Maternal}$), mother is on a high-fat diet during lactation and the offspring is on control diet during the post-weaning phase. Offspring´s genotype is $MYD88^{Myd88}\ RANK^{Cre/+}$(n=3-4).
(A) Body weight of adult offspring born to obese or lean mothers, represented as gram (g) of body weight. No genotype-specific significant difference was detected in the single dietary groups, according to unpaired t-test and Turkey´s multiple comparisons method. Dietary group related differences were addressed in the wild type (WT) model. **(B)** Liver weight of 11 weeks old adult offspring, represented as gramm (g) of weight. No genotype-specific significant difference was detected in the single dietary groups, according to unpaired t-test and Turkey´s multiple comparisons method. **(C)** Shotgun lipidomics analysis of liver, represented as total lipid content in picomol per milligram of liver tissue (pmol/mg) **(D)** Extracted accumulation of triacylglyceride species (TAGs), represented as pmol/mg of liver tissue.

Oil-red-O staining of Myd88 livers confirms lipidomics findings; NAFLD is present in both $HFD_MCD\ WT^{Myd88}$ and $HFD_MCD\ KO^{Myd88}$. Moreover, a slightly higher lipid accumulation can be detected in $HFD_MHFD\ KO^{Myd88}$ compared to $HFD_MHFD\ KO^{Myd88}$, which may explain the increasing trend in body weight and liver weight (Figure 19).

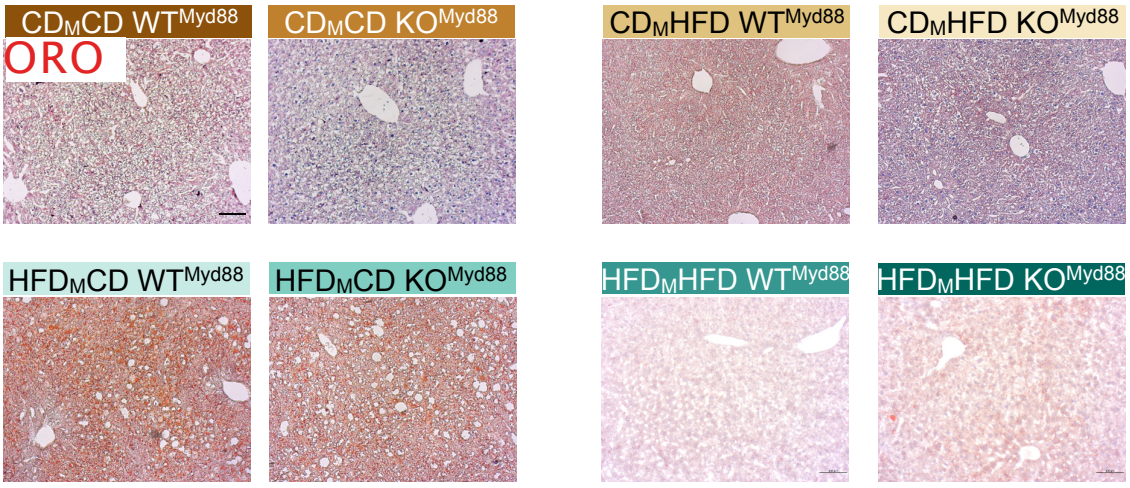

Figure 19. Oil-red-o histological staining shows that KO^{Myd88} does not rescue maternal obesity-induced steatosis. Representative records of adult offspring´s Oil-red-o (ORO)-stained livers. The scale represents 100µm, objective 10x. Perfused liver isolated from 11 weeks-old male offspring was fixed with 4% PFA and cryopreserved with sucrose. 10-micron thick cryosections were stained according to the ORO-staining protocol, where lipids are stained red.

Flow cytometric analysis of the myeloid cell populations was performed to shed light on potential modulations upon Myd88 KO in maternal obesity. There is no genotype-specific difference between CD_MCD and CD_MHFD groups. $HFD_MCD\ WT^{Myd88}$ and KO^{Myd88} show an equally high KC recruitment compared to maternal

lean groups. HFD_MHFD WT^{Myd88} KC numbers are slightly increased compared to CD_M. HFD_MHFD KO^{Myd88} KCs are significantly more than WT, which gives the only genotype-specific difference in myeloid cell quantification for the Myd88 model (Figure 20). Monocyte and granulocyte proliferation gives an insight into hepatic inflammation. Increased monocyte and granulocyte cell numbers were detected in all maternal obese livers, with no genotype-specific difference. LCM-related changes could not be addressed due to the high spread of data points (Figure 20).

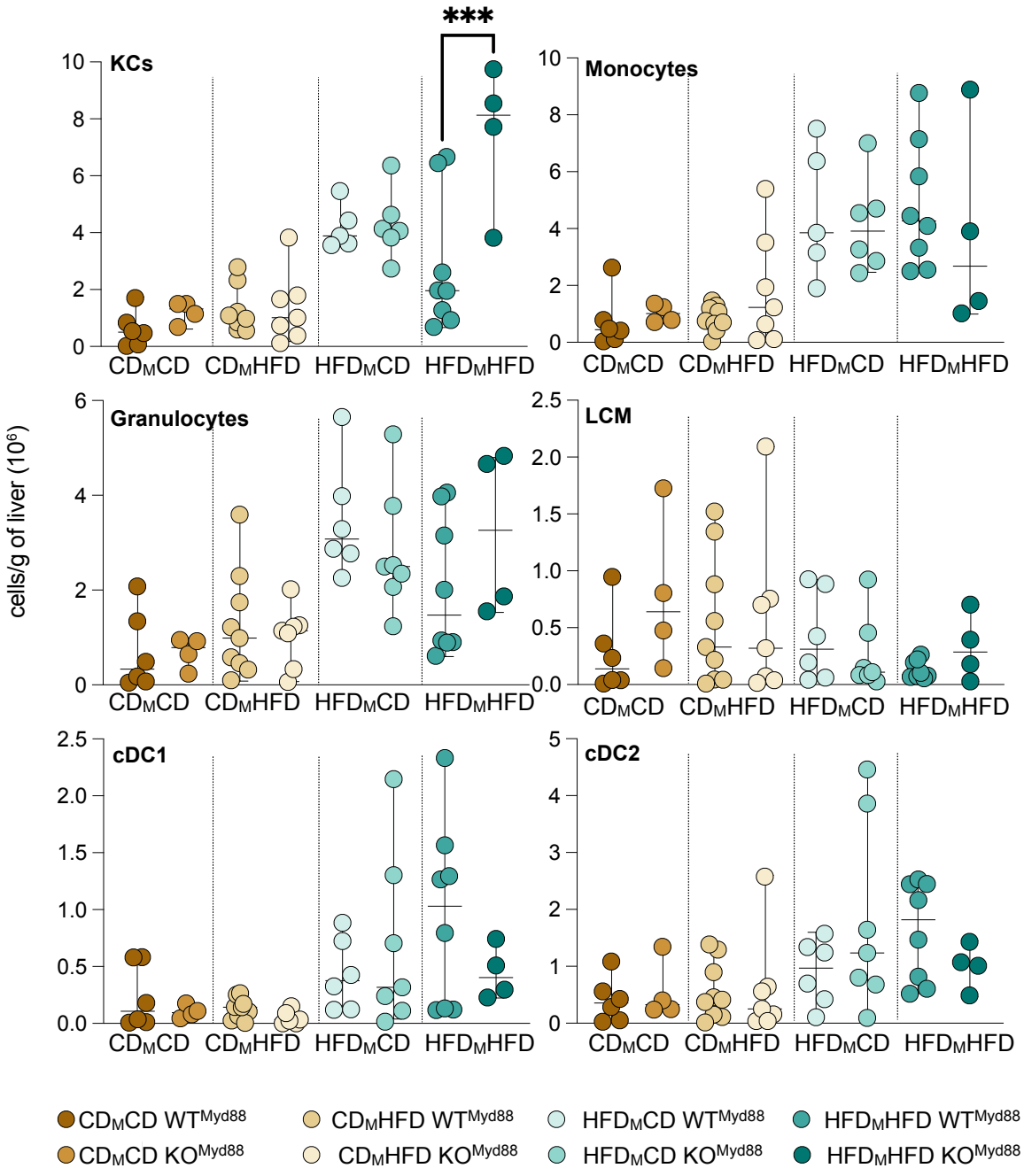

Figure 20. Flow cytometry quantification of myeloid cells from the Myd88 model
Cell numbers are normalized to liver weight. Single circles represent single offspring. In every dietary group, mice are at least from two different litters. Statistical assessment was performed via one-way ANOVA - Turkey´s multiple comparisons method. (Legend continues on the next page.)

Statistical significance is represented only for genotype specific difference. Statistical significance is represented via the probability (p-value) as follows: ***=p<0.001. KC-Kupffer cell, LCM - liver capsullar macrophages, cDC1 - classical dendritic cells type 1, cDC2 - classical dendritic cells type 2. Data are represented as mean ± ROD. ROD - Range of distribution.
Dark-brown - $CD_MCD\ WT^{Myd88}$- mother is on control diet before and during pregnancy (Control Diet $_{Maternal}$), mother is on control diet during lactation and the offspring is on control diet during the post-weaning phase. Offspring´s genotype is MYD88 $^{f/f}$ $RANK^{+/+}$ (n=6).
Light-brown - $CD_MCD\ KO^{Myd88}$- mother is on control diet before and during pregnancy (Control Diet $_{Maternal}$), mother is on control diet during lactation and the offspring is on control diet during the post-weaning phase. Offspring´s genotype is MYD88 $^{f/f}$ $RANK^{Cre/+}$(n=4).
Dark-yellow - $CD_MHFD\ WT^{Myd88}$- mother is on control diet before and during pregnancy (Control Diet $_{Maternal}$), mother is on control diet during lactation and the offspring is on a high-fat diet during the post-weaning phase. Offspring´s genotype is MYD88 $^{f/f}$ $RANK^{+/+}$ (n=9).Light-yellow - $CD_MHFD\ KO^{Myd88}$- mother is on control diet before and during pregnancy (Control Diet $_{Maternal}$), mother is on control diet during lactation and the offspring is on a high-fat diet during the post-weaning phase. Offspring´s genotype is MYD88 $^{f/f}$ $RANK^{Cre/+}$ (n=7).
Light-blue - $HFD_MCD\ WT^{Myd88}$- mother is on a high-fat diet before and during pregnancy High-fat Diet $_{Maternal}$), mother is on control diet during lactation and the offspring is on control diet during the post-weaning phase. Offspring´s genotype is MYD88 $^{f/f}$ $RANK^{+/+}$ (n=6).
Dark-blue - $HFD_MCD\ KO^{Myd88}$- mother is on a high-fat diet before and during pregnancy High-fat Diet $_{Maternal}$), mother is on control diet during lactation and the offspring is on control diet during the post-weaning phase. Offspring´s genotype is MYD88 $^{f/f}$ $RANK^{Cre/+}$ (n=7).
Light-green - $HFD_MHFD\ WT^{Myd88}$- mother is on a high-fat diet before and during pregnancy High-fat Diet $_{Maternal}$), mother is on a high-fat diet during lactation and the offspring is on control diet during the post-weaning phase. Offspring´s genotype is MYD88 $^{f/f}$ RANK $^{+/+}$ (n=8).
Dark-green - $HFD_MHFD\ KO^{Myd88}$- mother is on a high-fat diet before and during pregnancy High-fat Diet $_{Maternal}$), mother is on a high-fat diet during lactation and the offspring is on control diet during the post-weaning phase. Offspring´s genotype is MYD88 ^{Myd88} $RANK^{Cre/+}$ (n=4).

In summary, a macrophage-specific KO model was used to target Myd88 related signaling pathway. Our aim was to rescue maternal obesity-induced NASH with KO^{Myd88} via targeting the inflammatory phenotype. Unfortunately, macrophage-specific KO did neither rescue maternal obesity-induced hepatic lipid accumulation nor myeloid cell recruitment.

4.4.2 Macrophage-specific HIF-1α deletion rescues metabolic programming and NASH

In order to see, if macrophage-specific mitochondrial reprogramming can resolve the fatty liver phenotype we induced a macrophage-specific HIF-1α deletion to the metabolic programming model. Taking advantage of the Lysm CRE system, we introduced our maternal obesity model using a macrophage-specific HIF-1α KO model. The body weight and liver weight of adult offspring did not show any genotype-specific difference (Figure 21). Body weight – liver weight ratio shows a decreasing trend at the maternal obese HFD_MCD HIF-1α $^{fl/fl}$ LysMCre $^{+/wt}$ ($KO^{HIF-1α}$) samples compared to HFD_MCD HIF-1α $^{fl/fl}$ LysMCre $^{wt/wt}$ ($WT^{HIF-1α}$) (Figure 21).

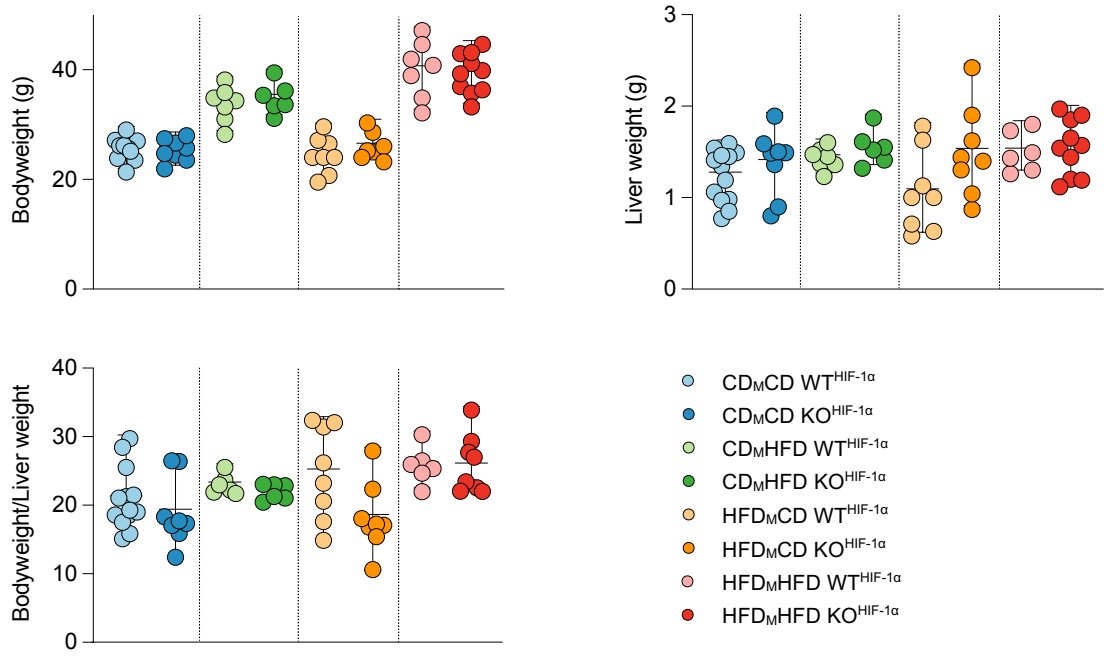

Figure 21. Physiological analysis of maternal obesity HIF-1α model
Body weight of 11-weeks-old adult offspring did not show any genotype-specific difference between the genotypes and diet conditions. Liver weight of adult offspring was measured as gram (g) of tissue. Neither genotype nor condition related difference was observed. Body weight/liver weight ratio of adult offspring was measured as division of body weight with the weight of liver. Here, no significant difference was observed, but a genotype-specific decreasing trend was detected between HFD_MCD WT $^{HIF\text{-}1\alpha}$ vs KO $^{HIF\text{-}1\alpha}$. Single circles represent single offspring. In every dietary group, mice are at least from two different litters. Statistical assessment was performed via one-way ANOVA - Turkey´s multiple comparisons method. Statistical significance is represented only for genotype specific difference. Statistical significance is represented via the probability (p-value) as follows: *= p<0.05, ** = p<0.01, ***=p<0.001, ****=p<0.001. Data are represented as mean ± ROD. ROD - Range of distribution. Groups are represented as follows:
Light-blue - CD_MCD WT $^{HIF\text{-}1\alpha}$- mother is on control diet before and during pregnancy (Control Diet $_{Maternal}$), mother is on control diet during lactation and the offspring is on control diet during the post-weaning phase. Offspring´s genotype is HIF-1α $^{fl/fl}$ LysMCre $^{wt/wt}$ (n=11).
Dark-blue - CD_MCD KO $^{HIF\text{-}1\alpha}$- mother is on control diet before and during pregnancy (Control Diet $_{Maternal}$), mother is on control diet during lactation and the offspring is on control diet during the post-weaning phase. Offspring´s genotype is HIF-1α $^{fl/fl}$ LysMCre $^{+/wt}$ (n=8).
Light-green - CD_MHFD WT $^{HIF\text{-}1\alpha}$ - mother is on control diet before and during pregnancy (Control Diet $_{Maternal}$), mother is on control diet during lactation and the offspring is on a high-fat diet during the post-weaning phase. Offspring´s genotype is HIF-1α $^{fl/fl}$ LysMCre $^{wt/wt}$ (n=6).
Dark-green - CD_MHFD KO $^{HIF\text{-}1\alpha}$ - mother is on control diet before and during pregnancy (Control Diet $_{Maternal}$), mother is on control diet during lactation and the offspring is on a high-fat diet during the post-weaning phase. Offspring´s genotype is HIF-1α $^{fl/fl}$ LysMCre $^{+/wt}$ (n=6).
Yellow - HFD_MCD WT $^{HIF\text{-}1\alpha}$ - mother is on a high-fat diet before and during pregnancy High-fat Diet $_{Maternal}$), mother is on control diet during lactation and the offspring is on control diet during the post-weaning phase. Offspring´s genotype is HIF-1α $^{fl/fl}$ LysMCre $^{wt/wt}$ (n=8).
Orange - HFD_MCD KO $^{HIF\text{-}1\alpha}$ - mother is on a high-fat diet before and during pregnancy High-fat Diet $_{Maternal}$), mother is on control diet during lactation and the offspring is on control diet during the post-weaning phase. Offspring´s genotype is HIF-1α $^{fl/fl}$ LysMCre $^{+/wt}$ (n=8).
Pink - HFD_MHFD WT $^{HIF\text{-}1\alpha}$ - mother is on a high-fat diet before and during pregnancy High-fat Diet $_{Maternal}$), mother is on a high-fat diet during lactation and the offspring is on control diet during the post-weaning phase. Offspring´s genotype is HIF-1α $^{fl/fl}$ LysMCre $^{wt/wt}$ (n=6).
Red - HFD_MHFD KO $^{HIF\text{-}1\alpha}$ - mother is on a high-fat diet before and during pregnancy High-fat Diet $_{Maternal}$), mother is on a high-fat diet during lactation and the offspring is on control diet during the post-weaning phase. Offspring´s genotype is HIF-1α $^{fl/fl}$ LysMCre $^{+/wt}$ (n=8).

Histological and lipidomic analysis confirmed that HFD_MCD KO$^{HIF\text{-}1\alpha}$ do not accumulate fat in their liver. Regarding hepatic lipid accumulation, no other genotype-specific difference was observed (Figure 22A-C).

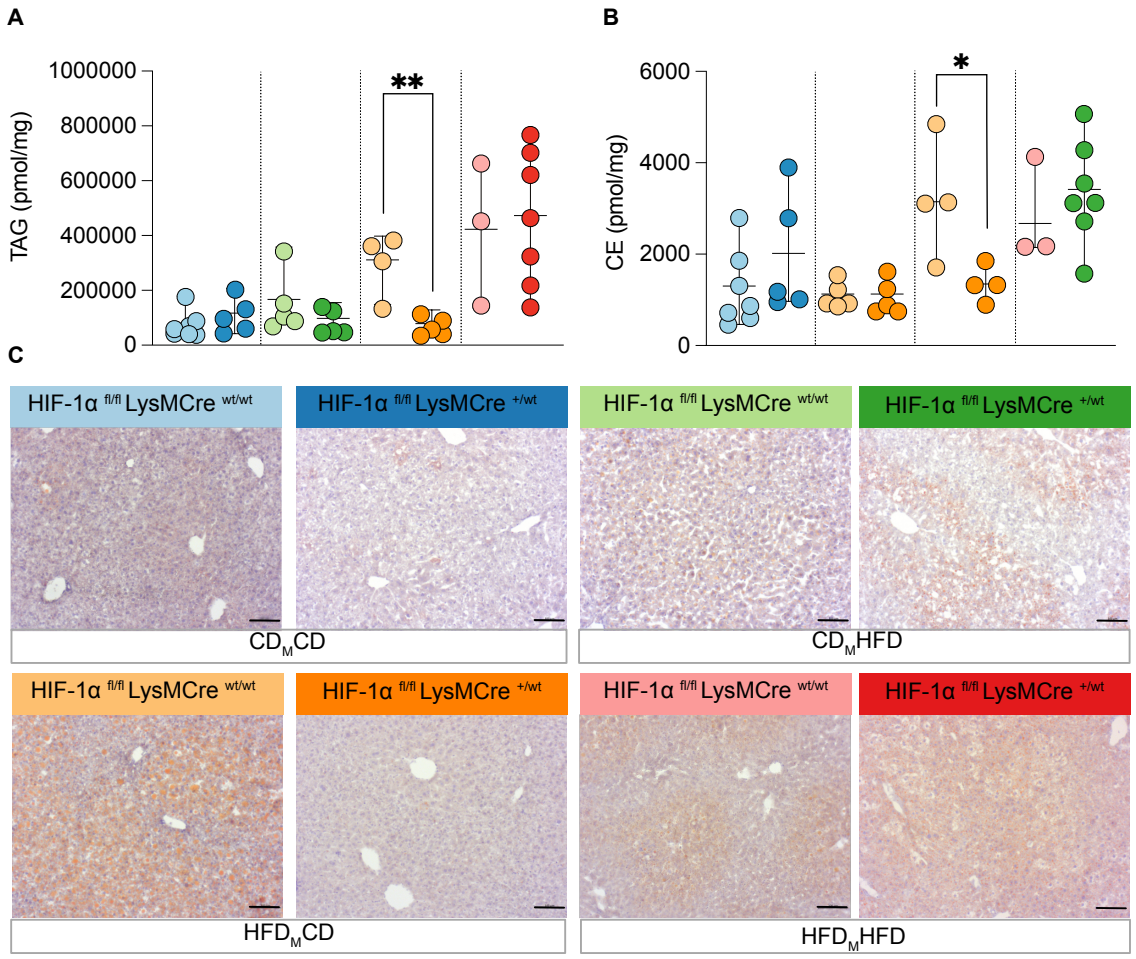

Figure 22. KO$^{HIF\text{-}1\alpha}$ rescued maternal obesity-induced hepatic lipid accumulation

Triacylglycerol and cholesterol ester lipid species are reduced to normal amount upon macrophage-specific HIF-1α deletion in the HFD$_M$CD maternal obese condition. HFD$_M$CD KO $^{HIF\text{-}1\alpha}$ offspring show significantly reduced amount of lipid accumulation in the liver shown via both mass spectrometry and histology. Data are represented as mean ± ROD. Every circle represents a single offspring. In the dietary groups, mice are at least from two different litters. Statistical assessment was performed via one-way ANOVA - Turkey´s multiple comparisons method. Statistical significance is represented only for genotype specific differences. Statistical significance is represented via the probability (p-value) as follows: *= p<0.05, ** = p<0.01.

(A) Quantification of triacylglycerol lipid species (TAG), based on shotgun lipidomics analysis, represented as pmol/mg of liver. **(B)** Quantification of cholesterol ester lipid species (CE), based on shotgun lipidomics analysis, represented as pmol/mg of liver.

(C) Representative records of adult offspring´s Oil-red-o (ORO)-stained livers. The scale represents 100µm, objective 10x. Perfused liver isolated from 11 weeks-old male offspring was fixed with 4% PFA and cryopreserved with sucrose. 10-micron thick cryosections were stained according to the ORO-staining protocol, where lipids are stained red. Groups are represented as follows:

Light-blue - CD$_M$CD WT $^{HIF\text{-}1\alpha}$- mother is on control diet before and during pregnancy (Control Diet $_{Maternal}$), mother is on control diet during lactation and the offspring is on control diet during the post-weaning phase. Offspring´s genotype is HIF-1α $^{fl/fl}$ LysMCre $^{wt/wt}$ (n=7).

Dark-blue - CD$_M$CD KO $^{HIF\text{-}1\alpha}$- mother is on control diet before and during pregnancy (Control Diet $_{Maternal}$), mother is on control diet during lactation and the offspring is on control diet during the post-weaning phase. Offspring´s genotype is HIF-1α $^{fl/fl}$ LysMCre $^{+/wt}$ (n=5).

Light-green - CD$_M$HFD WT $^{HIF\text{-}1\alpha}$ - mother is on control diet before and during pregnancy (Control Diet $_{Maternal}$), mother is on control diet during lactation and the offspring is on a high-fat diet during the post-weaning phase. Offspring´s genotype is HIF-1α $^{fl/fl}$ LysMCre $^{wt/wt}$ (n=5).

Dark-green - CD$_M$HFD KO $^{HIF\text{-}1\alpha}$ - mother is on control diet before and during pregnancy (Control Diet $_{Maternal}$), mother is on control diet during lactation and the offspring is on a high-fat diet during the post-weaning phase. Offspring´s genotype is HIF-1α $^{fl/fl}$ LysMCre $^{+/wt}$ (n=5).

Yellow - HFD$_M$CD WT $^{HIF\text{-}1\alpha}$ - mother is on a high-fat diet before and during pregnancy High-fat Diet $_{Maternal}$), mother is on control diet during lactation and the offspring is on control diet during the post-weaning phase. Offspring´s genotype is HIF-1α $^{fl/fl}$ LysMCre $^{wt/wt}$ (n=4).

Orange - HFD$_M$CD KO $^{HIF\text{-}1\alpha}$ - mother is on a high-fat diet before and during pregnancy High-fat Diet $_{Maternal}$), mother is on control diet during lactation and the offspring is on control diet during the post-weaning phase. Offspring´s genotype is HIF-1α $^{fl/fl}$ LysMCre $^{+/wt}$ (n=5).

Pink - HFD$_M$HFD WT $^{HIF\text{-}1\alpha}$ - mother is on a high-fat diet before and during pregnancy High-fat Diet $_{Maternal}$), mother is on a high-fat diet during lactation and the offspring is on control diet during the post-weaning phase. Offspring´s genotype is HIF-1α $^{fl/fl}$ LysMCre $^{wt/wt}$ (n=3). (Legend continues on the next page.)

Red - $HFD_MHFD\ KO^{HIF\text{-}1\alpha}$ - mother is on a high-fat diet before and during pregnancy High-fat Diet $_{Maternal}$), mother is on a high-fat diet during lactation and the offspring is on control diet during the post-weaning phase. Offspring´s genotype is $HIF\text{-}1\alpha^{fl/fl}$ $LysMCre^{+/wt}$ (n=7).

Flow cytometric analysis confirmed that $HFD_MCD\ KO^{HIF\text{-}1\alpha}$ offspring are rescued from the inflammatory accumulation of KCs and monocytes. In other myeloid cells, no genotype-specific difference was detected (Figure 23).

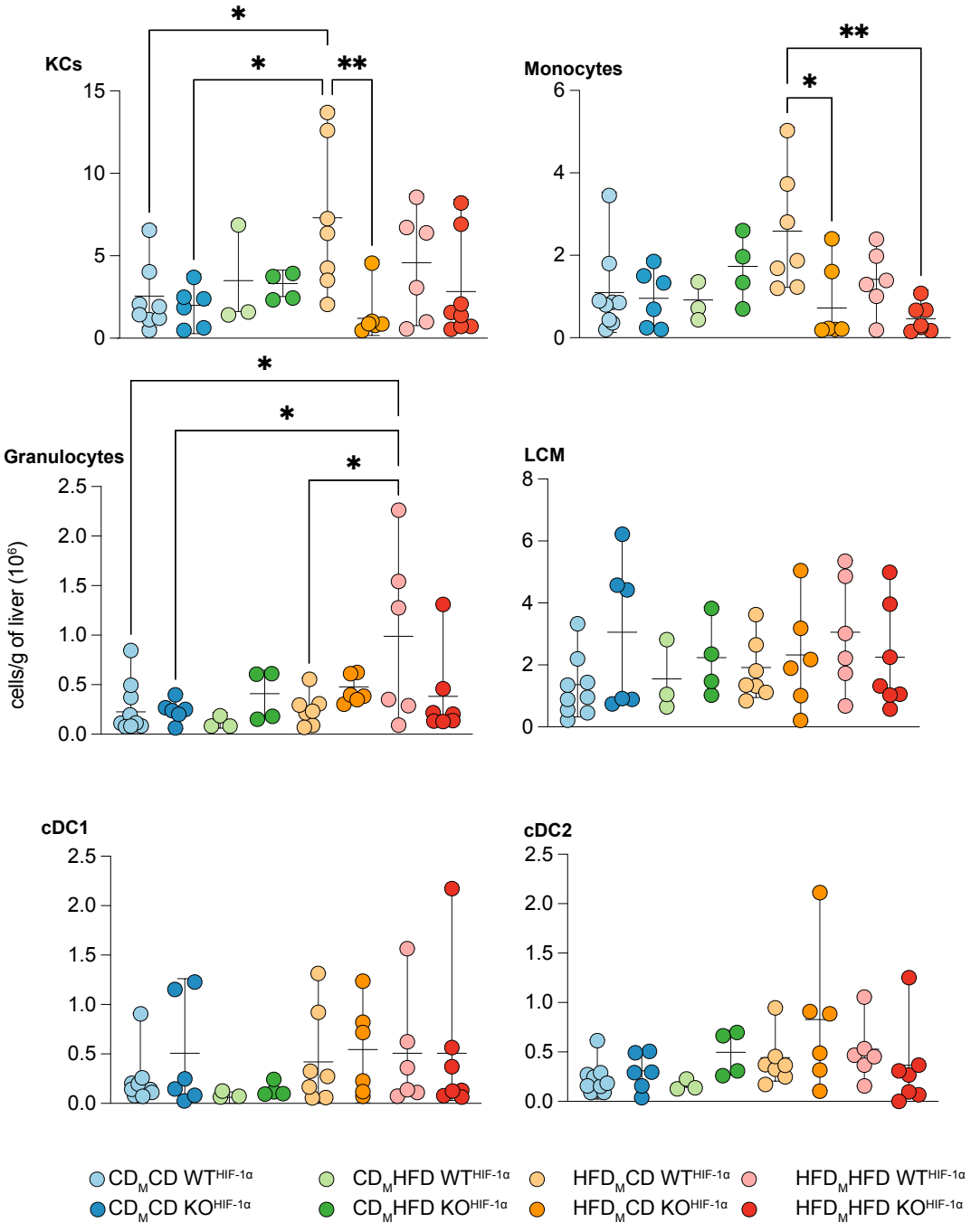

Figure 23. Flow cytometric analysis of myeloid cells upon HIF-1α KO
Myeloid cell population was quantified as cell numbers pergram (g) of the liver. Cell numbers are normalized to liver weight. Data are represented as mean ± ROD. Every circle represents a single offspring. In every dietary group, mice are at least from two different litters. Statistical assessment was performed via one-way ANOVA - Turkey´s multiple comparisons method. Statistical significance is represented via the probability (p-value) as follows: *= p<0.05, ** = p<0.01, ***=p<0.001.
KC-Kupffer cell, LCM - liver capsullar macrophages, cDC1 - classical dendritic cells type 1, cDC2 - classical dendritic cells type 2
Groups are represented as follows: (Legend continues on the next page.)

Light-blue - CD_MCD WT $^{HIF-1α}$- mother is on control diet before and during pregnancy (Control Diet $_{Maternal}$), mother is on control diet during lactation and the offspring is on control diet during the post-weaning phase. Offspring´s genotype is HIF-1α $^{fl/fl}$ LysMCre $^{wt/wt}$ (n=9).
Dark-blue - CD_MCD KO $^{HIF-1α}$- mother is on control diet before and during pregnancy (Control Diet $_{Maternal}$), mother is on control diet during lactation and the offspring is on control diet during the post-weaning phase. Offspring´s genotype is HIF-1α $^{fl/fl}$ LysMCre $^{+/wt}$ (n=6).
Light-green - CD_MHFD WT $^{HIF-1α}$ - mother is on control diet before and during pregnancy (Control Diet $_{Maternal}$), mother is on control diet during lactation and the offspring is on a high-fat diet during the post-weaning phase. Offspring´s genotype is HIF-1α $^{fl/fl}$ LysMCre $^{wt/wt}$ (n=3).
Dark-green - CD_MHFD KO $^{HIF-1α}$ - mother is on control diet before and during pregnancy (Control Diet $_{Maternal}$), mother is on control diet during lactation and the offspring is on a high-fat diet during the post-weaning phase. Offspring´s genotype is HIF-1α $^{fl/fl}$ LysMCre $^{+/wt}$ (n=4).
Yellow - HFD_MCD WT $^{HIF-1α}$ - mother is on a high-fat diet before and during pregnancy High-fat Diet $_{Maternal}$), mother is on control diet during lactation and the offspring is on control diet during the post-weaning phase. Offspring´s genotype is HIF-1α $^{fl/fl}$ LysMCre $^{wt/wt}$ (n=7).
Orange - HFD_MCD KO $^{HIF-1α}$ - mother is on a high-fat diet before and during pregnancy High-fat Diet $_{Maternal}$), mother is on control diet during lactation and the offspring is on control diet during the post-weaning phase. Offspring´s genotype is HIF-1α $^{fl/fl}$ LysMCre $^{+/wt}$ (n=6).
Pink - HFD_MHFD WT $^{HIF-1α}$ - mother is on a high-fat diet before and during pregnancy High-fat Diet $_{Maternal}$), mother is on a high-fat diet during lactation and the offspring is on control diet during the post-weaning phase. Offspring´s genotype is HIF-1α $^{fl/fl}$ LysMCre $^{wt/wt}$ (n=6).
Red - HFD_MHFD KO $^{HIF-1α}$ - mother is on a high-fat diet before and during pregnancy High-fat Diet $_{Maternal}$), mother is on a high-fat diet during lactation and the offspring is on control diet during the post-weaning phase. Offspring´s genotype is HIF-1α $^{fl/fl}$ LysMCre $^{+/wt}$ (n=7).

Next, we analyzed how the macrophage-specific HIF-1α KO system influences KC transcriptomics. We performed bulk RNA-sequencing of fluorescence sorted KC for every dietary and genetic condition in the HIF-1α model. Differential expression analysis of the sequenced cells shows that HIF-1α depletion in macrophages induce only minor changes is most of the dietary groups (Figure 24B). The quantification of DEG shows that in the control group (CD_MCD) no genotype-specific DEG is present. In obese condition (CD_MHFD) 29 genes were upregulated and 12 genes were downregulated for the comparison of WT $^{HIF-1α}$ vs KO $^{HIF-1α}$. None of the CD_MHFD DEG were differentially regulated in the transgenerational obese condition (HFD_MHFD), which indicates that developmental programming targets a unique transcriptomic profile (Figure 24B).

Macrophage-specific HIF-1α KO induced the highest number of DEG in the two metabolic programming conditions (HFD_MHFD and HFD_MCD). HFD_MHFD WT $^{HIF-1α}$ vs KO $^{HIF-1α}$ resulted with 259 upregulated and 57 downregulated genes. HFD_MCD WT $^{HIF-1α}$ vs KO $^{HIF-1α}$ induced the complete downregulation of 1142 and upregulation of 809 genes, which indicates the pivotal role of HIF-1α in developmental programming (Figure 24A). There were only 1 downregulated and 33 upregulated genes, which were present in both maternal obesity groups (HFD_MHFD and HFD_MCD). Therefore, we conclude that postnatal diet has a specific role in developmental programming induced NASH and the role of HIF-1α is specific for maternal obesity followed by postnatal control diet (HFD_MCD).

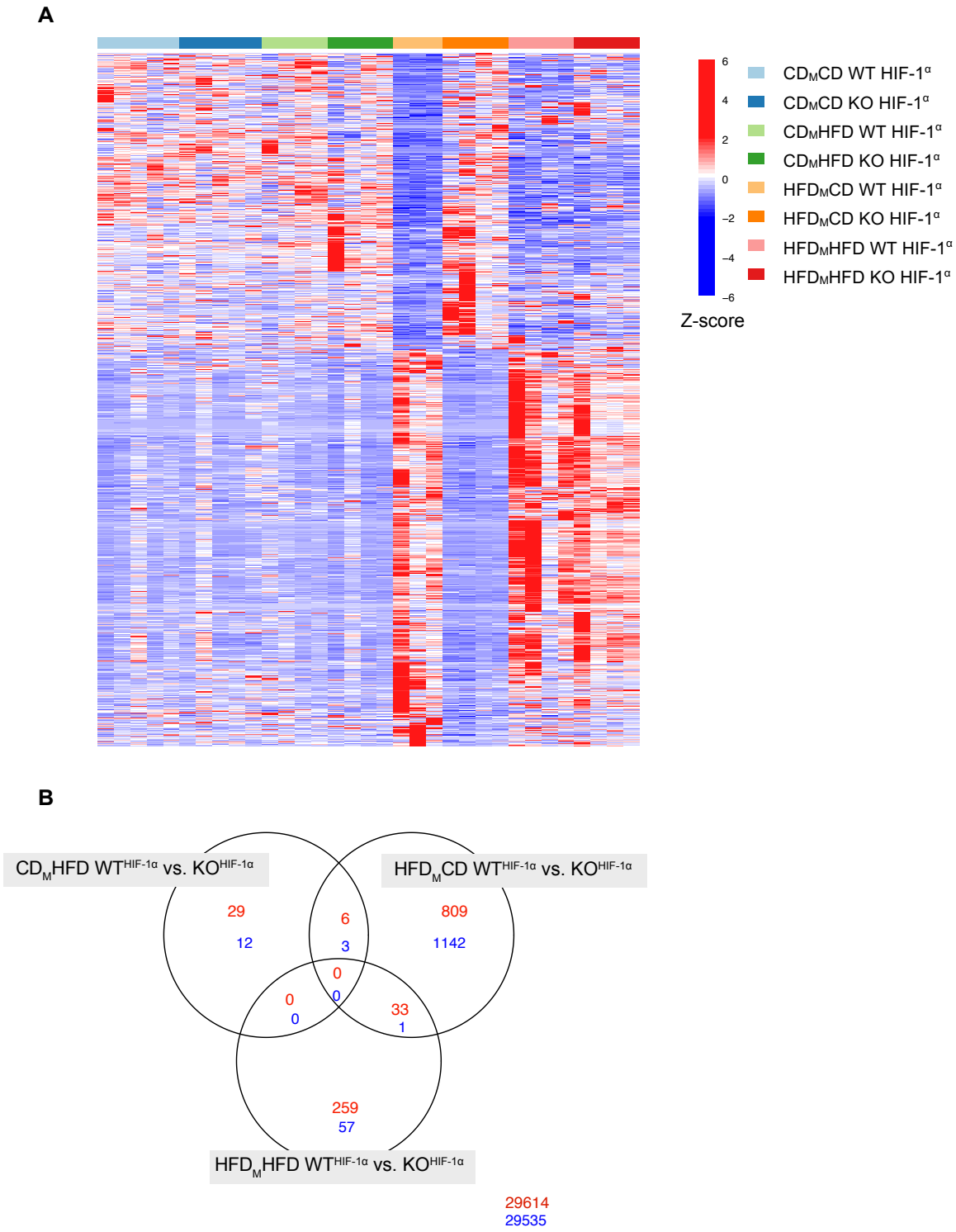

Figure 24. Differentially expressed gene analysis of the HIF-1α KC transcriptomics.
(A) Differentially expressed genes between HFD_MCD $WT^{HIF\text{-}1\alpha}$ vs. $KO^{HIF\text{-}1\alpha}$ represented as a heatmap. Every row represents differentially expressed genes between maternal obese lean mouse (HFD_MCD) HIF-$1\alpha^{f/f}$ $Lysm^{+/+}$ ($WT^{HIF\text{-}1\alpha}$) versus HIF-$1\alpha^{f/f}$ $Lysm^{cre/+}$ ($KO^{HIF\text{-}1\alpha}$). Expression pattern of genes is represented as row-scaled Z-score between every samples. Every column represents a single adult mouse sorted Kupffer cell (KC) expression profile. Samples are colour coded based on their dietary pattern and genotype as follows:
Light-blue - CD_MCD $WT^{HIF\text{-}1\alpha}$ (n=5) - mother is on control diet before and during pregnancy (Control Diet $_{Maternal}$), and the offspring is on control diet after birth. Mouse is HIF-$1\alpha^{f/f}$ $Lysm^{+/+}$ comparable genotype to wild-type (WT). Dark-blue - CD_MCD $KO^{HIF\text{-}1\alpha}$ (n=5) - mother is on control diet before and during pregnancy (Control Diet $_{Maternal}$), and the offspring is on control diet after birth. Mouse is HIF-$1\alpha^{f/f}$ $Lysm^{cre/+}$, macrophage-specific knock-out of hypoxia-inducible factor 1a (HIF-1α). (Legend continues on the next page.)

Light-green - $CD_MHFD\ WT^{HIF\text{-}1\alpha}$ (n=4) - mother is on control diet before and during pregnancy (Control Diet $_{Maternal}$), and the offspring is on a high-fat diet after birth. Mouse is $HIF\text{-}1\alpha^{f/f}\ Lysm^{+/+}$ comparable genotype to wild-type (WT).
Dark-green - $CD_MHFD\ KO^{HIF\text{-}1\alpha}$ (n=4) - mother is on control diet before and during pregnancy (Control Diet $_{Maternal}$), and the offspring is on a high-fat diet after birth. Mouse is $HIF\text{-}1\alpha^{f/f}\ Lysm^{cre/+}$, macrophage-specific knock-out of (HIF-1α).
Yellow - $HFD_MCD\ WT^{HIF\text{-}1\alpha}$ (n=3) - mother is on a high-fat diet before and during pregnancy (High-fat Diet $_{Maternal}$), and the offspring is on control diet after birth. Mouse is $HIF\text{-}1\alpha^{f/f}\ Lysm^{+/+}$ comparable genotype to wild-type (WT).
Orange - $HFD_MCD\ KO^{HIF\text{-}1\alpha}$ (n=4) - mother is on a high-fat diet before and during pregnancy (High-fat Diet $_{Maternal}$), and the offspring is on control diet after birth. Mouse is $HIF\text{-}1\alpha^{f/f}\ Lysm^{cre/+}$, macrophage-specific knock-out of HIF-1α.
Pink - $HFD_MHFD\ WT^{HIF\text{-}1\alpha}$ (n=4) - mother is on a high-fat diet before and during pregnancy (High-fat Diet $_{Maternal}$), and the offspring is on a high-fat diet after birth. Mouse is $HIF\text{-}1\alpha^{f/f}\ Lysm^{+/+}$ comparable genotype to wild-type (WT).
Red - $HFD_MHFD\ KO^{HIF\text{-}1\alpha}$ (n=4) - mother is on a high-fat diet before and during pregnancy (High-fat Diet $_{Maternal}$), and the offspring is on a high-fat diet after birth. Mouse is $HIF\text{-}1\alpha^{f/f}\ Lysm^{cre/+}$, macrophage-specific knock-out of HIF-1α.
(B) Representation of the differentially expressed gene (DEG) numbers between genotypes and dietary conditions. DEG calculation was performed by independent hypothesis weighting with a significance limit $p<0.05$ and significant fold-change equals or above 2. Upregulated gene numbers are marked with red, downregulated genes are marked with blue. Upon macrophage-specific KO of HIF-1α, HFD_MCD had the highest number of DEG, with 809 upregulated and 1142 downregulated genes. Only 1 downregulated and 33 upregulated genes are shared between HFD_MHFD and HFD_MCD genotype specific DEG.

In summary, a macrophage-specific KO model was used to target HIF-1α related metabolic shift from oxidative phosphorylation to glycolysis. Our aim was to rescue maternal obesity-induced NASH with $KO^{HIF\text{-}1\alpha}$ in the HFD_MCD group. According to histological, flow cytometric and shotgun lipidomic analysis, $HFD_MCD\ KO^{HIF\text{-}1\alpha}$ is rescued from NASH. Myeloid cell recruitment and lipid accumulation are both reduced. Transcriptomic analysis shows that most of the DEGs are in the $HFD_MCD\ WT^{HIF\text{-}1\alpha}$ vs. $KO^{HIF\text{-}1\alpha}$ groups. This finding motivated us to further analyze the transcriptomics of HFD_MCD hepatocytes. As hepatocytes accumulate lipid in NASH, we aimed to find the possible cellular interaction between KC and hepatocytes which is responsible for developmental programming induced NASH.

4.4.2.1 Ligand-receptor interaction between Kupffer cells and hepatocytes

In order to understand, how KCs interact with hepatocytes in the terms of maternal obesity-induced NASH and how macrophage-specific KO of HIF-1α protects offspring from hepatic lipid accumulation, we analyzed the ligand-receptor interactions between KC and hepatocytes.

Transcriptomic analysis of sorted KCs and hepatocytes shed light on ligand-receptor interactions between those cells, especially in the sense of maternal obesity-induced hepatic lipid accumulation. In total, 848 KC DEG were found via comparing $HFD_MCD\ WT^{HIF\text{-}1\alpha}$ vs. $KO^{HIF\text{-}1\alpha}$. Of those, 12 ligands were found to have receptor interaction with $HFD_MCD\ WT^{HIF\text{-}1\alpha}$ vs. $KO^{HIF\text{-}1\alpha}$ hepatocytes (Figure 29A). Nine of those ligands show a similar expression pattern between the eight conditions in KC. Namely, upregulation in $HFD_MCD\ WT^{HIF\text{-}1\alpha}$ and $HFD_MHFD\ WT^{HIF\text{-}1\alpha}$ & $KO^{HIF\text{-}1\alpha}$, while in all maternal lean conditions and $HFD_MCD\ KO^{HIF\text{-}1\alpha}$, those transcripts are downregulated (Figure 25B). In the hepatocyte DEG

receptors, we found two transcripts with enzymatic activity, Cd36 (EC1.2.1.67) and Dpp4 (EC3.4.14.5). Those two enzymes are receptors of ApoB and Cxcl12. Moreover, we extracted all possible receptors of the 48 DE ligands, which are upregulated in $HFD_MCD\ WT^{HIF\text{-}1\alpha}$ but come to a steady-state in $HFD_MCD\ KO^{HIF\text{-}1\alpha}$ compared to maternal lean conditions. Between those transcripts, we found even more ligands belonging to the Apolipoprotein family, such as ApoE and ApoA1 (Figure 26). We retrieved the regulatory potential between those ligands and receptors using the Nichenet prediction matrix (Figure 27). A high regulatory potential was detected between *ApoA1* with *Tlr4* and *Abca1*, *ApoE* with *Lrp1*, *Ldr*, *Itgb2*, *Itgam*, *F3*, *Cxcr4*, *Cd44*, *C3ar1,* and *Abca1*.

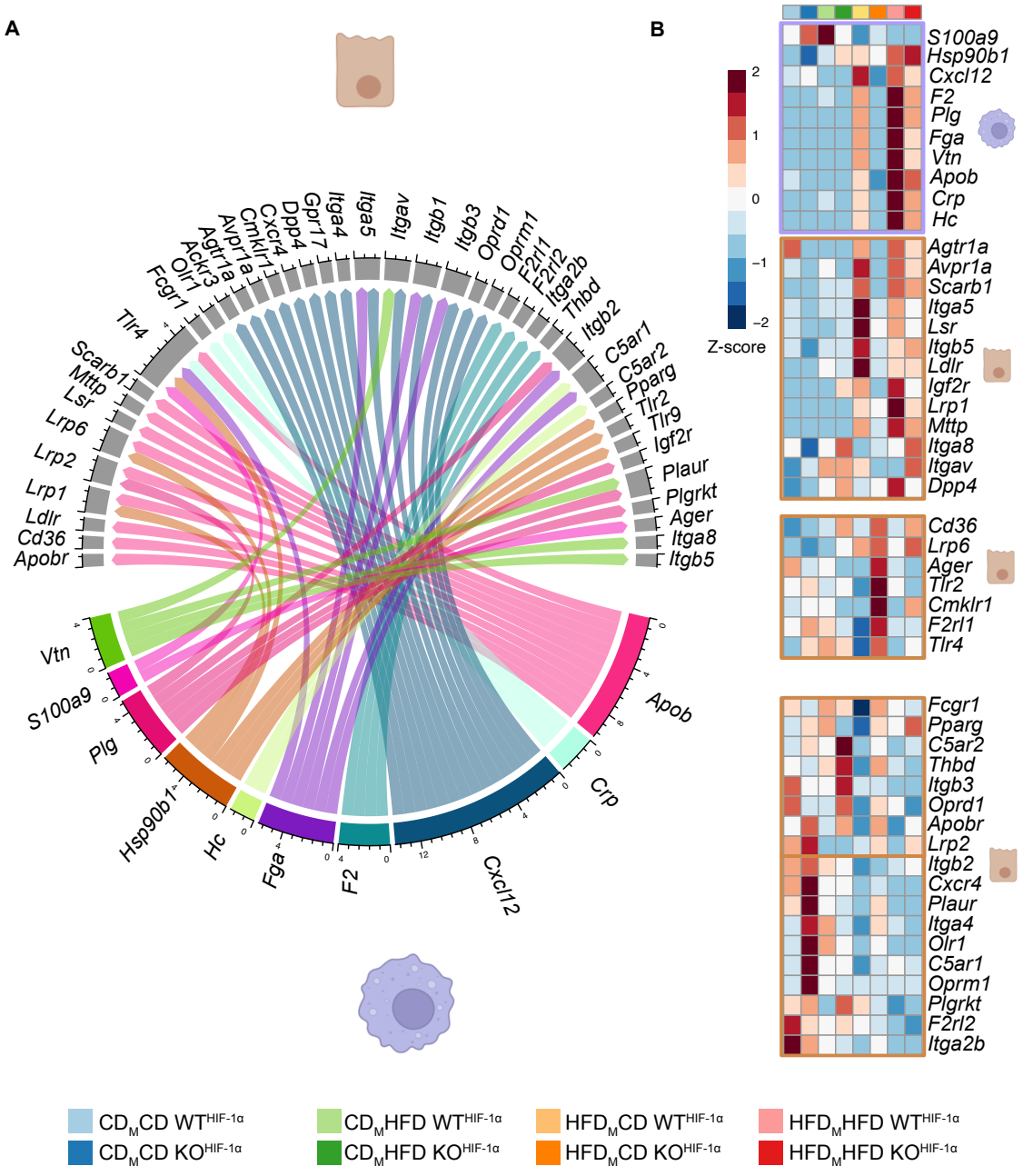

Figure 25. Ligand-receptor interactions between HFDCDCD DEGs KC and hepatocytes

(A) CelltalkDB was used to extract the ligand-receptor (LR) pairs between KC HFD_MCD WT vs. HFD_MCD KO DEG as ligands (colored), and hepatocyte HFD_MCD WT vs. HFD_MCD KO DEG as receptors (grey). LR-pairs are visualized as a circle plot. **(B)** The expression of ligands and receptors is represented as heatmap. Every row represents a differentially expressed gene between maternal obese lean mouse (HFD_MCD) HIF-$1\alpha^{f/f}$ $Lysm^{+/+}$ ($WT^{HIF\text{-}1\alpha}$) versus HIF-$1\alpha^{f/f}$ $Lysm^{cre/+}$ ($KO^{HIF\text{-}1\alpha}$). Expression pattern of genes is represented as row-scaled z-score between every condition. Every column represents a condition-based expression profile. Heatmaps surrounded with purple are KC ligands, and heatmaps surrounded with brown identifies hepatocyte receptors. DEG calculation was performed by independent hypothesis weighting with a significance limit $p<0.05$ and significant fold-change equals or above 2. Conditions are color-coded based on their dietary pattern and genotype as follows:

Light-blue - CD_MCD $WT^{HIF\text{-}1\alpha}$ (n=5) - mother is on control diet before and during pregnancy (Control Diet $_{Maternal}$), and the offspring is on control diet after birth. Mouse is HIF-$1\alpha^{f/f}$ $Lysm^{+/+}$ comparable genotype to wild-type (WT).

Dark-blue - CD_MCD $KO^{HIF\text{-}1\alpha}$ (n=5) - mother is on control diet before and during pregnancy (Control Diet $_{Maternal}$), and the offspring is on control diet after birth. Mouse is HIF-$1\alpha^{f/f}$ $Lysm^{cre/+}$, macrophage-specific knock-out of hypoxia-inducible factor 1a (HIF-1α).

Light-green - CD_MHFD $WT^{HIF\text{-}1\alpha}$ (n=4) - mother is on control diet before and during pregnancy (Control Diet $_{Maternal}$), and the offspring is on a high-fat diet after birth. Mouse is HIF-$1\alpha^{f/f}$ $Lysm^{+/+}$ comparable genotype to wild-type (WT).

Dark-green - CD_MHFD $KO^{HIF\text{-}1\alpha}$ (n=4) - mother is on control diet before and during pregnancy (Control Diet $_{Maternal}$), and the offspring is on a high-fat diet after birth. Mouse is HIF-$1\alpha^{f/f}$ $Lysm^{cre/+}$, macrophage-specific knock-out of (HIF-1α). (Legend continues on the next page.)

Yellow - $HFD_MCD\ WT^{HIF\text{-}1\alpha}$ (n=3) - mother is on a high-fat diet before and during pregnancy (High-fat Diet $_{Maternal}$), and the offspring is on control diet after birth. Mouse is $HIF\text{-}1\alpha^{f/f}$ $Lysm^{+/+}$ comparable genotype to wild-type (WT).
Orange - $HFD_MCD\ KO^{HIF\text{-}1\alpha}$ (n=4) - mother is on a high-fat diet before and during pregnancy (High-fat Diet $_{Maternal}$), and the offspring is on control diet after birth. Mouse is $HIF\text{-}1\alpha^{f/f}$ $Lysm^{cre/+}$, macrophage-specific knock-out of HIF-1α.
Pink - $HFD_MHFD\ WT^{HIF\text{-}1\alpha}$ (n=4) - mother is on a high-fat diet before and during pregnancy (High-fat Diet $_{Maternal}$), and the offspring is on a high-fat diet after birth. Mouse is $HIF\text{-}1\alpha^{f/f}$ $Lysm^{+/+}$ comparable genotype to wild-type (WT).
Red - $HFD_MHFD\ KO^{HIF\text{-}1\alpha}$ (n=4) - mother is on a high-fat diet before and during pregnancy (High-fat Diet $_{Maternal}$), and the offspring is on a high-fat diet after birth. Mouse is $HIF\text{-}1\alpha^{f/f}$ $Lysm^{cre/+}$, macrophage-specific knock-out of HIF-1α.

The Nichenet regulation potential matrix did not recognize other Apolipoprotein ligands with the expression mentioned above, but literature-based ligand-receptor pairs got extracted. This procedure allows retrieving the possible hepatocyte receptors which are not necessarily differentially expressed. Those KC-specific ligands are *Apoc1*, *Apom,* and *Apoc3*. Their receptors are *Vldlr*; *Lrp2*; *Lrp1*, *Ldlr,* and *Gpihbp1,* respectively (Figure 26).

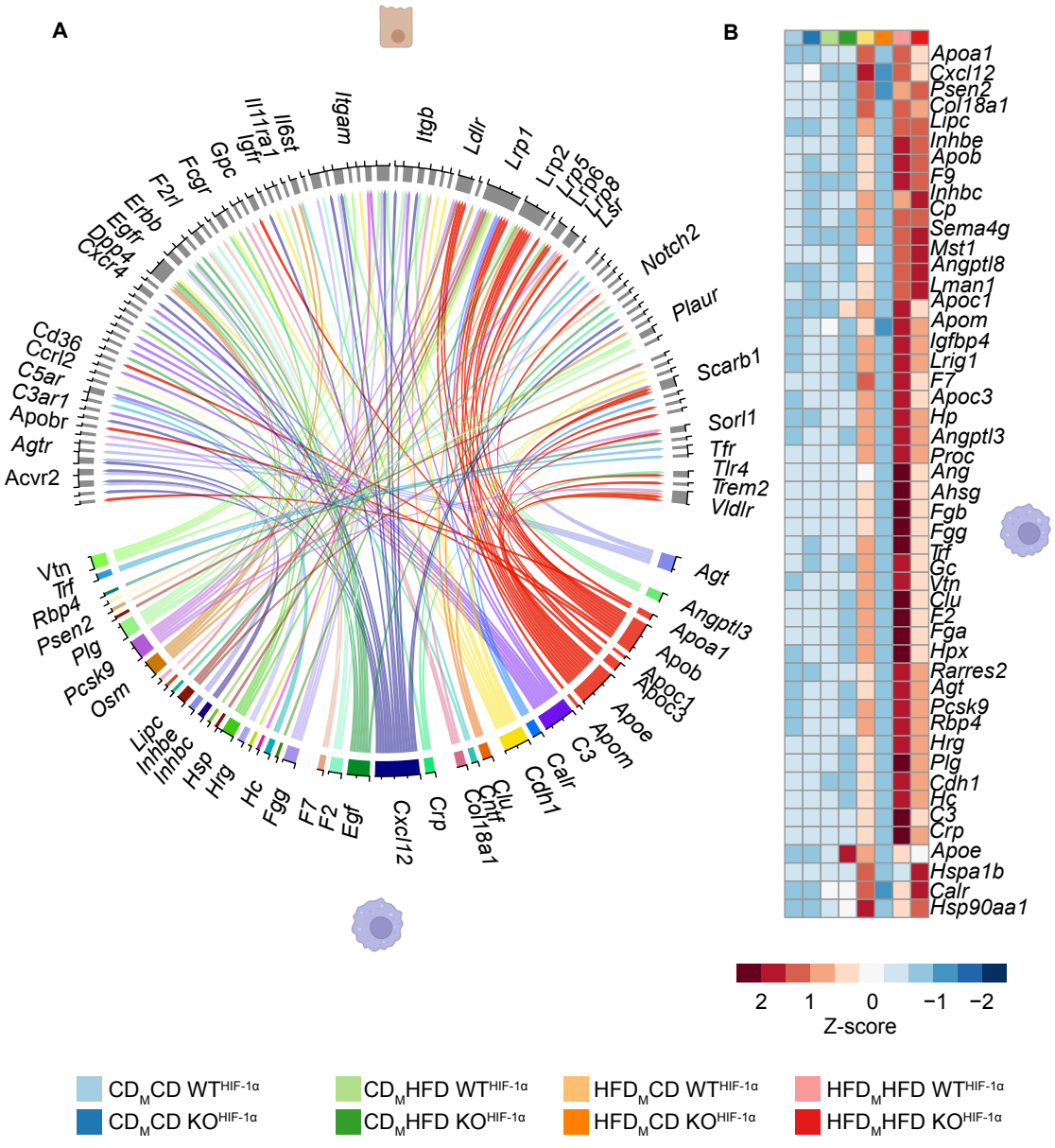

Figure 26. Receptor prediction of maternal obese rescued KC
(A) All possible receptors and their connecting $HFD_MCD\ WT^{HIF\text{-}1\alpha}$ VS $KO^{HIF\text{-}1\alpha}$ KC ligands. (Legend continues on the next page.)

Grey-labeled genes represent the possible predicted receptors, and color-labeled genes represent the KC DEG ligands. The colored lines represent the ligand-receptor interactions between KC and hepatocytes. **(B)** Gene expression profile of KC-ligands across the subgroups is represented as a heatmap. Expression pattern of ligand-genes is represented as row-scaled Z-score between every condition. Every column represents a condition-based expression profile and every row represents a gene that was differentially expressed in $HFD_{M}CD\ WT^{HIF\text{-}1\alpha}$ VS $KO^{HIF\text{-}1\alpha}$ KCs. Conditions are colour coded based on their dietary pattern and genotype as follows:
Light-blue - $CD_{M}CD\ WT^{HIF\text{-}1\alpha}$ (n=5) - mother is on control diet before and during pregnancy (Control Diet $_{Maternal}$), and the offspring is on control diet after birth. Mouse is $HIF\text{-}1\alpha^{f/f}\ Lysm^{+/+}$ comparable genotype to wild-type (WT).
Dark-blue - $CD_{M}CD\ KO^{HIF\text{-}1\alpha}$ (n=5) - mother is on control diet before and during pregnancy (Control Diet $_{Maternal}$), and the offspring is on control diet after birth. Mouse is $HIF\text{-}1\alpha^{f/f}\ Lysm^{cre/+}$, macrophage-specific knock-out of hypoxia-inducible factor 1a (HIF-1α).
Light-green - $CD_{M}HFD\ WT^{HIF\text{-}1\alpha}$ (n=4) - mother is on control diet before and during pregnancy (Control Diet $_{Maternal}$), and the offspring is on a high-fat diet after birth. Mouse is $HIF\text{-}1\alpha^{f/f}\ Lysm^{+/+}$ comparable genotype to wild-type (WT).
Dark-green - $CD_{M}HFD\ KO^{HIF\text{-}1\alpha}$ (n=4) - mother is on control diet before and during pregnancy (Control Diet $_{Maternal}$), and the offspring is on a high-fat diet after birth. Mouse is $HIF\text{-}1\alpha^{f/f}\ Lysm^{cre/+}$, macrophage-specific knock-out of (HIF-1α).
Yellow - $HFD_{M}CD\ WT^{HIF\text{-}1\alpha}$ (n=3) - mother is on a high-fat diet before and during pregnancy (High-fat Diet $_{Maternal}$), and the offspring is on control diet after birth. Mouse is $HIF\text{-}1\alpha^{f/f}\ Lysm^{+/+}$ comparable genotype to wild-type (WT).
Orange - $HFD_{M}CD\ KO^{HIF\text{-}1\alpha}$ (n=4) - mother is on a high-fat diet before and during pregnancy (High-fat Diet $_{Maternal}$), and the offspring is on control diet after birth. Mouse is $HIF\text{-}1\alpha^{f/f}\ Lysm^{cre/+}$, macrophage-specific knock-out of HIF-1α.
Pink - $HFD_{M}HFD\ WT^{HIF\text{-}1\alpha}$ (n=4) - mother is on a high-fat diet before and during pregnancy (High-fat Diet $_{Maternal}$), and the offspring is on a high-fat diet after birth. Mouse is $HIF\text{-}1\alpha^{f/f}\ Lysm^{+/+}$ comparable genotype to wild-type (WT).
Red - $HFD_{M}HFD\ KO^{HIF\text{-}1\alpha}$ (n=4) - mother is on a high-fat diet before and during pregnancy (High-fat Diet $_{Maternal}$), and the offspring is on a high-fat diet after birth. Mouse is $HIF\text{-}1\alpha^{f/f}\ Lysm^{cre/+}$, macrophage-specific knock-out of HIF-1α.

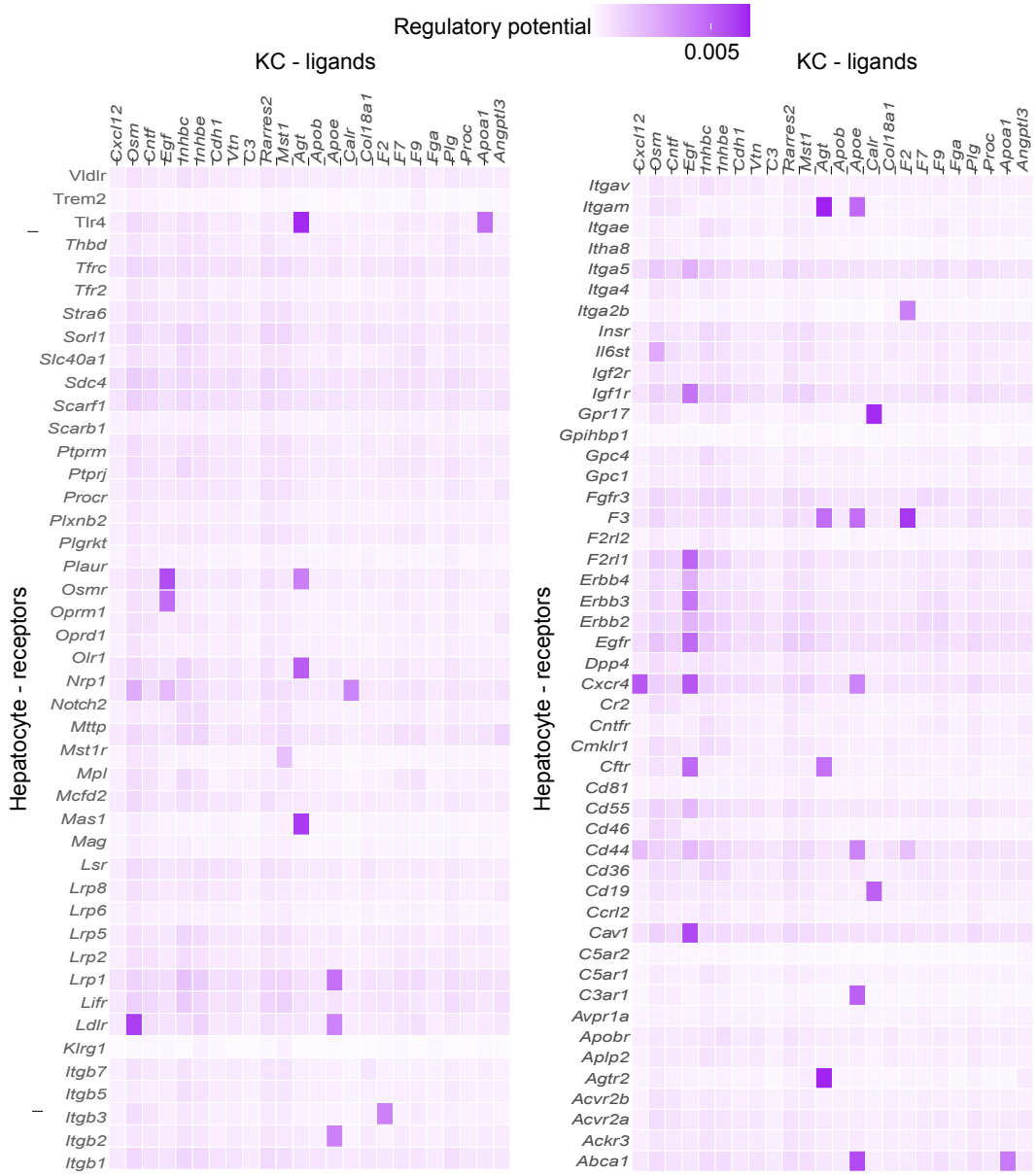

Figure 27. Regulatory potential prediction of rescued KC DEG
Ligand-Receptor regulatory potential prediction using the Nichenet DB with all possible receptors and their connecting HFD_MCD WT $^{HIF\text{-}1\alpha}$ VS KO $^{HIF\text{-}1\alpha}$ KC ligands. Regulatory potential is scaled by purple. The higher regulatory potential score visualizes the absolute ligand-target (KC-hepatocyte) regulatory potential. This confidence score relates to the number of data sources, which confirmed the regulatory interaction between ligand and receptor. KC - Kupffer cell; DEG - differentially expressed genes (performed by independent hypothesis weighting with a significance limit $p<0.05$ and significant fold-change equals or above 2); HFD_MCD WT $^{HIF\text{-}1\alpha}$(n=3) - mother is on a high-fat diet before and during pregnancy (High-fat Diet $_{Maternal}$), and the offspring is on control diet after birth. Mouse is HIF-1$\alpha^{f/f}$ Lysm$^{+/+}$ comparable genotype to wild-type (WT); HFD_MCD KO$^{HIF\text{-}1\alpha}$ (n=4) - mother is on a high-fat diet before and during pregnancy (High-fat Diet $_{Maternal}$), and the offspring is on control diet after birth. Mouse is HIF-1$\alpha^{f/f}$ Lysm$^{cre/+}$, macrophage-specific knock-out of HIF-1α. Receptors are in alphabetic order, split into two heatmaps due to space considerations.

In summary, LR interactions were predicted between HFD_MCD KC and hepatocytes via the Nichenet pipeline. In this way, we gained an understanding of how the macrophage-specific KO of HIF-1α can rescue the offspring from NASH. We found several apolipoproteins and Cxcl12 chemokine ligands in KC, which send signals to Cd36 and Dpp4 hepatocyte receptors to promote lipid

accumulation. Both receptors are well known in the NASH field and differentially expressed in HFD_MCD hepatocytes. Those gained knowledge makes ApoB - Cd36 and Cxcl2 - Dpp4 promiscuous candidates to gain mechanistic insight into developmental programming-induced NASH.

4.4.2.2 Multiomics: Hepatocyte - lipid interaction upon maternal obesity-induced NASH

In order to find the joint variables which may drive maternal obesity-induced transgenerational NASH, a simultaneous integrated analysis was performed on hepatocyte transcriptome and liver lipidome. The hepatocyte transcriptome dataset was gained via bulk RNA sequencing of sorted hepatocytes from the HIF-1α maternal obesity model. The same mice were used for the RNA-sequencing and lipidomics; therefore, we joined the lipidomics and transcriptomics dataset through the joint samples. We used the orthogonal partial least square mathematical model to visualize relationships between liver lipidomics and hepatocyte transcriptomic datasets.

Joint lipidome analysis exposed that cholesterol esters (CE) are the main drivers of NASH, even though TAGs are accumulated in significant amounts. CE-dynamic was joint with Alb, ApoE, Trf, ApoA1, and mt-Co3. The most prominent species in the lipidome-transcriptome crosstalk are TAG (48:1), CE (18:2), CE (18:1), and DAG (34:2). Furthermore, TAG, DAG, and CE are the critical modulators of NASH, and their regulation is triggered by mitochondrial hepatocyte transcripts. Those key modulators are *mt-Co1*, *mt-Cyb*, *mt-Nd4*, *mt-Nd1,* and *mt-Atp6* (Figure 28).

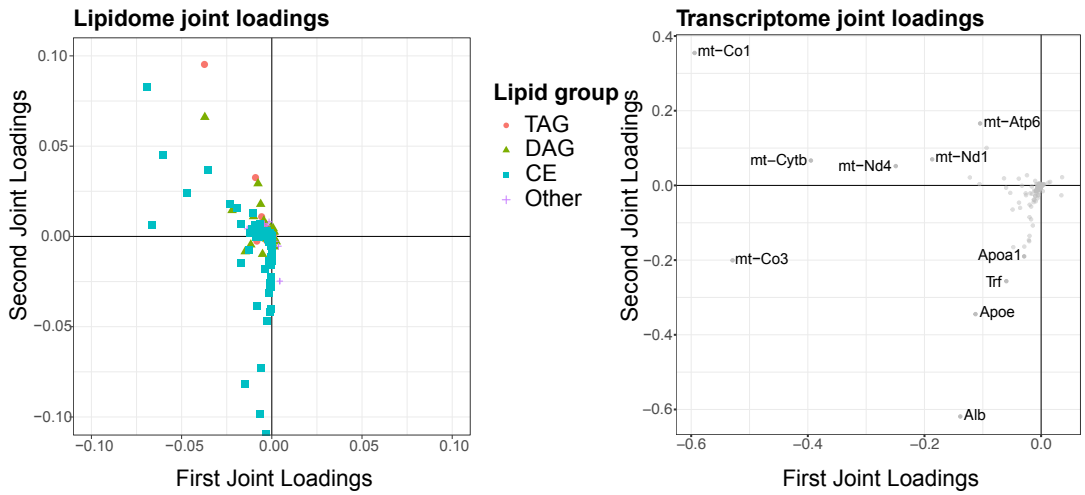

Figure 28. O2PLS multi-omics analysis of hepatocyte transcriptome and liver lipidome.
Joint factors are predicted between lipid species and transcripts. The orthogonal partial least square (O2PLS) model got imputed the shotgun lipidomics matrix with 439 lipid species and the hepatocyte RNA-seq count table with 11.382 transcripts and 29 joint samples between the two matrices. Transcriptomic data was scaled down to the top 75% of most variable transcripts. Lipidomics and transcriptomics were joined through the shared host. Dimension reduction took place through cross-validation to find the triplet (joint components, lipid-specific components, and RNA-specific components), which enables the best prediction power. The joint predictional power was 0.83 for both transcriptome and lipidome.

To sum up, the O2PLS analysis confirmed our findings related to the pivotal role of apolipoproteins in maternal obesity-induced NASH development. This method enabled us to involve the lipidomic dataset and join it with transcriptomics. In this combined analysis, we could identify CE as the most affecting lipid type in NASH.

In this thesis, I have demonstrated how maternal obesity induces KC metabolic programming, which leads to NASH in the offspring. NAFLD was found in every maternal obese condition and NASH if maternal obese offspring followed a different diet than the mother. NASH was accompanied by a high accumulation of LCM, monocytes, granulocytes and cDCs. Transcriptomic analysis manifested that developmentally programmed KCs go through a metabolic shift from oxidative phosphorylation to glycolysis. Three possible mechanisms were identified which may lead to maternal obesity-induced NASH. Those are ontogeny, inflammation and immunometabolic shift. Two macrophage-specific maternal obesity KO models were established targeting Myd88 and HIF-1α. Macrophage-specific HIF-1α deletion rescued maternal obesity-induced NASH through the metabolic reprogramming of KC.

5.1 Maternal obesity induces NAFLD and NASH

We proved that maternal obesity induces NAFLD and also NASH in the case of HFD_MCD_LCD and HFD_MHFD_LCD. Transgenerational NASH was already shown in mice, humans, and other species[98–101]. Usually, fatty liver positively correlates with liver weight. However, in diet-induced obesity, liver weight reduction is reported[102]. Our model showed a slight decrease in liver weight upon NASH phenotype. Elevated liver weight has also been reported upon NASH[103,104]. It needs to be further investigated what is the causality and correlation between NASH and liver weight. The fatty liver phenotype was defined via ORO staining, lipid droplet quantification, and shotgun lipidomics. We found a negative correlation between neutral lipid and glycogen accumulation, published already in another NASH model[85]. Glucose and lipid homeostasis disturbance is a clear signature of developing metabolic syndrome and insulin resistance. Metabolic syndrome and insulin resistance are the most common risk factors for NASH. Hepatic insulin resistance upon maternal obesity was remarkable in the macrophage transcriptome analysis. Glutamine and carbohydrate transporting solute carriers were immensely upregulated in all maternal obese groups, suggesting insulin resistance. However, this study did not address systemic insulin resistance due to physiological reasons. We need to fast the mice before the experiment to target systemic insulin resistance. Upon fasting, the liver accumulates lipid immediately. We could not perform any other

experiments on those mice with this procedure. Therefore, we decided to target systemic insulin resistance in a future cohort, which is not included in this thesis.

TAG and CE species are increased upon maternal obesity-induced NASH and also decreased upon rescue. However, CE gives only a small proportion of all identified lipids (~5%). TAG and Phospholipids are the key players in lipid accumulation. However, CE was found to be the key driver, according to O2PLS analysis. CE and TAG are known to incorporate into ultra low-density lipoproteins. Those lipoproteins enter the bloodstream, where they are subjected to lipoprotein lipase, which is a possible mechanism to induce whole body metabolic disturbances, which needs to be addressed in the future.

5.2 Myd88 expression is upregulated upon hepatic fibrosis, not upon developmental programming

The macrophage-specific Myd88 model aimed to rescue the phenotype of developmental programming via the Myd88-related inflammatory mechanism. However, Myd88 was upregulated in KC for all maternal obese conditions; developmental programming is not rescued via its macrophage-specific KO. Myd88 deficiency in macrophages resulted in no change upon maternal obesity, and the lipid accumulation got worse upon transgenerational obesity.

Myeloid cell-specific Myd88 deficiency induced liver fibrosis even without maternal obesity[105]. Myd88 deficiency in macrophages inhibits CXCL2, which leads to the activation of the NLRP3 inflammasome. Myd88 upregulation in our WT model was not a result of developmental programming but a consequence of maternal obesity-induced NAFLD. Therefore, Myd88 was not the key regulator of developmental programming, and we could not rescue the phenotype via its macrophage-specific KO-model. Prior knowledge combined with our results let us assume that maternal obesity-induced steatosis has a different trigger than other hepatic steatosis-related diseases.

5.3 HIF1-α is the key regulator of maternal obesity-induced metabolic programming

Macrophage-specific $KO^{HIF1\text{-}\alpha}$ rescued the maternal obesity-induced NASH phenotype. Lipid accumulation of the liver got rescued, which was assessed by histological, and lipidomics approaches. The inflammatory phenotype of the liver got rescued as well in the HFD_MCD $KO^{HIF1\text{-}\alpha}$ group, which we could address via flow cytometric quantification of monocyte and granulocyte populations. As a macrophage-specific KO model can rescue NASH, the lipid accumulation signal must originate from macrophages. Hepatocytes are the main cells in the liver that accumulate lipids upon NASH. Therefore, we tracked the ligand-receptor interactions between KC and hepatocytes. ApoB and Cxcl12 are the main ligands that send signals in maternal obesity-induced NASH. The predicted ligand-receptor interactions between HFD_MCD $WT^{HIF1\text{-}\alpha}$ vs. $KO^{HIF1\text{-}\alpha}$ DEG macrophages and their receptors further raise the role of apolipoproteins, such as ApoA1, ApoB, Apoc1, Apoc3, ApoE, and Apom. Those upregulated ligands send signals to hepatocyte low-density lipoprotein receptors (LDLRs), for example, Ldlr and Lrp families. That LDLRs bind to LDLs, which are the primary carriers of cholesterol in the blood. LDLRs are highly present in the liver, which is the responsible organ for removing most excess cholesterol from the body. The number of LDLRs in the liver determines how fast cholesterol is removed from the bloodstream. HFD_MCD $WT^{HIF1\text{-}\alpha}$ develop NASH, with a high accumulation of TAGs, CEs, upregulated Apolipoprotein transcripts in KC and upregulated LDLRs in hepatocytes. HFD_MCD $KO^{HIF1\text{-}\alpha}$ rescued the NASH phenotype. HFD_MCD $KO^{HIF\text{-}1\alpha}$ measures are the same in the whole liver, hepatocyte, and KC as in the CD_MCD group and downregulated if we compare with the HFD_MCD $WT^{HIF1\text{-}\alpha}$ group. O2PLS multi-omics analysis of hepatocyte transcriptome and liver lipidomics confirmed the key role of apolipoproteins, CEs, and TAGs; moreover, their interaction in maternal obesity-induced NASH. Maternal obesity induces developmental programming of the macrophages through Apolipoproteins, which send signals to hepatocyte LDLRs. LDLRs activation leads to the accumulation of CE, TAG and, in this way to NAFLD.

How does $KO^{HIF1\text{-}\alpha}$ rescue metabolic programming through Apolipoproteins? Recently, Ppar-α was suggested as the regulator between HIF1-α and NAFLD[106].

We can confirm those findings; the resolution of liver lipid accumulation through KO $^{HIF1-\alpha}$ resulted in the downregulation of Ppar-α as well.

Another potential connection is Trem2 between HIF-1α and ApoE, which is well described in the brain. In Alzheimer's disease models, HIF-1α expression is increased in microglia in a Trem2-dependent manner[107,108]. Moreover, Trem2 recognizes many of the ligands on the surface of lipoproteins, including Ldl, Hdl, and ApoE[109–111]. Trem2 identifies SAM as well in the context of NASH. There is a clear pattern in the Trem2 expression, and it is also identified as a DEG between HFD_MCD KO $^{HIF1-\alpha}$ and WT $^{HIF1\alpha}$. Neither Trem2 nor Pparα is recognized as part of the HIF-1α signaling pathway in the common bioinformatics databases, such as KEGG or GO, which makes unbiased analysis challenging.

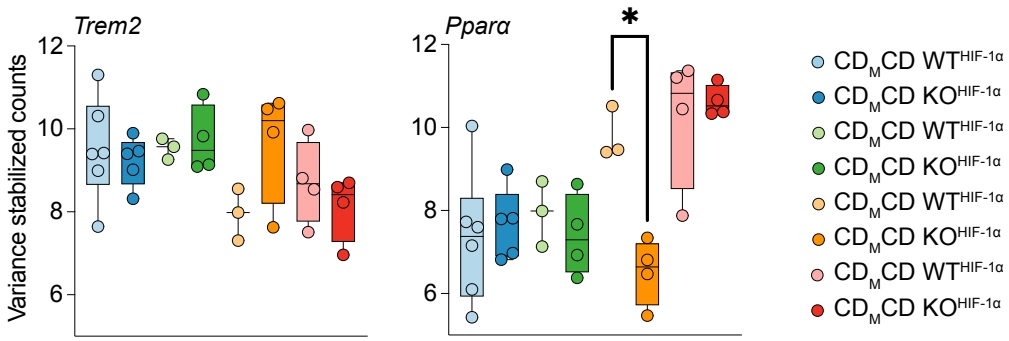

Figure 29. Pparα is the key mediator between HIF-1α and NASH.

Boxplot of variance stabilized gene expression counts for Trem2 and Pparα in the KCs from the HIF-1α maternal obesity model. Every circle represents a single offspring. In every dietary group, mice are at least from two different litters. Statistical assessment was performed via one-way ANOVA - Turkey's multiple comparisons method. Statistical significance is represented only for genotype-specific differences. Statistical significance is represented via the probability (p-value) as follows: *= p<0.05. *Groups are represented as follows:*
Light-blue - CD_MCD WT $^{HIF-1\alpha}$- mother is on control diet before and during pregnancy (Control Diet $_{Maternal}$), mother is on control diet during lactation and offspring is on control diet during post-weaning diet. Offspring's genotype is HIF-1α $^{fl/fl}$ LysMCre $^{wt/wt}$.
Dark-blue - CD_MCD KO $^{HIF-1\alpha}$- mother is on control diet before and during pregnancy (Control Diet $_{Maternal}$), mother is on control diet during lactation and offspring is on control diet during post-weaning diet. Offspring's genotype is HIF-1α $^{fl/fl}$ LysMCre $^{+/wt}$
Light-green - CD_MHFD WT $^{HIF-1\alpha}$ - mother is on control diet before and during pregnancy (Control Diet $_{Maternal}$), mother is on control diet during lactation and offspring is on High-fat diet during post-weaning diet. Offspring's genotype is HIF-1α $^{fl/fl}$ LysMCre $^{wt/wt}$.
Dark-green - CD_MHFD KO $^{HIF-1\alpha}$ - mother is on control diet before and during pregnancy (Control Diet $_{Maternal}$), mother is on control diet during lactation and offspring is on High-fat diet during post-weaning diet. Offspring's genotype is HIF-1α $^{fl/fl}$ LysMCre $^{+/wt}$.
Yellow - HFD_MCD WT $^{HIF-1\alpha}$ - mother is on High-fat diet before and during pregnancy High-fat Diet $_{Maternal}$), mother is on control diet during lactation and offspring is on control diet during post-weaning diet. Offspring's genotype is HIF-1α $^{fl/fl}$ LysMCre $^{wt/wt}$.
Orange - HFD_MCD KO $^{HIF-1\alpha}$ - mother is on High-fat diet before and during pregnancy High-fat Diet $_{Maternal}$), mother is on control diet during lactation and offspring is on control diet during post-weaning diet. Offspring's genotype is HIF-1α $^{fl/fl}$ LysMCre $^{+/wt}$.
Pink - HFD_MHFD WT $^{HIF-1\alpha}$ - mother is on High-fat diet before and during pregnancy High-fat Diet $_{Maternal}$), mother is on High-fat diet during lactation and offspring is on control diet during post-weaning diet. Offspring's genotype is HIF-1α $^{fl/fl}$ LysMCre $^{wt/wt}$.
Red - HFD_MHFD KO $^{HIF-1\alpha}$ - mother is on High-fat diet before and during pregnancy High-fat Diet $_{Maternal}$), mother is on High-fat diet during lactation and offspring is on control diet during post-weaning diet. Offspring's genotype is HIF-1α $^{fl/fl}$ LysMCre $^{+/wt}$.

5.3.1 Mitochondrial DNA, as key regulators of CE accumulation

O2PLS multi-omics analysis of the HIF-1α dataset identified mitochondrial transcripts as key regulators of lipidome, next to apolipoproteins. Those are *mt-Co1*, *mt-Cyb*, *mt-Nd4*, *mt-Nd1,* and *mt-Atp6.*

Epigenetic analysis shed light on liver mitochondrial DNA (mtDNA) in selected regions of the mtDNA genome, such as the D-loop control region and mitochondrially encoded NADH dehydrogenase 6 (MT-Nd6) and cytochrome C oxidase I (MT-Co1), and their methylation was correlated to NASH severity[112]. mt-Atp6 was associated with childhood obesity[113], pregnancy complications[114], and with NAFLD as well[115]. Our study could not cover epigenetic changes related to developmental programming, but those mitochondrially encoded transcripts serve as good candidates for further epigenetic analysis. O2PLS analysis highlighted those mitochondrial transcripts as main possible regulators of CE accumulation in hepatocytes. However, the high prevalence of mitochondrial genes can also be a sign for low sample quality. Therefore, stringent quality assessment was performed also for the hepatocyte transcriptome data. We excluded low sample quality issues, via read count assesment (at least 5 mio reads per sample), Kallisto alignment quality check, and variance analysis of O2PLS target genes (Appendix K). This analysis gave a hint for further epigenetic investigation, but due to the low sample size and unspecific measurement, different experiments need to be done to prove those findings. As a general praxis, mitochondrial transcripts are excluded from the transcriptome input data. In metabolic research, mitochondrial transcripts have a pivotal role and need to be included into the analysis[116–118].

5.3.2 HIF-1α as a pharmaceutical target

HIF-1α rescues maternal obesity-induced NASH in a macrophage-specific manner. Its key mechanism is related to the metabolic shift from OXPHOS to glycolysis, and it is also the mechanism where macrophages rescue maternal obesity induced NASH.

HIF-1α has various functions, coordinating the activity of many transcription factors and their downstream molecules in cancer, NASH and neurodegenerative diseases. Thus, HIF-1α signaling pathways became the most prominent pharmacological target in cancer research[119,120].

For that purpose, inhibitors of HIF-1α or their target genes have to be identified. HSP90 (also DE-ligand in HFD_MCD KC) is a molecular chaperone involved in the proper folding of HIF-1a protein. Two drugs, geldanamycin and KF58333 show that HSP90 inhibition decrease HIF-1α stabilization as well. In vitro, HSP-90 modulates PPAR activity upon NAFLD[121]. However, none of the drugs were tested to treat NAFLD.

Resmetirom is the most promising HIF-1α-related candidate to treat NASH, currently in the phase-3 clinical trial. It is a liver-directed thyroid hormone receptor (Thr) β-selective agonist. Non-genomic actions of thyroid hormone include HIF-1α transcriptional activation, which is another possible scenario of how HIF-1α is involved in NASH development upon developmental programming. Thrβ is also DEG in HFD_MCD KC; potentially, its inhibition would be sufficient to rescue maternal obesity-induced NASH[122].

Metformin, an antidiabetic drug, was shown as well to decrease HIF-1α protein levels, and with it offers a potential drug to treat NASH as well[123]. Prior studies have shown a pleiotropic effect of HIF-1α, which has a key role in many disease-related mechanisms, from cancer to neurodegeneration through diabetes. Our work suggests that HIF-1α does only affected by the macrophage-specific metabolic programming, which may subsequentially lead to many disease-causing mechanisms.

5.4 The effects of developmental programming on the body

This work focused on the chronic effects of metabolic programming in the liver. We collected and analyzed liver samples during embryonic development E14.5 and at the perinatal stage P0 as well. The pre-and perinatal effects of developmental programming are conveyed in Malin Jessen's thesis[84].

Certainly, maternal obesity has a significant effect on many other organs as well. We collected and initially analyzed the EWAT, BM, BAT, blood, cortex, hippocampus, heart, and muscle (data not shown). Prior knowledge relates maternal diabetes and offspring heart dysfunction through HIF-1α[124]. Metabolic dysfunction of adipose tissue upon maternal obesity highlights the effect of epigenetic programming through DNA demethylation[125,126]. Neuropsychiatric disorders and other chronic diseases related to maternal obesity give a hint that developmental programming induces a long-term dysregulation in the offspring's

body. The fact that a macrophage-specific KO-model could reverse metabolic programming, at least in the liver, makes certain that KC and immune metabolism have a crucial role in this transgenerational process.

5.5 Conclusion

Maternal obesity induced NAFLD is unrelated to the lactational and offspring diet. Inflammation joins NAFLD and develops into NASH if maternal and offspring diets are different. Neither NASH nor NAFLD shows any effect on offspring bodyweight. In NASH, CE and TAG are accumulated in the liver. Macrophages, monocytes, granulocytes, and dendritic cells are recruited upon chronic inflammation. Triggered by maternal obesity, KCs go through a metabolic shift from OXPHOS to glycolysis. Metabolic programmed macrophages rely on glycolysis, which leads to inefficient energy production.

Myd88 was upregulated in maternal obese KC, but it is an effect of NAFLD and not a cause. Macrophage-specific KO of HIF-1α did rescue NASH. TAG and CE amounts become normal. Macrophage metabolism is reprogrammed, and efficient ATP production takes place through the mitochondrion. Ligand-receptor interactions between KC and hepatocytes reveal the role of apolipoproteins in sending the signal to LDLRs. LDLRs bind to LDLs, which are the primary carriers of cholesterol in the blood and possibly induce a whole-body metabolic challenge and further chronic diseases related to macrophage metabolism. This work shows how maternal lifestyle effects the innate immune system and proves the causative role of Kupffer cells in developmental programming and NASH.

References

1. Gluckman, P. D., Buklijas, T. & Hanson, M. A. The Developmental Origins of Health and Disease (DOHaD) Concept. in *The Epigenome and Developmental Origins of Health and Disease* 1–15 (Elsevier, 2016). doi:10.1016/B978-0-12-801383-0.00001-3.

2. Mandy, M. & Nyirenda, M. Developmental Origins of Health and Disease: the relevance to developing nations. *Int Health* **10**, (2018).

3. Lumey, L. *et al.* Cohort Profile: The Dutch Hunger Winter Families Study. *International Journal of Epidemiology* **36**, 1196–1204 (2007).

4. Gyllenhammer, L. E., Entringer, S., Buss, C. & Wadhwa, P. D. Developmental programming of mitochondrial biology: a conceptual framework and review. *Proceedings of the Royal Society B: Biological Sciences* **287**, 20192713 (2020).

5. Tain, Y.-L. & Hsu, C.-N. Developmental Programming of the Metabolic Syndrome: Can We Reprogram with Resveratrol? *International Journal of Molecular Sciences* **19**, 2584 (2018).

6. Balistreri, C. R., Garagnani, P., Madonna, R., Vaiserman, A. & Melino, G. Developmental programming of adult haematopoiesis system. *Ageing Research Reviews* **54**, 100918 (2019).

7. Balistreri, C. R., Garagnani, P., Madonna, R., Vaiserman, A. & Melino, G. Developmental programming of adult haematopoiesis system. *Ageing Research Reviews* **54**, 100918 (2019).

8. Friedman, J. E. Developmental Programming of Obesity and Diabetes in Mouse, Monkey, and Man in 2018: Where Are We Headed? *Diabetes* **67**, 2137–2151 (2018).

9. Hsu & Tain. The Good, the Bad, and the Ugly of Pregnancy Nutrients and Developmental Programming of Adult Disease. *Nutrients* **11**, 894 (2019).

10. Schulz, L. C. The Dutch Hunger Winter and the developmental origins of health and disease. *Proc Natl Acad Sci U S A* **107**, 16757–8 (2010).

11. Tobi, E. W. *et al.* DNA methylation signatures link prenatal famine exposure to growth and metabolism. *Nature Communications* **5**, 5592 (2014).

12. Bleker, L. S., de Rooij, S. R., Painter, R. C., Ravelli, A. C. & Roseboom, T. J. Cohort profile: the Dutch famine birth cohort (DFBC)— a prospective birth cohort study in the Netherlands. *BMJ Open* **11**, e042078 (2021).

13. Lumey, L. H., Ekamper, P., Bijwaard, G., Conti, G. & van Poppel, F. Overweight and obesity at age 19 after pre-natal famine exposure. *International Journal of Obesity* **45**, 1668–1676 (2021).

14. Fruh, S. M. Obesity. *J Am Assoc Nurse Pract* **29**, S3–S14 (2017).

15. Hedermann, G. *et al.* Maternal obesity and metabolic disorders associate with congenital heart defects in the offspring: A systematic review. *PLoS One* **16**, e0252343 (2021).

16. Strauss, A. *et al.* Obesity in pregnant women: a 20-year analysis of the German experience. *Eur J Clin Nutr* **75**, 1757–1763 (2021).

17. Denison, F. C. *et al.* Care of Women with Obesity in Pregnancy: Green-top Guideline No. 72. *BJOG* **126**, e62–e106 (2019).

18. Hedermann, G. *et al.* Maternal obesity and metabolic disorders associate with congenital heart defects in the offspring: A systematic review. *PLoS One* **16**, e0252343 (2021).

19. Chen, Y.-Y. & Yeh, M. M. Non-alcoholic fatty liver disease: A review with clinical and pathological correlation. *Journal of the Formosan Medical Association* **120**, 68–77 (2021).

20. Vuppalanchi, R. & Chalasani, N. Nonalcoholic fatty liver disease and nonalcoholic steatohepatitis: Selected practical issues in their evaluation and management. *Hepatology* **49**, 306–317 (2009).

21. Masuoka, H. C. & Chalasani, N. Nonalcoholic fatty liver disease: an emerging threat to obese and diabetic individuals. *Ann N Y Acad Sci* **1281**, 106–122 (2013).

22. Singh, S. *et al.* Fibrosis Progression in Nonalcoholic Fatty Liver vs Nonalcoholic Steatohepatitis: A Systematic Review and Meta-analysis of

Paired-Biopsy Studies. *Clinical Gastroenterology and Hepatology* **13**, 643-654.e9 (2015).

23. Sanal, M. G. Biomarkers in nonalcoholic fatty liver disease-the emperor has no clothes? *World Journal of Gastroenterology* **21**, 3223–3231 (2015).

24. Wu, X.-X. *et al.* acNASH index to diagnose nonalcoholic steatohepatitis: a prospective derivation and global validation study. *EClinicalMedicine* **41**, 101145 (2021).

25. Bertrando, S. & Vajro, P. NAFLD at the Interface of the Mother-Infant Dyad. *Current Pharmaceutical Design* **26**, 1119–1125 (2020).

26. Brumbaugh, D. E. & Friedman, J. E. Developmental origins of nonalcoholic fatty liver disease. *Pediatric Research* **75**, 140–147 (2014).

27. Thompson, M. D. Developmental Programming of <scp>NAFLD</scp> by Parental Obesity. *Hepatology Communications* **4**, 1392–1403 (2020).

28. Ludvigsson, J. F. & Lashkariani, M. Cohort profile: ESPRESSO (Epidemiology Strengthened by histoPathology Reports in Sweden). *Clin Epidemiol* **11**, 101–114 (2019).

29. Ayonrinde, O. T. *et al.* Infant nutrition and maternal obesity influence the risk of non-alcoholic fatty liver disease in adolescents. *Journal of Hepatology* **67**, 568–576 (2017).

30. Hagström, H. *et al.* Maternal obesity increases the risk and severity of NAFLD in offspring. *Journal of Hepatology* **75**, 1042–1048 (2021).

31. Ayonrinde, O. T. *et al.* Infant nutrition and maternal obesity influence the risk of non-alcoholic fatty liver disease in adolescents. *J Hepatol* **67**, 568–576 (2017).

32. Sekkarie, A. *et al.* Associations of maternal diet and nutritional status with offspring hepatic steatosis in the Avon longitudinal study of parents and children. *BMC Nutr* **7**, 28 (2021).

33. Li, Y., Pollock, C. A. & Saad, S. Aberrant DNA Methylation Mediates the Transgenerational Risk of Metabolic and Chronic Disease Due to Maternal Obesity and Overnutrition. *Genes (Basel)* **12**, 1653 (2021).

34. Szabo, G., Mandrekar, P. & Dolganiuc, A. Innate immune response and hepatic inflammation. *Semin Liver Dis* **27**, 339–50 (2007).

35. Gordillo, M., Evans, T. & Gouon-Evans, V. Orchestrating liver development. *Development* **142**, 2094–108 (2015).

36. Si-Tayeb, K., Lemaigre, F. P. & Duncan, S. A. Organogenesis and Development of the Liver. *Developmental Cell* **18**, 175–189 (2010).

37. Soares-da-Silva, F., Peixoto, M., Cumano, A. & Pinto-do-Ó, P. Crosstalk Between the Hepatic and Hematopoietic Systems During Embryonic Development. *Frontiers in Cell and Developmental Biology* **8**, (2020).

38. Giancotti *et al.* Functions and the Emerging Role of the Foetal Liver into Regenerative Medicine. *Cells* **8**, 914 (2019).

39. Lewis, K., Yoshimoto, M. & Takebe, T. Fetal liver hematopoiesis: from development to delivery. *Stem Cell Research & Therapy* **12**, 139 (2021).

40. Bonnardel, J. *et al.* Stellate Cells, Hepatocytes, and Endothelial Cells Imprint the Kupffer Cell Identity on Monocytes Colonizing the Liver Macrophage Niche. *Immunity* **51**, 638-654.e9 (2019).

41. Weston, C. J., Zimmermann, H. W. & Adams, D. H. The Role of Myeloid-Derived Cells in the Progression of Liver Disease. *Front Immunol* **10**, 893 (2019).

42. Krenkel, O. *et al.* Myeloid cells in liver and bone marrow acquire a functionally distinct inflammatory phenotype during obesity-related steatohepatitis. *Gut* **69**, 551–563 (2020).

43. Schulz, C. *et al.* A Lineage of Myeloid Cells Independent of Myb and Hematopoietic Stem Cells. *Science (1979)* **336**, 86–90 (2012).

44. Gomez Perdiguero, E. *et al.* Tissue-resident macrophages originate from yolk-sac-derived erythro-myeloid progenitors. *Nature* **518**, 547–551 (2015).

45. Mass, E. *et al.* Specification of tissue-resident macrophages during organogenesis. *Science (1979)* **353**, (2016).

46. Palis, J., Robertson, S., Kennedy, M., Wall, C. & Keller, G. Development of erythroid and myeloid progenitors in the yolk sac and embryo proper of the mouse. *Development* **126**, 5073–5084 (1999).

47. Kingsley, P. D., Malik, J., Fantauzzo, K. A. & Palis, J. Yolk sac–derived primitive erythroblasts enucleate during mammalian embryogenesis. *Blood* **104**, 19–25 (2004).

48. Freyer, L. *et al.* Fetal Hematopoiesis is Driven by Privileged Expansion and Differentiation of HSC-Independent Erythro-Myeloid Progenitors. *Nature journals - in Review* (2021).

49. Palis, J. Interaction of the Macrophage and Primitive Erythroid Lineages in the Mammalian Embryo. *Frontiers in Immunology* **7**, (2017).

50. Scott, C. L. *et al.* The Transcription Factor ZEB2 Is Required to Maintain the Tissue-Specific Identities of Macrophages. *Immunity* **49**, 312-325.e5 (2018).

51. Buttgereit, A. *et al.* Sall1 is a transcriptional regulator defining microglia identity and function. *Nature Immunology* **17**, 1397–1406 (2016).

52. Nguyen-Lefebvre, A. T. & Horuzsko, A. Kupffer Cell Metabolism and Function. *J Enzymol Metab* **1**,.

53. Scott, C. L. & Guilliams, M. The role of Kupffer cells in hepatic iron and lipid metabolism. *Journal of Hepatology* **69**, 1197–1199 (2018).

54. Kanamori, Y. *et al.* Iron-rich Kupffer cells exhibit phenotypic changes during the development of liver fibrosis in NASH. *iScience* **24**, 102032 (2021).

55. Wen, Y., Lambrecht, J., Ju, C. & Tacke, F. Hepatic macrophages in liver homeostasis and diseases-diversity, plasticity and therapeutic opportunities. *Cellular & Molecular Immunology* **18**, 45–56 (2021).

56. Roohani, S. & Tacke, F. Liver Injury and the Macrophage Issue: Molecular and Mechanistic Facts and Their Clinical Relevance. *International Journal of Molecular Sciences* **22**, 7249 (2021).

57. Ramachandran, P. *et al.* Resolving the fibrotic niche of human liver cirrhosis at single-cell level. *Nature* **575**, 512–518 (2019).

58. Jaitin, D. A. *et al.* Lipid-Associated Macrophages Control Metabolic Homeostasis in a Trem2-Dependent Manner. *Cell* **178**, 686-698.e14 (2019).

59. Sierro, F. *et al.* A Liver Capsular Network of Monocyte-Derived Macrophages Restricts Hepatic Dissemination of Intraperitoneal Bacteria by Neutrophil Recruitment. *Immunity* **47**, 374-388.e6 (2017).

60. Schulz, D., Severin, Y., Zanotelli, V. R. T. & Bodenmiller, B. In-Depth Characterization of Monocyte-Derived Macrophages using a Mass Cytometry-Based Phagocytosis Assay. *Scientific Reports* **9**, 1925 (2019).

61. Nahrendorf, M. & Swirski, F. K. Abandoning M1/M2 for a Network Model of Macrophage Function. *Circulation Research* **119**, 414–417 (2016).

62. Helm, O., Held-Feindt, J., Schäfer, H. & Sebens, S. M1 and M2: there is no “good” and “bad”—How macrophages promote malignancy-associated features in tumorigenesis. *OncoImmunology* **3**, e946818 (2014).

63. Scott, C. L. *et al.* Bone marrow-derived monocytes give rise to self-renewing and fully differentiated Kupffer cells. *Nature Communications* **7**, 10321 (2016).

64. Shemer, A. *et al.* Engrafted parenchymal brain macrophages differ from microglia in transcriptome, chromatin landscape and response to challenge. *Nature Communications* **9**, 5206 (2018).

65. van de Laar, L. *et al.* Yolk Sac Macrophages, Fetal Liver, and Adult Monocytes Can Colonize an Empty Niche and Develop into Functional Tissue-Resident Macrophages. *Immunity* **44**, 755–768 (2016).

66. Guilliams, M. & Svedberg, F. R. Does tissue imprinting restrict macrophage plasticity? *Nature Immunology* **22**, 118–127 (2021).

67. Hashimoto, D. *et al.* Tissue-Resident Macrophages Self-Maintain Locally throughout Adult Life with Minimal Contribution from Circulating Monocytes. *Immunity* **38**, 792–804 (2013).

68. Viola, A., Munari, F., Sánchez-Rodríguez, R., Scolaro, T. & Castegna, A. The Metabolic Signature of Macrophage Responses. *Frontiers in Immunology* **10**, (2019).

69. Iacobini, C., Vitale, M., Pugliese, G. & Menini, S. Normalizing HIF-1α Signaling Improves Cellular Glucose Metabolism and Blocks the Pathological Pathways of Hyperglycemic Damage. *Biomedicines* **9**, 1139 (2021).

70. Netea, M. G. *et al.* Defining trained immunity and its role in health and disease. *Nature Reviews Immunology* **20**, 375–388 (2020).

71. van den Bossche, J., Baardman, J. & de Winther, M. P. J. Metabolic Characterization of Polarized M1 and M2 Bone Marrow-derived Macrophages Using Real-time Extracellular Flux Analysis. *J Vis Exp* (2015) doi:10.3791/53424.

72. Tan, Z. *et al.* Pyruvate dehydrogenase kinase 1 participates in macrophage polarization via regulating glucose metabolism. *J Immunol* **194**, 6082–9 (2015).

73. Cruz-Carrillo, G. & Camacho-Morales, A. Metabolic Flexibility Assists Reprograming of Central and Peripheral Innate Immunity During Neurodevelopment. *Molecular Neurobiology* **58**, 703–718 (2021).

74. Kwon, E. J. & Kim, Y. J. What is fetal programming?: a lifetime health is under the control of in utero health. *Obstetrics & Gynecology Science* **60**, 506 (2017).

75. Magalhaes, M. S., Potter, H. G., Ahlback, A. & Gentek, R. Developmental programming of macrophages by early life adversity. in 213–259 (2022). doi:10.1016/bs.ircmb.2022.02.003.

76. Mass, E. & Gentek, R. Fetal-Derived Immune Cells at the Roots of Lifelong Pathophysiology. *Frontiers in Cell and Developmental Biology* **9**, (2021).

77. Fernandez-Twinn, D. S. *et al.* Exercise rescues obese mothers' insulin sensitivity, placental hypoxia and male offspring insulin sensitivity. *Scientific Reports* **7**, 44650 (2017).

78. Giussani, D. A. Breath of Life: Heart Disease Link to Developmental Hypoxia. *Circulation* **144**, 1429–1443 (2021).

79. Gohir, W. *et al.* High-fat diet intake modulates maternal intestinal adaptations to pregnancy and results in placental hypoxia, as well as altered fetal gut barrier proteins and immune markers. *The Journal of Physiology* **597**, 3029–3051 (2019).

80. Åmark, H., Sirotkina, M., Westgren, M., Papadogiannakis, N. & Persson, M. Is obesity in pregnancy associated with signs of chronic fetal hypoxia? *Acta Obstetricia et Gynecologica Scandinavica* **99**, 1649–1656 (2020).

81. Cerychova, R. & Pavlinkova, G. HIF-1, Metabolism, and Diabetes in the Embryonic and Adult Heart. *Frontiers in Endocrinology* **9**, (2018).

82. Baker, P. R. & Friedman, J. E. Mitochondrial role in the neonatal predisposition to developing nonalcoholic fatty liver disease. *Journal of Clinical Investigation* **128**, 3692–3703 (2018).

83. Abate, M. *et al.* Mitochondria as playmakers of apoptosis, autophagy and senescence. *Seminars in Cell & Developmental Biology* **98**, 139–153 (2020).

84. Malin Jessen. Developmental Programming of Kupffer Cells by Maternal Obesity. Pre- and Perinatal Effects. (2021).

85. Kern, P. *et al.* Creld2 function during unfolded protein response is essential for liver metabolism homeostasis. *The FASEB Journal* **35**, (2021).

86. Byers, S. L., Wiles, M. v., Dunn, S. L. & Taft, R. A. Mouse Estrous Cycle Identification Tool and Images. *PLoS ONE* **7**, e35538 (2012).

87. Picelli, S. *et al.* Full-length RNA-seq from single cells using Smart-seq2. *Nature Protocols* **9**, 171–181 (2014).

88. Bray, N. L., Pimentel, H., Melsted, P. & Pachter, L. Near-optimal probabilistic RNA-seq quantification. *Nature Biotechnology* **34**, 525–527 (2016).

89. Love, M. I., Huber, W. & Anders, S. Moderated estimation of fold change and dispersion for RNA-seq data with DESeq2. *Genome Biology* **15**, 550 (2014).

90. Ignatiadis, N., Klaus, B., Zaugg, J. B. & Huber, W. Data-driven hypothesis weighting increases detection power in genome-scale multiple testing. *Nature Methods* **13**, 577–580 (2016).

91. Ulas, T. Cocena2 workflow: https://github.com/Ulas-lab/CoCena2. *2020*.

92. Ritchie, M. E. *et al.* limma powers differential expression analyses for RNA-sequencing and microarray studies. *Nucleic Acids Research* **43**, e47–e47 (2015).

93. Shao, X. *et al.* CellTalkDB: a manually curated database of ligand–receptor interactions in humans and mice. *Briefings in Bioinformatics* **22**, (2021).

94. Browaeys, R., Saelens, W. & Saeys, Y. NicheNet: modeling intercellular communication by linking ligands to target genes. *Nature Methods* **17**, 159–162 (2020).

95. Schomburg, I. BRENDA, enzyme data and metabolic information. *Nucleic Acids Research* **30**, 47–49 (2002).

96. Bouhaddani, S. el *et al.* Integrating omics datasets with the OmicsPLS package. *BMC Bioinformatics* **19**, 371 (2018).

97. Bouhaddani, S. el *et al.* Evaluation of O2PLS in Omics data integration. *BMC Bioinformatics* **17**, S11 (2016).

98. Hagström, H. *et al.* Maternal obesity increases the risk and severity of NAFLD in offspring. *Journal of Hepatology* **75**, 1042–1048 (2021).

99. Mouralidarane, A. *et al.* Maternal obesity programs offspring nonalcoholic fatty liver disease by innate immune dysfunction in mice. *Hepatology* **58**, 128–138 (2013).

100. Alfaradhi, M. Z. *et al.* Oxidative stress and altered lipid homeostasis in the programming of offspring fatty liver by maternal obesity. *American Journal of Physiology-Regulatory, Integrative and Comparative Physiology* **307**, R26–R34 (2014).

101. Puppala, S. *et al.* Primate fetal hepatic responses to maternal obesity: epigenetic signalling pathways and lipid accumulation. *The Journal of Physiology* **596**, 5823–5837 (2018).

102. Zhu, N. *et al.* Metabolomic Study of High-Fat Diet-Induced Obese (DIO) and DIO Plus CCl4-Induced NASH Mice and the Effect of Obeticholic Acid. *Metabolites* **11**, (2021).

103. Montandon, S. A. *et al.* Multi-technique comparison of atherogenic and MCD NASH models highlights changes in sphingolipid metabolism. *Scientific Reports* **9**, 16810 (2019).

104. Simon, J. *et al.* Sphingolipids in Non-Alcoholic Fatty Liver Disease and Hepatocellular Carcinoma: Ceramide Turnover. *Int J Mol Sci* **21**, (2019).

105. Ge, S. *et al.* Myd88 in Macrophages Enhances Liver Fibrosis by Activation of NLRP3 Inflammasome in HSCs. *International Journal of Molecular Sciences* **22**, 12413 (2021).

106. He, Y. *et al.* Silencing HIF-1α aggravates non-alcoholic fatty liver disease in vitro through inhibiting PPAR-α/ANGPTL4 singling pathway. *Gastroenterologia y hepatologia* **44**, 355–365 (2021).

107. Wolfe, C. M., Fitz, N. F., Nam, K. N., Lefterov, I. & Koldamova, R. The Role of APOE and TREM2 in Alzheimer's Disease-Current Understanding and Perspectives. *Int J Mol Sci* **20**, (2018).

108. Keren-Shaul, H. *et al.* A Unique Microglia Type Associated with Restricting Development of Alzheimer's Disease. *Cell* **169**, 1276-1290.e17 (2017).

109. Yeh, F. L., Wang, Y., Tom, I., Gonzalez, L. C. & Sheng, M. TREM2 Binds to Apolipoproteins, Including APOE and CLU/APOJ, and Thereby Facilitates Uptake of Amyloid-Beta by Microglia. *Neuron* **91**, 328–340 (2016).

110. Bailey, C. C., DeVaux, L. B. & Farzan, M. The Triggering Receptor Expressed on Myeloid Cells 2 Binds Apolipoprotein E. *Journal of Biological Chemistry* **290**, 26033–26042 (2015).

111. Atagi, Y. *et al.* Apolipoprotein E Is a Ligand for Triggering Receptor Expressed on Myeloid Cells 2 (TREM2). *Journal of Biological Chemistry* **290**, 26043–26050 (2015).

112. Pirola, C. J. *et al.* Epigenetic modification of liver mitochondrial DNA is associated with histological severity of nonalcoholic fatty liver disease. *Gut* **62**, 1356–1363 (2013).

113. Demir, D. *et al.* Mitochondrial ATPase Subunit 6 and Cytochrome B Gene Variations in Obese Turkish Children. *Journal of Clinical Research in Pediatric Endocrinology* **6**, 209–215 (2014).

114. Jones, R. *et al.* Mitochondrial and glycolysis-regulatory gene expression profiles are associated with intrauterine growth restriction. *The Journal of Maternal-Fetal & Neonatal Medicine* 1–10 (2018) doi:10.1080/14767058.2018.1518419.

115. Sookoian, S. *et al.* Mitochondrial genome architecture in non-alcoholic fatty liver disease. *The Journal of Pathology* **240**, 437–449 (2016).

116. Nicholls, T. J., Rorbach, J. & Minczuk, M. Mitochondria: Mitochondrial RNA metabolism and human disease. *The International Journal of Biochemistry & Cell Biology* **45**, 845–849 (2013).

117. Prasun, P. Mitochondrial dysfunction in metabolic syndrome. *Biochimica et Biophysica Acta (BBA) - Molecular Basis of Disease* **1866**, 165838 (2020).

118. Medini, H., Cohen, T. & Mishmar, D. Mitochondrial gene expression in single cells shape pancreatic beta cells' sub-populations and explain variation in insulin pathway. *Scientific Reports* **11**, 466 (2021).

119. Ma, Z. *et al.* Targeting hypoxia-inducible factor-1, for cancer treatment: Recent advances in developing small-molecule inhibitors from natural compounds. *Seminars in Cancer Biology* (2020) doi:10.1016/j.semcancer.2020.09.011.

120. Giaccia, A., Siim, B. G. & Johnson, R. S. HIF-1 as a target for drug development. *Nature Reviews Drug Discovery* **2**, 803–811 (2003).

121. Wheeler, M. C. & Gekakis, N. Hsp90 modulates PPARγ activity in a mouse model of nonalcoholic fatty liver disease. *Journal of Lipid Research* **55**, 1702–1710 (2014).

122. Luong, X. G. *et al.* Regulation of gene transcription by thyroid hormone receptor β agonists in clinical development for the treatment of non-alcoholic steatohepatitis (NASH). *PLoS One* **15**, e0240338 (2020).

123. Zhou, X. *et al.* Metformin suppresses hypoxia-induced stabilization of HIF-1α through reprogramming of oxygen metabolism in hepatocellular carcinoma. *Oncotarget* **7**, 873–884 (2016).

124. Cerychova, R. *et al.* Adverse effects of Hif1a mutation and maternal diabetes on the offspring heart. *Cardiovascular Diabetology* **17**, 68 (2018).

125. Liang, X. *et al.* Maternal obesity epigenetically alters visceral fat progenitor cell properties in male offspring mice. *The Journal of Physiology* **594**, 4453–4466 (2016).

126. O'Hara, S. E., Gembus, K. M. & Nicholas, L. M. Understanding the Long-Lasting Effects of Fetal Nutrient Restriction versus Exposure to an Obesogenic Diet on Islet-Cell Mass and Function. *Metabolites* **11**, 514 (2021).

Appendix A: WT GSEA Significantly enriched mechanisms - green

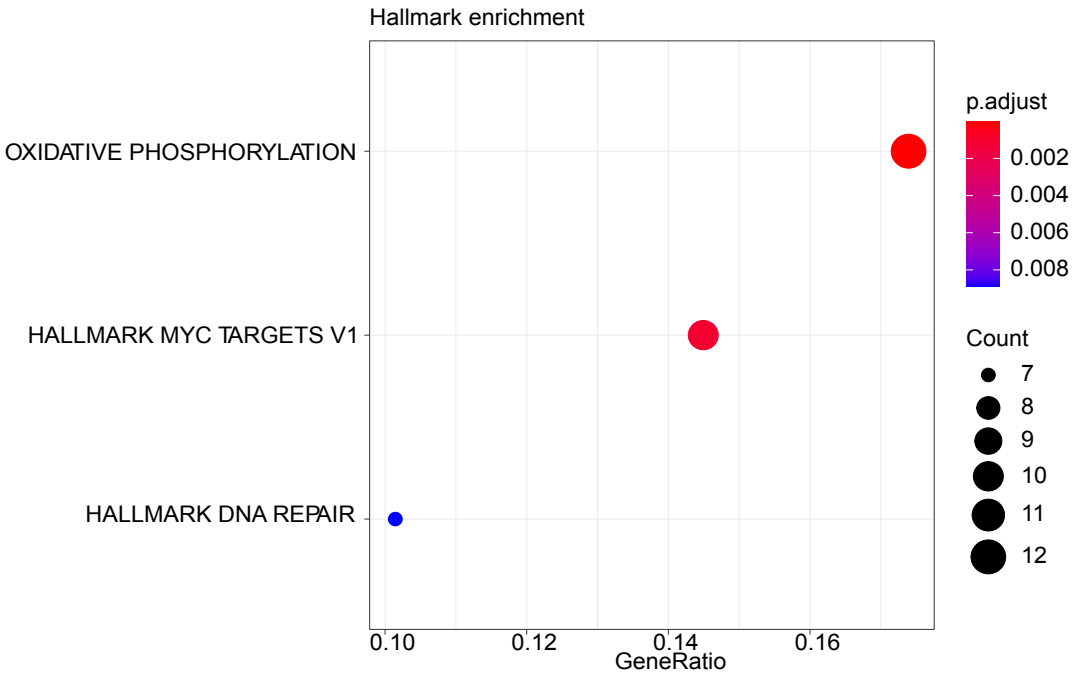

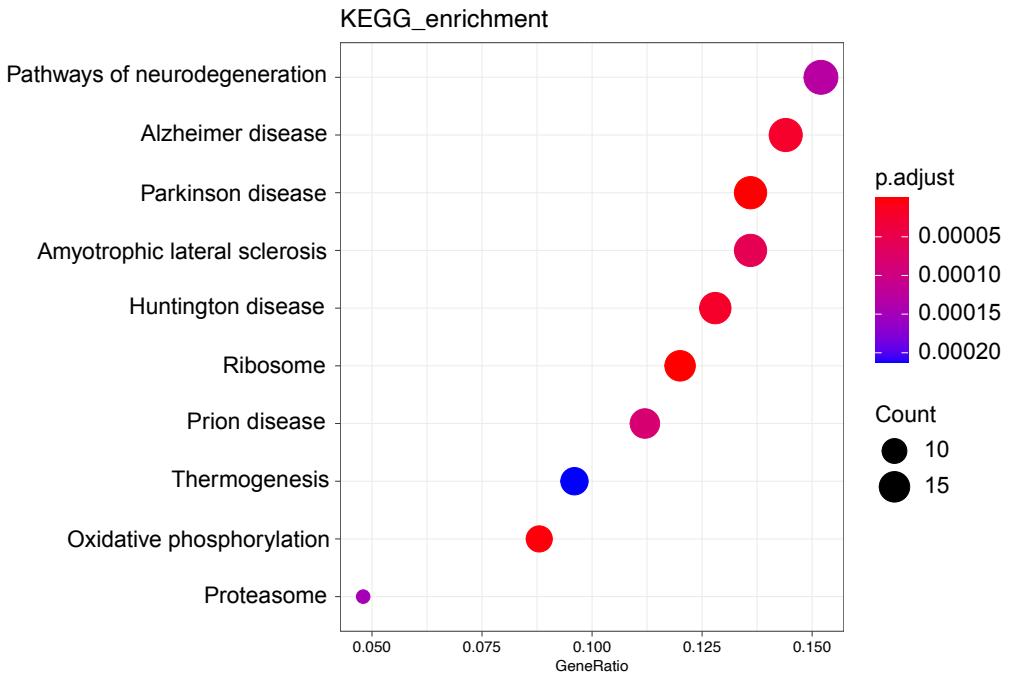

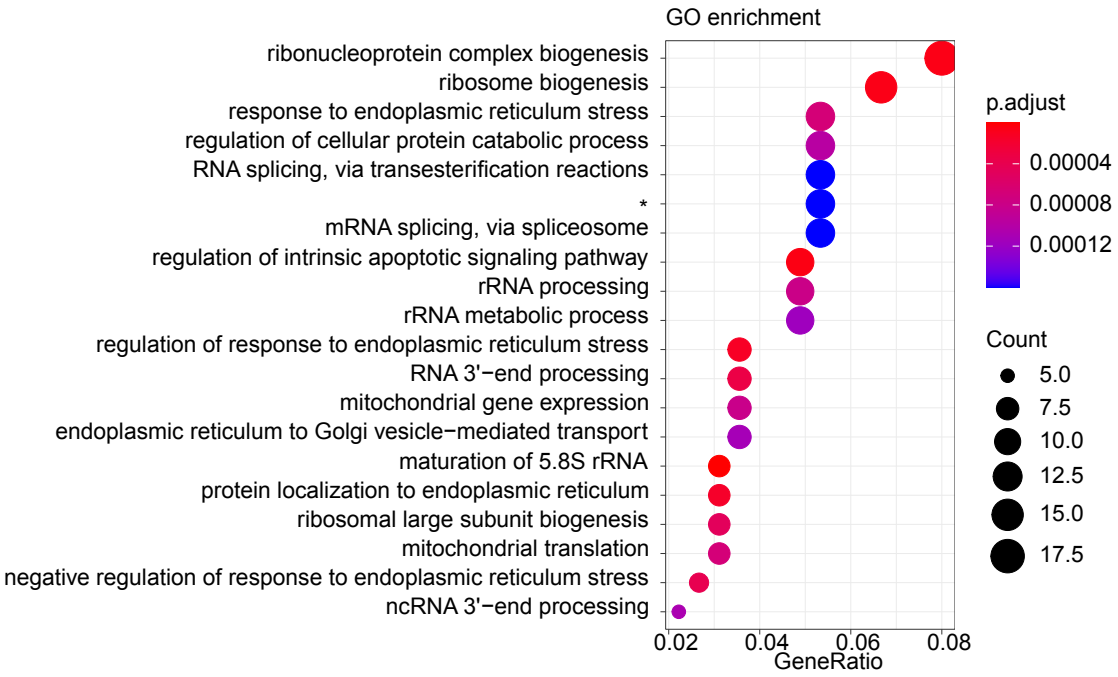

*RNA splicing, via transesterification reactions with bulged adenosine as nucleophile

Appendix A: Gene set enrichment analysis of the CO-CENA green cluster
Automatized gene set enrichment analysis (GSEA) plots of the WT maternal obesity dataset, belonging to the CO-CENA clusters (Figure 5 and Figure 16). GSEA plots belong to cluster green and contains all significantly enriched mechanisms ($p<0.05$). GSEA was performed with the following datasets: Hallmark, KEGG, GO, Reactome, Disease. On every plot, Y axis indicates the significantly enriched mechanisms and X axis shows the gene-ratio (number of genes from the specific CO-CENA cluster, which were enriched to the indicated mechanism, divided by the number of genes classified to the mechanism according to the dataset). The size of the dots relate to the number of enriched genes (counts) and the color code is defined by the adjusted p-value (p-adjust).

Appendix B: WT GSEA Significantly enriched mechanisms - grey

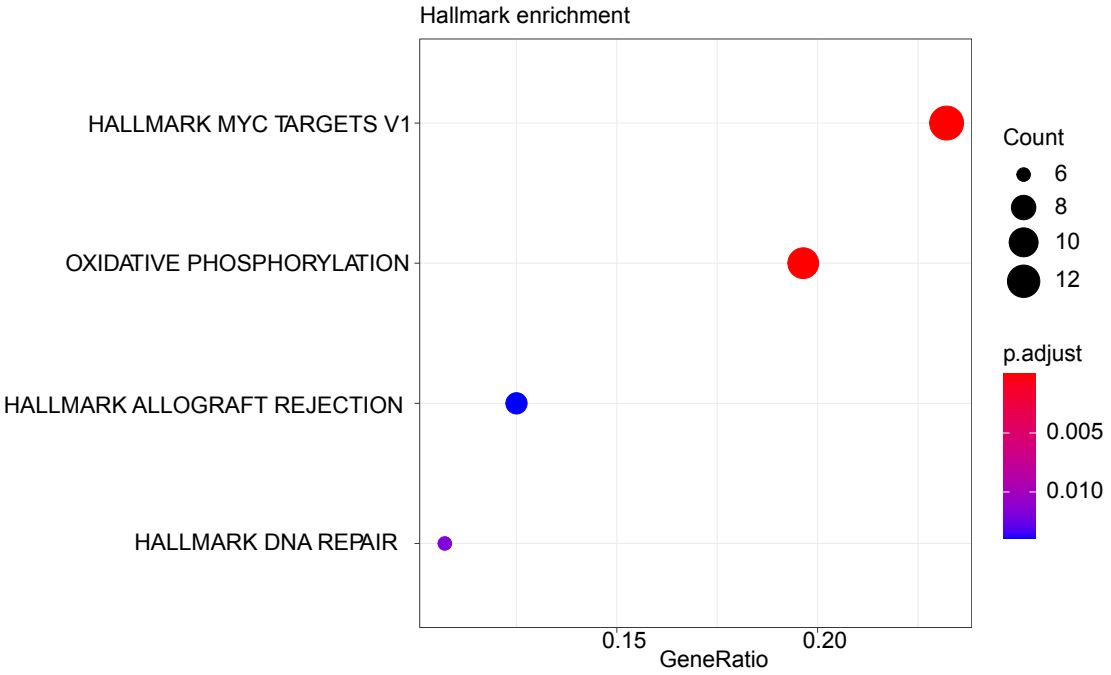

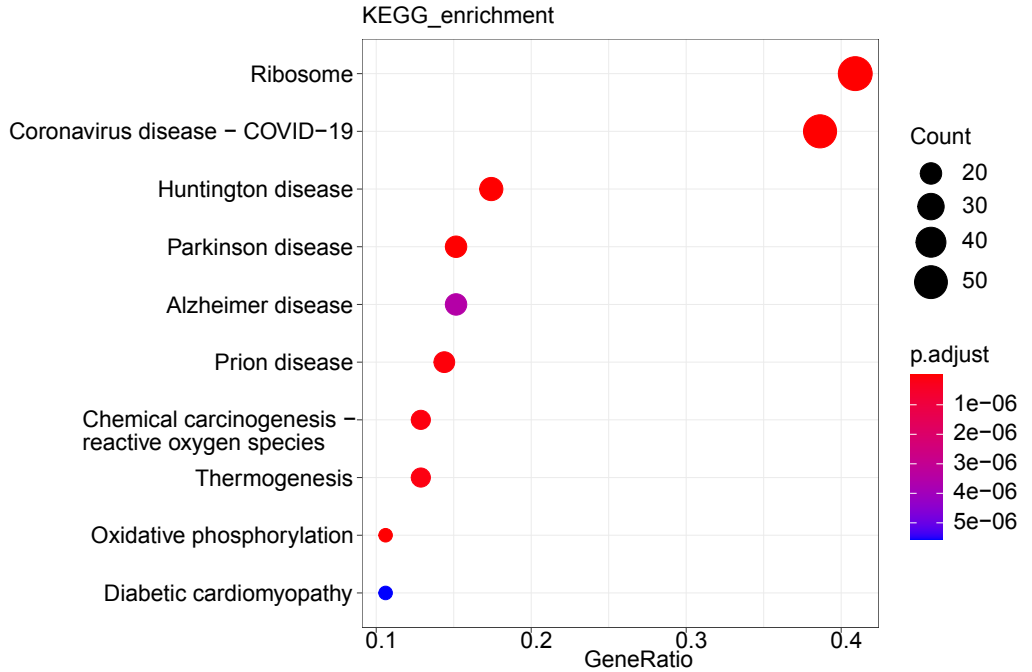

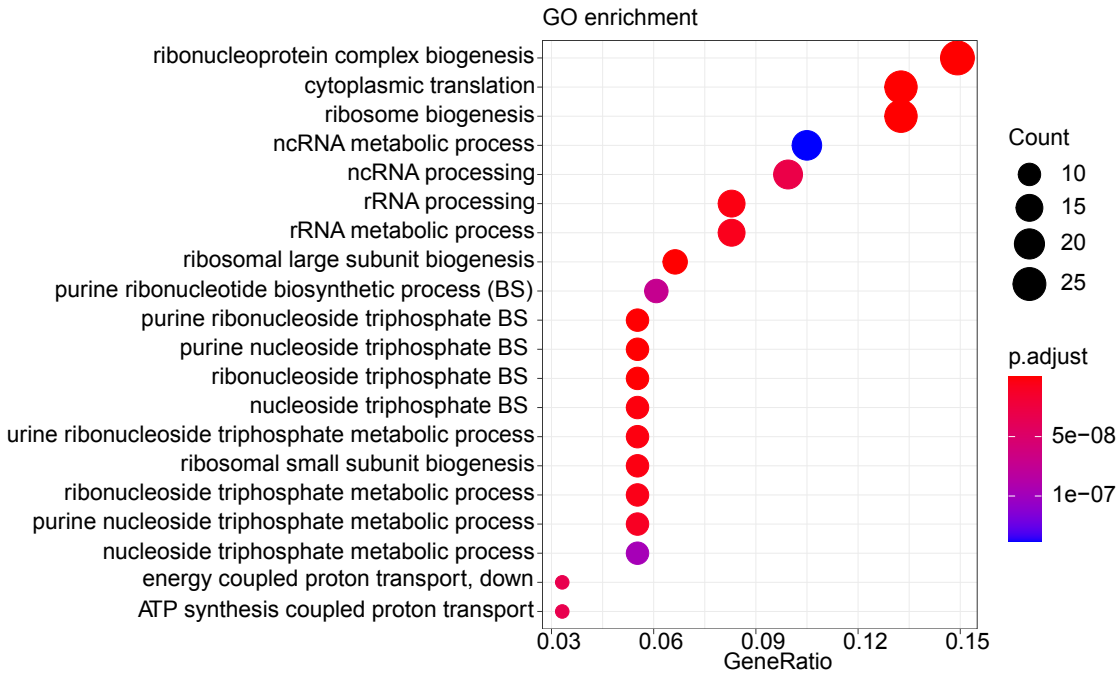
GO enrichment
ribonucleoprotein complex biogenesis
cytoplasmic translation
ribosome biogenesis
ncRNA metabolic process
ncRNA processing
rRNA processing
rRNA metabolic process
ribosomal large subunit biogenesis
purine ribonucleotide biosynthetic process (BS)
purine ribonucleoside triphosphate BS
purine nucleoside triphosphate BS
ribonucleoside triphosphate BS
nucleoside triphosphate BS
urine ribonucleoside triphosphate metabolic process
ribosomal small subunit biogenesis
ribonucleoside triphosphate metabolic process
purine nucleoside triphosphate metabolic process
nucleoside triphosphate metabolic process
energy coupled proton transport, down
ATP synthesis coupled proton transport
0.03
0.06
0.09
0.12
0.15
GeneRatio
Count
10
15
20
25
p.adjust
5e−08
1e−07

Appendix B: Gene set enrichment analysis of the CO-CENA grey cluster
Automatized gene set enrichment analysis (GSEA) plots of the WT maternal obesity dataset, belonging to the CO-CENA clusters (Figure 5 and Figure 16). GSEA plots belong to cluster grey and contains all significantly enriched mechanisms ($p<0.05$). GSEA was performed with the following datasets: Hallmark, KEGG, GO, Reactome, Disease. On every plot, Y axis indicates the significantly enriched mechanisms and X axis shows the gene-ratio (number of genes from the specific CO-CENA cluster, which were enriched to the indicated mechanism, divided by the number of genes classified to the mechanism according to the dataset). The size of the dots relate to the number of enriched genes (counts) and the color code is defined by the adjusted p-value (p-adjust).

Appendix C: WT GSEA Significantly enriched mechanisms - orange

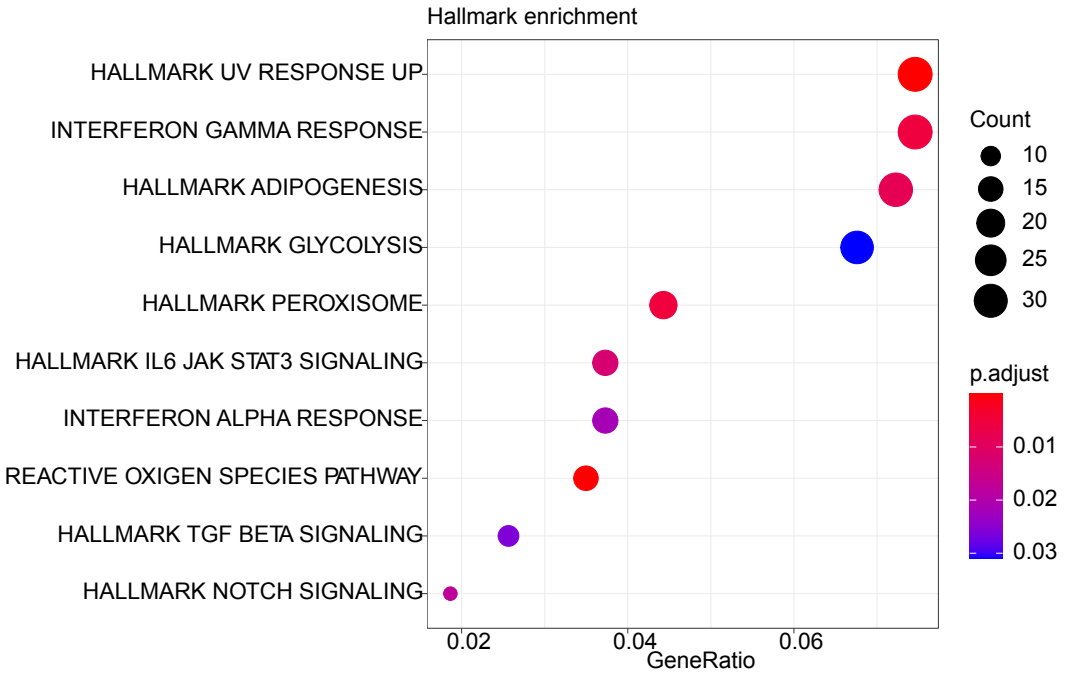

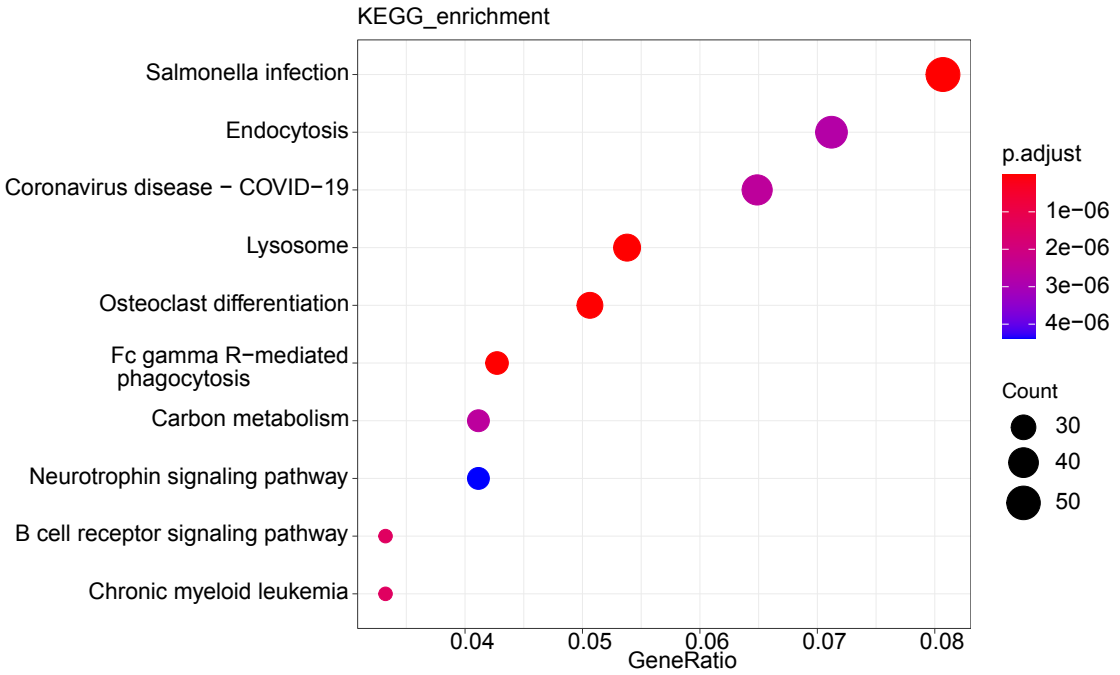

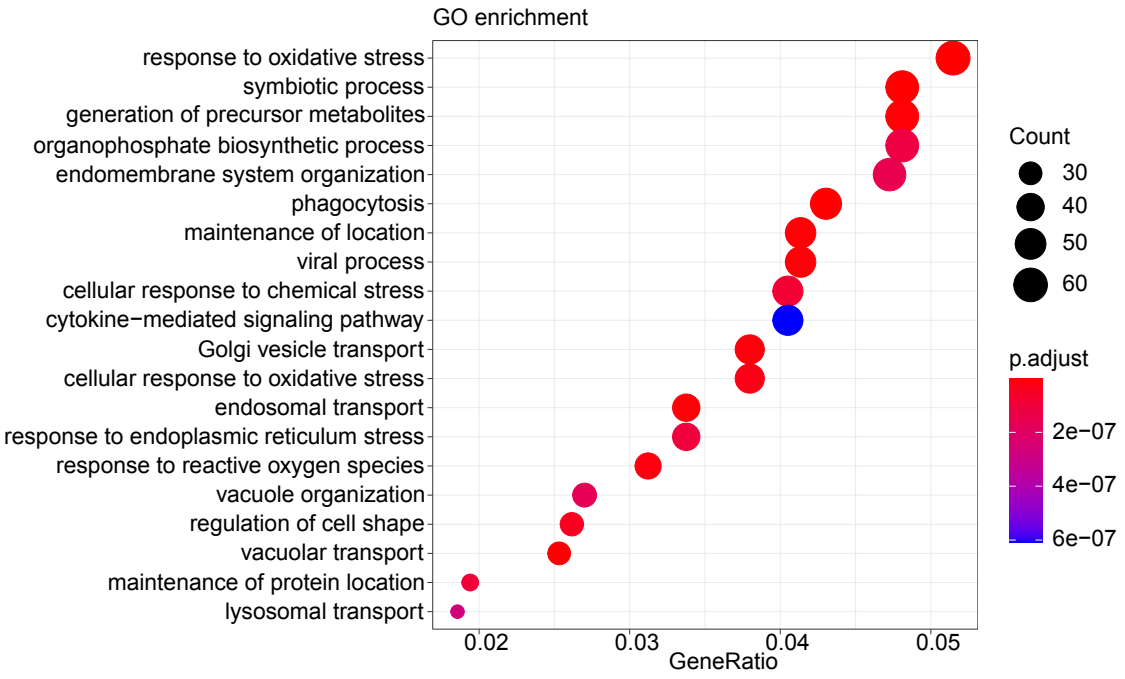
GO enrichment
response to oxidative stress
symbiotic process
generation of precursor metabolites
organophosphate biosynthetic process
endomembrane system organization
phagocytosis
maintenance of location
viral process
cellular response to chemical stress
cytokine−mediated signaling pathway
Golgi vesicle transport
cellular response to oxidative stress
endosomal transport
response to endoplasmic reticulum stress
response to reactive oxygen species
vacuole organization
regulation of cell shape
vacuolar transport
maintenance of protein location
lysosomal transport
0.02
0.03
0.04
0.05
GeneRatio
Count
30
40
50
60
p.adjust
2e−07
4e−07
6e−07

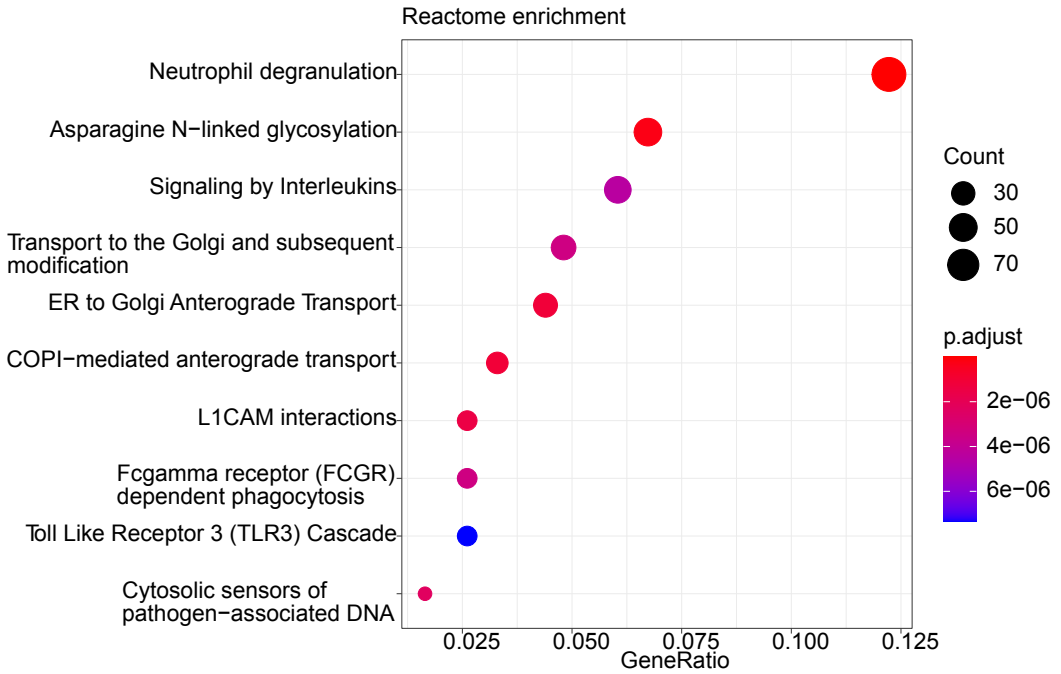

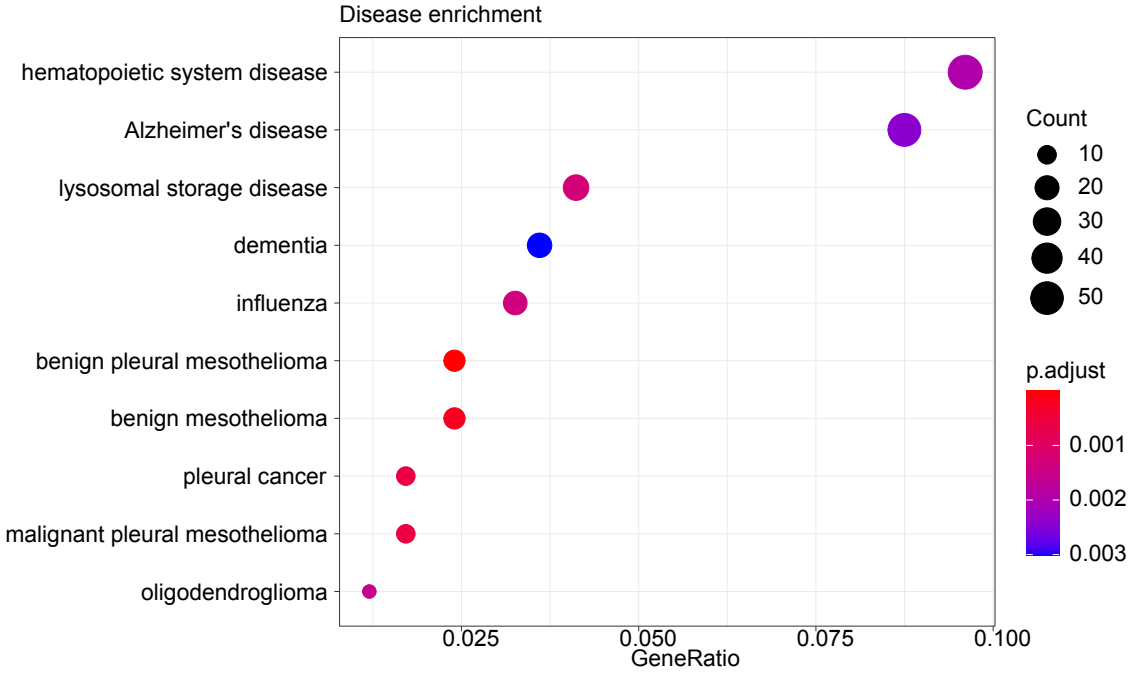

Appendix C: Gene set enrichment analysis of the CO-CENA orange cluster
Automatized gene set enrichment analysis (GSEA) plots of the WT maternal obesity dataset, belonging to the CO-CENA clusters (Figure 5 and Figure 16). GSEA plots belong to cluster orange and contains all significantly enriched mechanisms ($p<0.05$). GSEA was performed with the following datasets: Hallmark, KEGG, GO, Reactome, Disease. On every plot, Y axis indicates the significantly enriched mechanisms and X axis shows the gene-ratio (number of genes from the specific CO-CENA cluster, which were enriched to the indicated mechanism, divided by the number of genes classified to the mechanism according to the dataset). The size of the dots relate to the number of enriched genes (counts) and the color code is defined by the adjusted p-value (p-adjust).

Appendix D: WT GSEA Significantly enriched mechanisms - gold

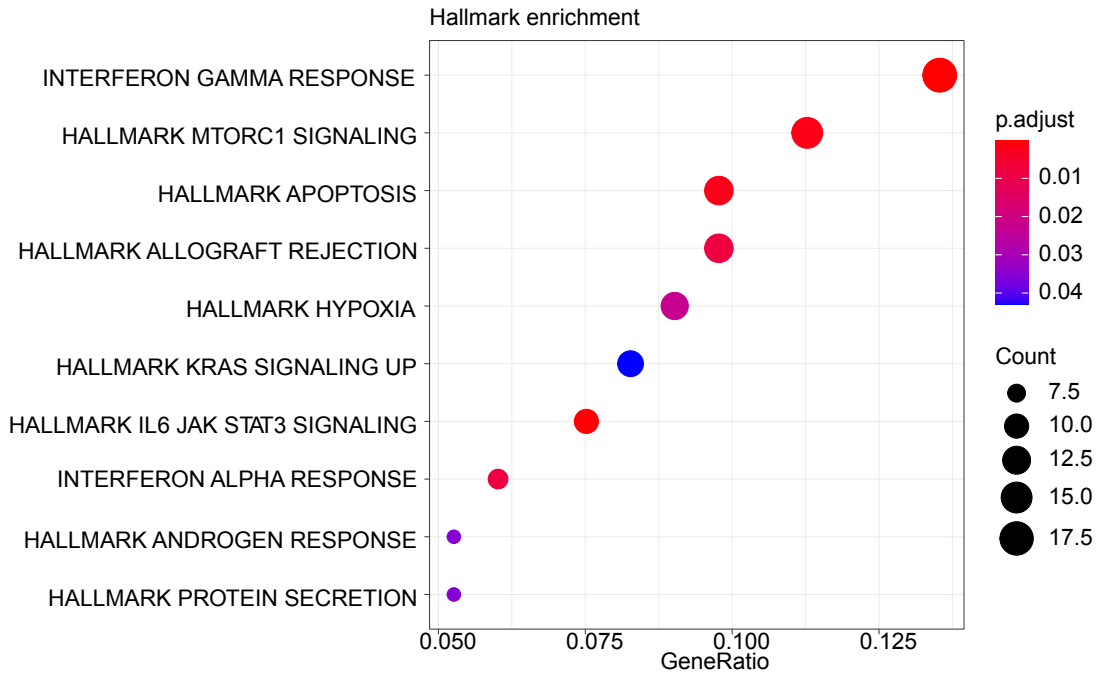

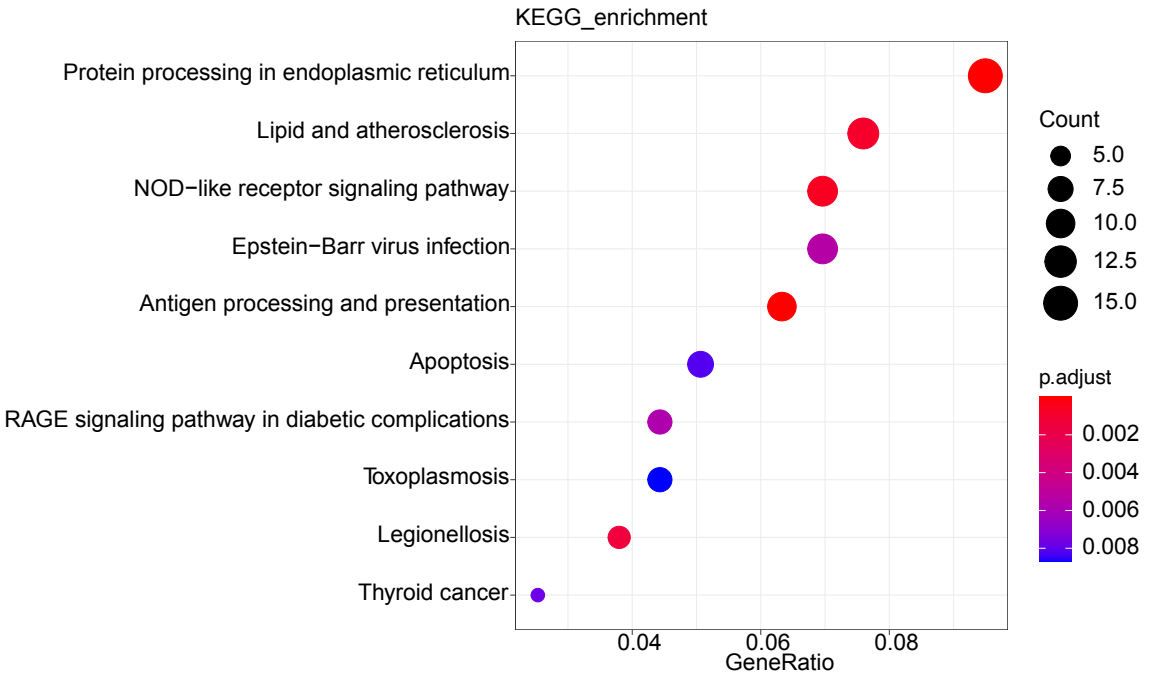

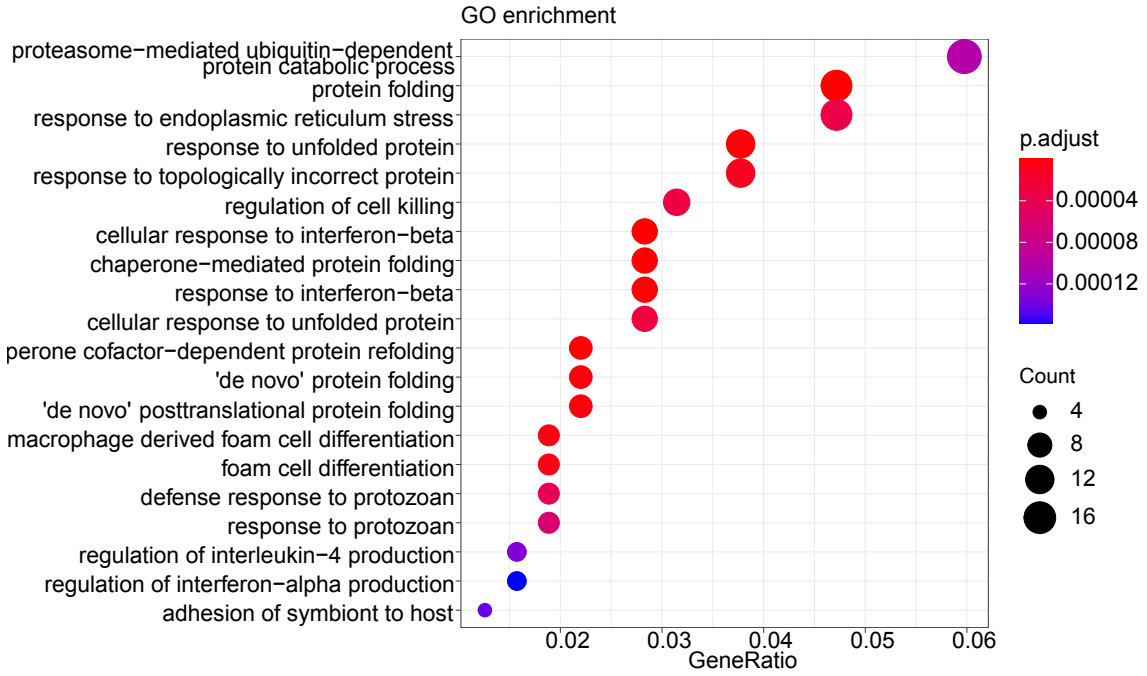
GO enrichment
proteasome−mediated ubiquitin−dependent protein catabolic process
protein folding
response to endoplasmic reticulum stress
response to unfolded protein
response to topologically incorrect protein
regulation of cell killing
cellular response to interferon−beta
chaperone−mediated protein folding
response to interferon−beta
cellular response to unfolded protein
perone cofactor−dependent protein refolding
'de novo' protein folding
'de novo' posttranslational protein folding
macrophage derived foam cell differentiation
foam cell differentiation
defense response to protozoan
response to protozoan
regulation of interleukin−4 production
regulation of interferon−alpha production
adhesion of symbiont to host
0.02
0.03
0.04
0.05
0.06
GeneRatio
p.adjust
0.00004
0.00008
0.00012
Count
4
8
12
16

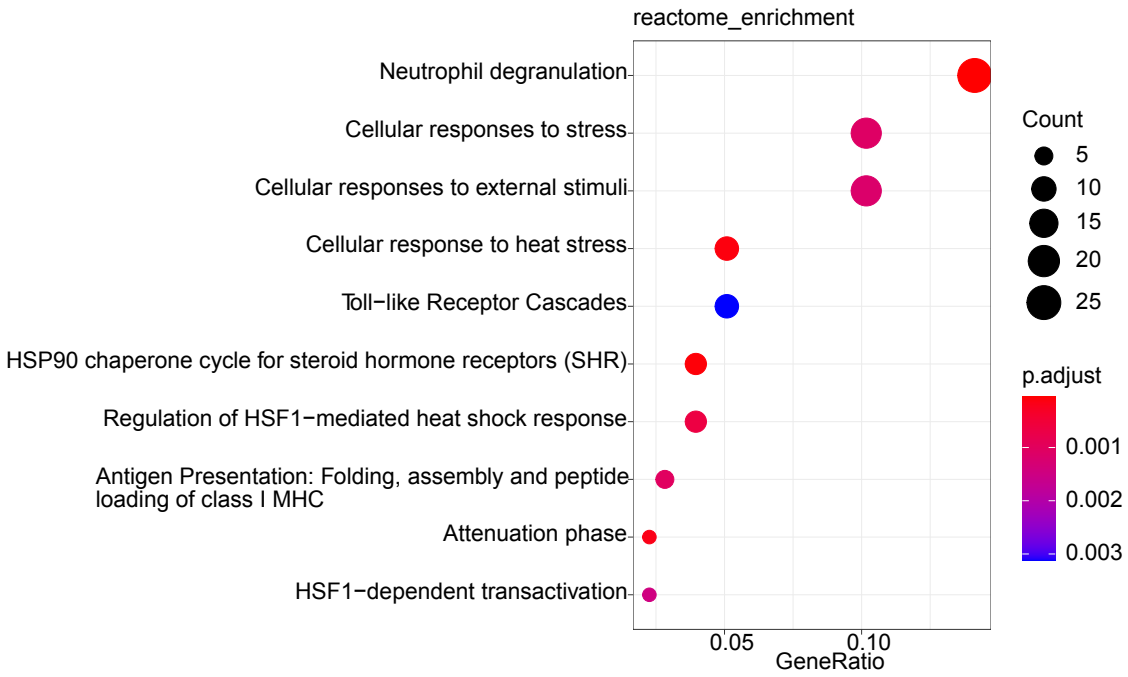

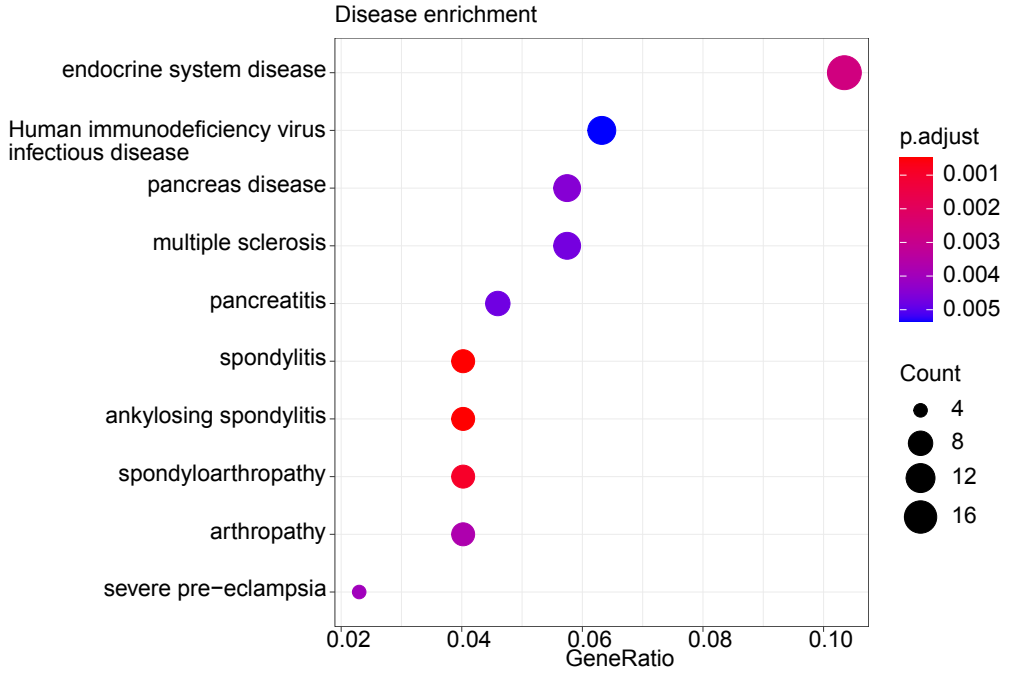

Appendix D: Gene set enrichment analysis of the CO-CENA gold cluster
Automatized gene set enrichment analysis (GSEA) plots of the WT maternal obesity dataset, belonging to the CO-CENA clusters (Figure 5 and Figure 16). GSEA plots belong to cluster gold and contains all significantly enriched mechanisms ($p<0.05$). GSEA was performed with the following datasets: Hallmark, KEGG, GO, Reactome, Disease. On every plot, Y axis indicates the significantly enriched mechanisms and X axis shows the gene-ratio (number of genes from the specific CO-CENA cluster, which were enriched to the indicated mechanism, divided by the number of genes classified to the mechanism according to the dataset). The size of the dots relate to the number of enriched genes (counts) and the color code is defined by the adjusted p-value (p-adjust).

Appendix E: WT GSEA Significantly enriched mechanisms - maroon

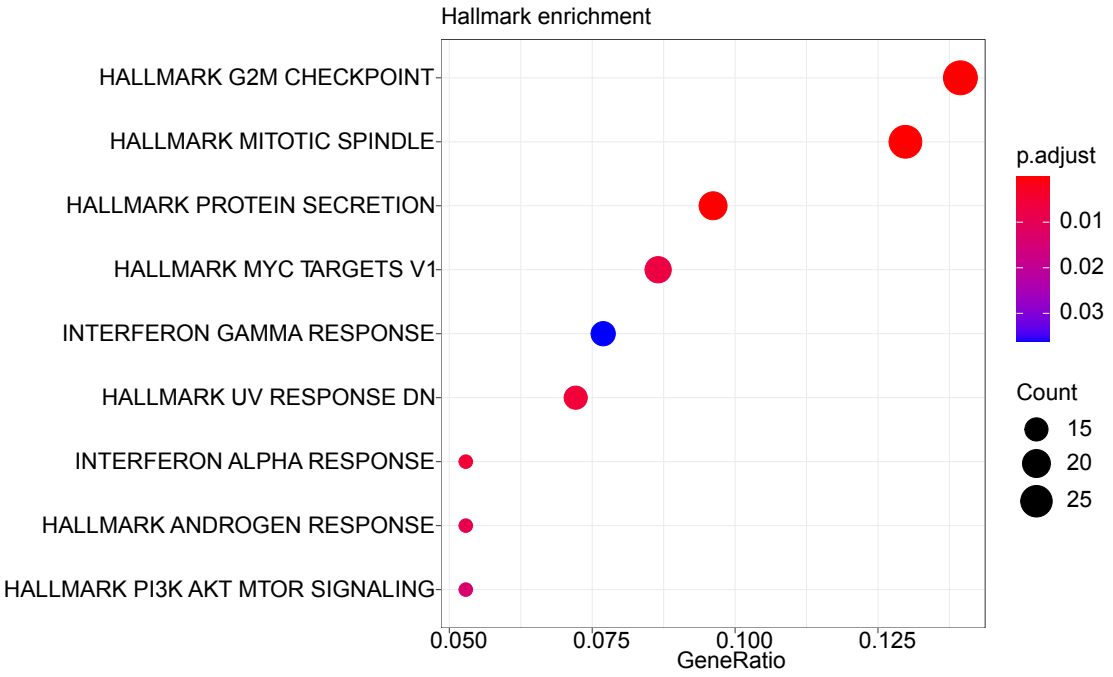

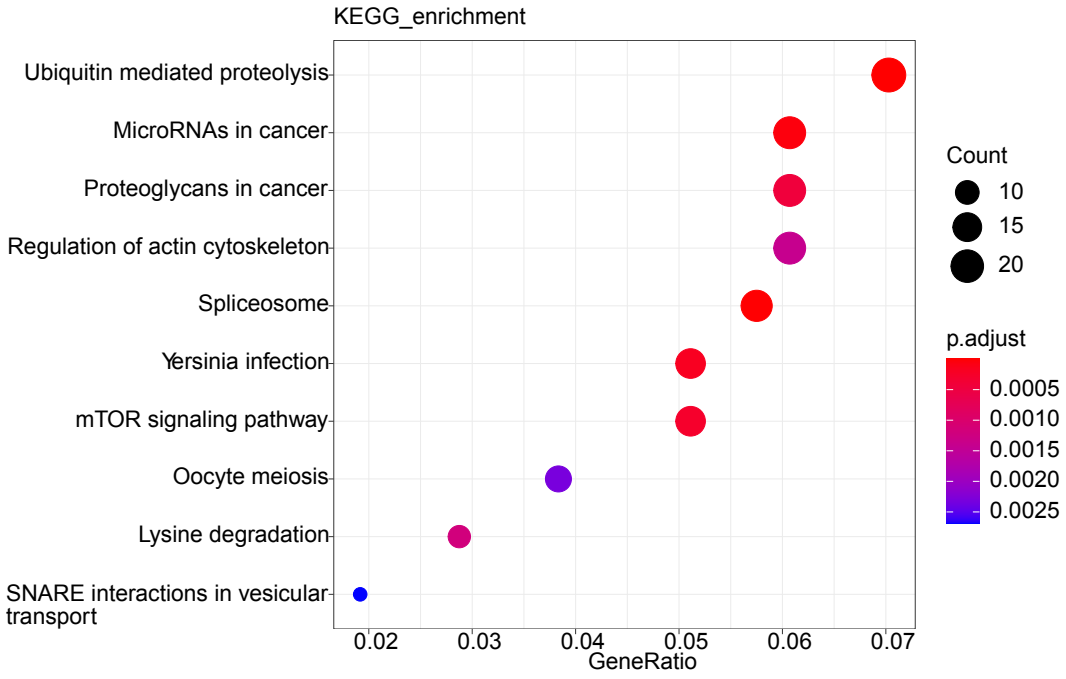

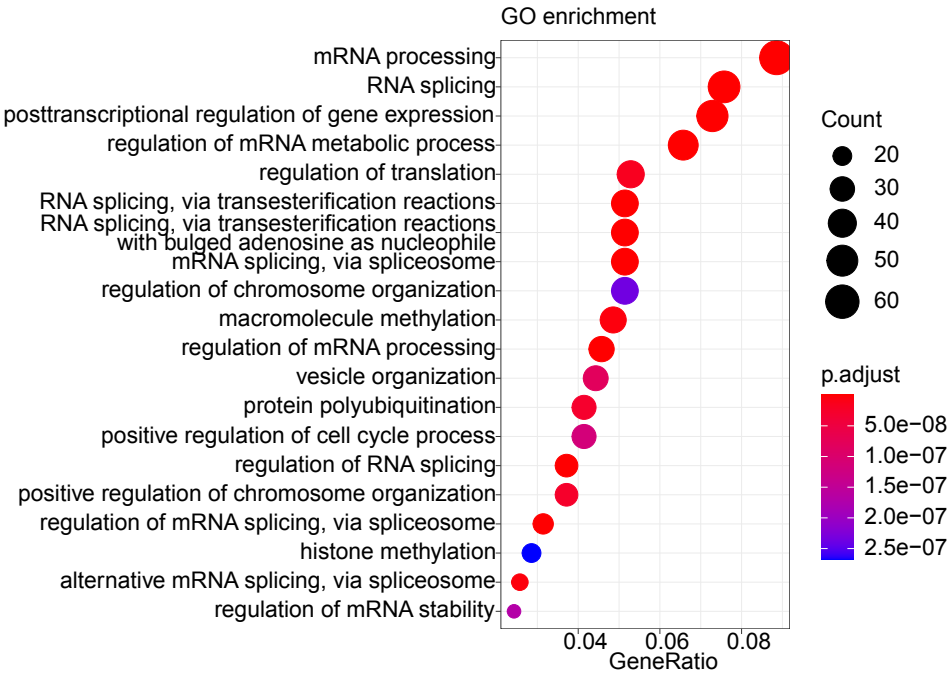
GO enrichment
mRNA processing
RNA splicing
posttranscriptional regulation of gene expression
regulation of mRNA metabolic process
regulation of translation
RNA splicing, via transesterification reactions
RNA splicing, via transesterification reactions with bulged adenosine as nucleophile
mRNA splicing, via spliceosome
regulation of chromosome organization
macromolecule methylation
regulation of mRNA processing
vesicle organization
protein polyubiquitination
positive regulation of cell cycle process
regulation of RNA splicing
positive regulation of chromosome organization
regulation of mRNA splicing, via spliceosome
histone methylation
alternative mRNA splicing, via spliceosome
regulation of mRNA stability
0.04
0.06
0.08
GeneRatio
Count
20
30
40
50
60
p.adjust
5.0e−08
1.0e−07
1.5e−07
2.0e−07
2.5e−07

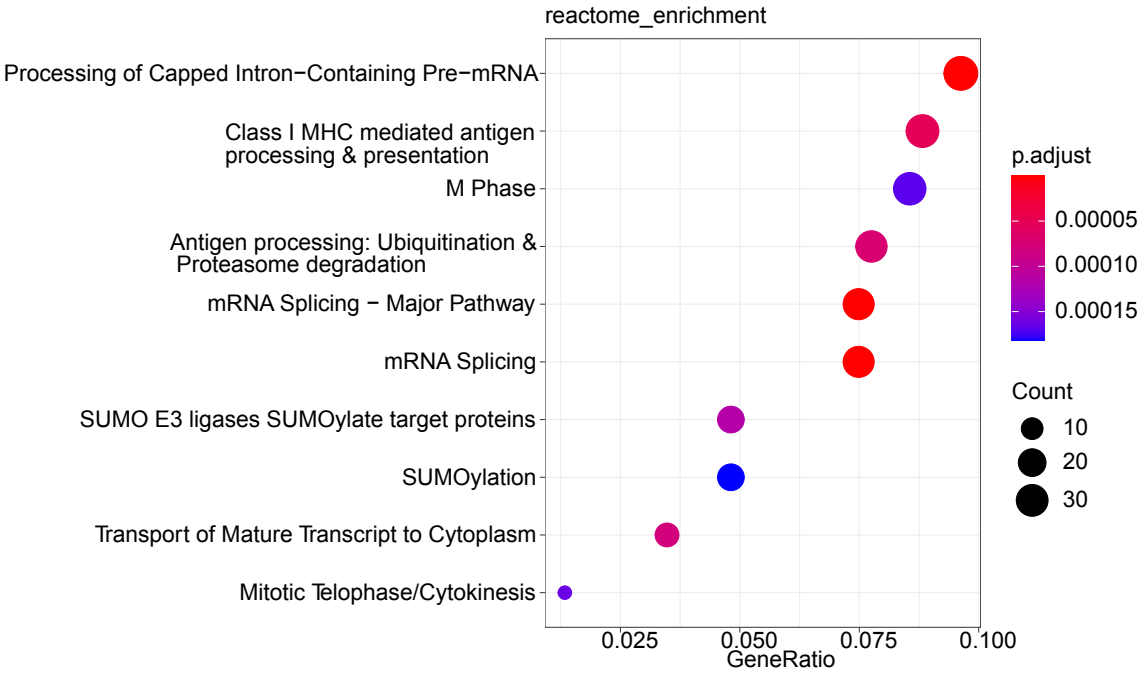

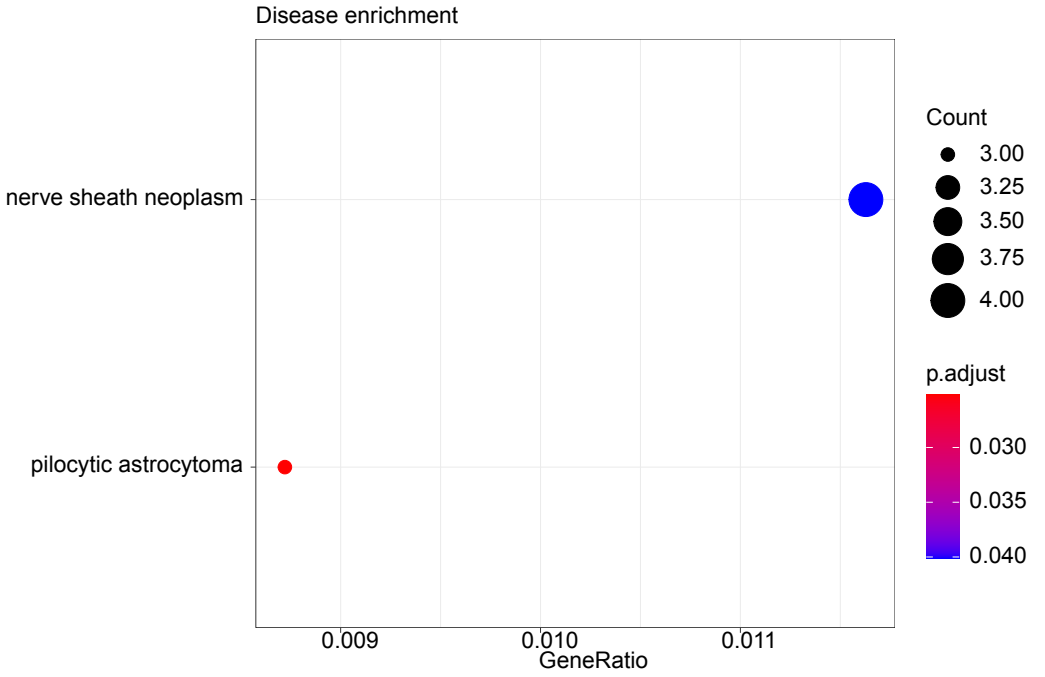

Appendix E: Gene set enrichment analysis of the CO-CENA maroon cluster
Automatized gene set enrichment analysis (GSEA) plots of the WT maternal obesity dataset, belonging to the CO-CENA clusters (Figure 5 and Figure 16). GSEA plots belong to cluster maroon and contains all significantly enriched mechanisms ($p<0.05$). GSEA was performed with the following datasets: Hallmark, KEGG, GO, Reactome, Disease. On every plot, Y axis indicates the significantly enriched mechanisms and X axis shows the gene-ratio (number of genes from the specific CO-CENA cluster, which were enriched to the indicated mechanism, divided by the number of genes classified to the mechanism according to the dataset). The size of the dots relate to the number of enriched genes (counts) and the color code is defined by the adjusted p-value (p-adjust).

Appendix F: WT GSEA Significantly enriched mechanisms - orchid

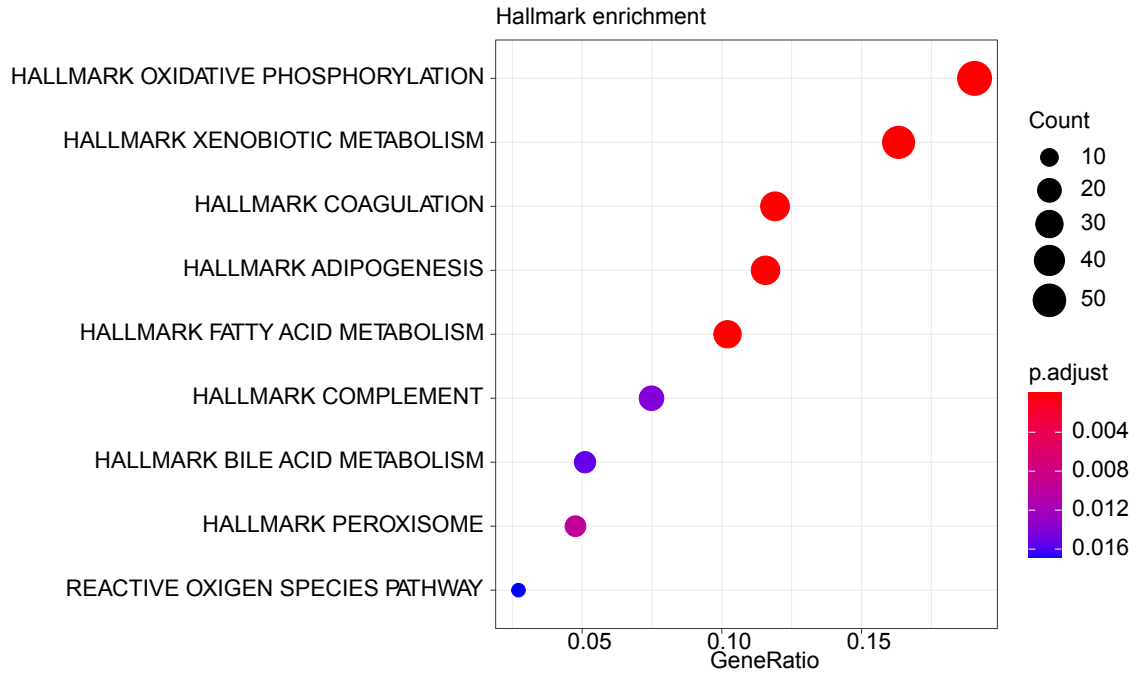

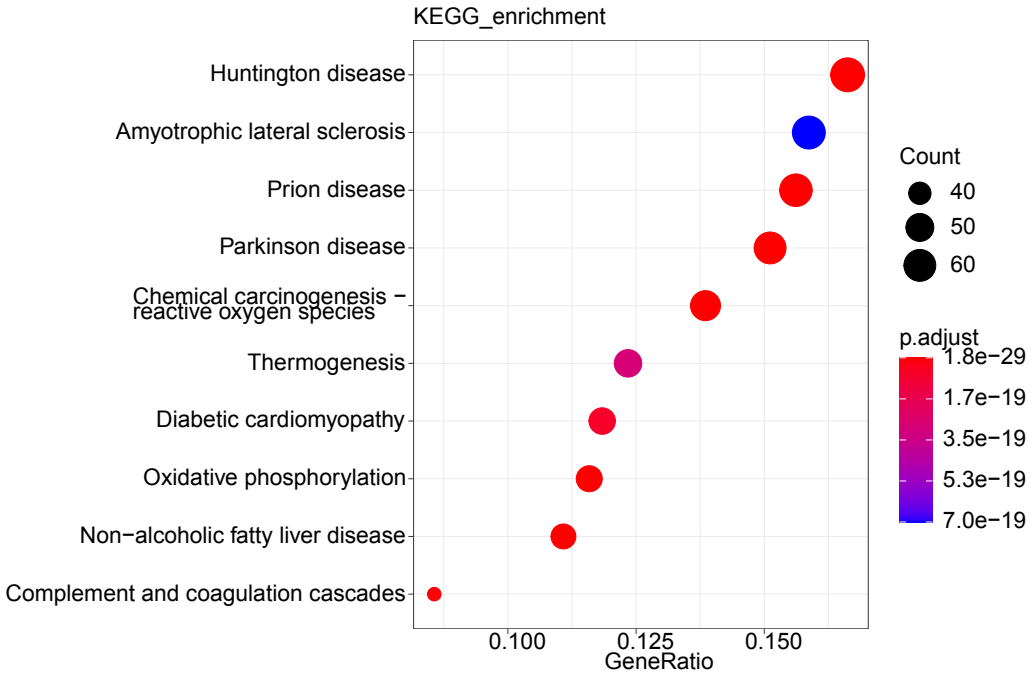

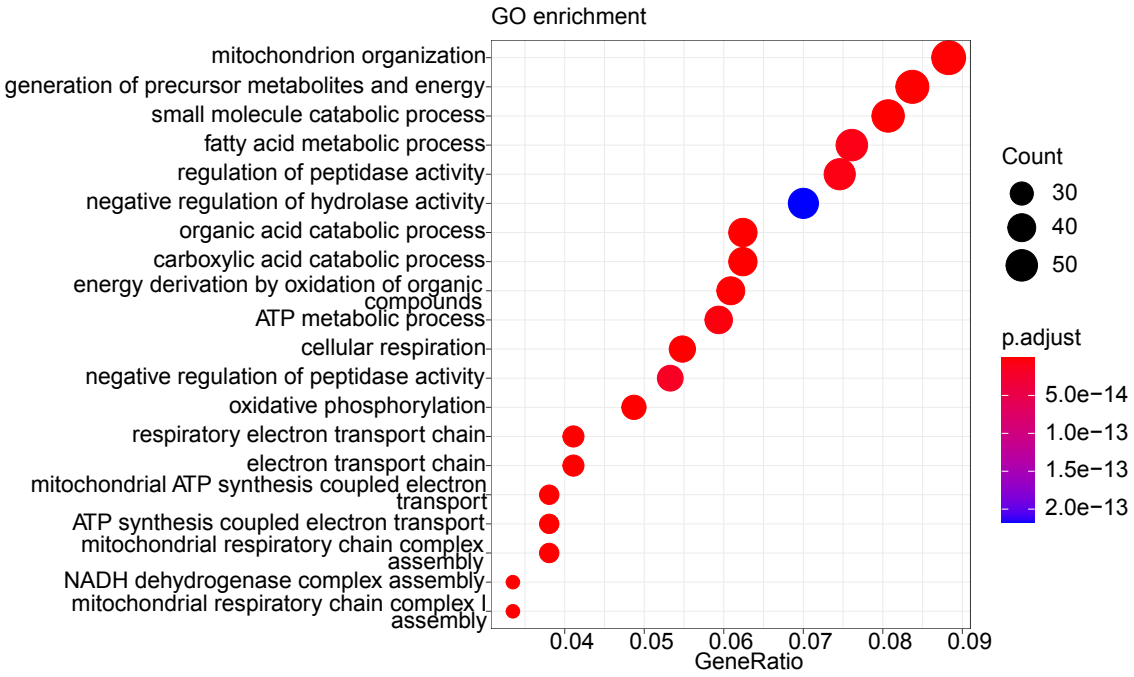
GO enrichment
mitochondrion organization
generation of precursor metabolites and energy
small molecule catabolic process
fatty acid metabolic process
regulation of peptidase activity
negative regulation of hydrolase activity
organic acid catabolic process
carboxylic acid catabolic process
energy derivation by oxidation of organic compounds
ATP metabolic process
cellular respiration
negative regulation of peptidase activity
oxidative phosphorylation
respiratory electron transport chain
electron transport chain
mitochondrial ATP synthesis coupled electron transport
ATP synthesis coupled electron transport
mitochondrial respiratory chain complex assembly
NADH dehydrogenase complex assembly
mitochondrial respiratory chain complex I assembly
0.04
0.05
0.06
0.07
0.08
0.09
GeneRatio
Count
30
40
50
p.adjust
5.0e−14
1.0e−13
1.5e−13
2.0e−13

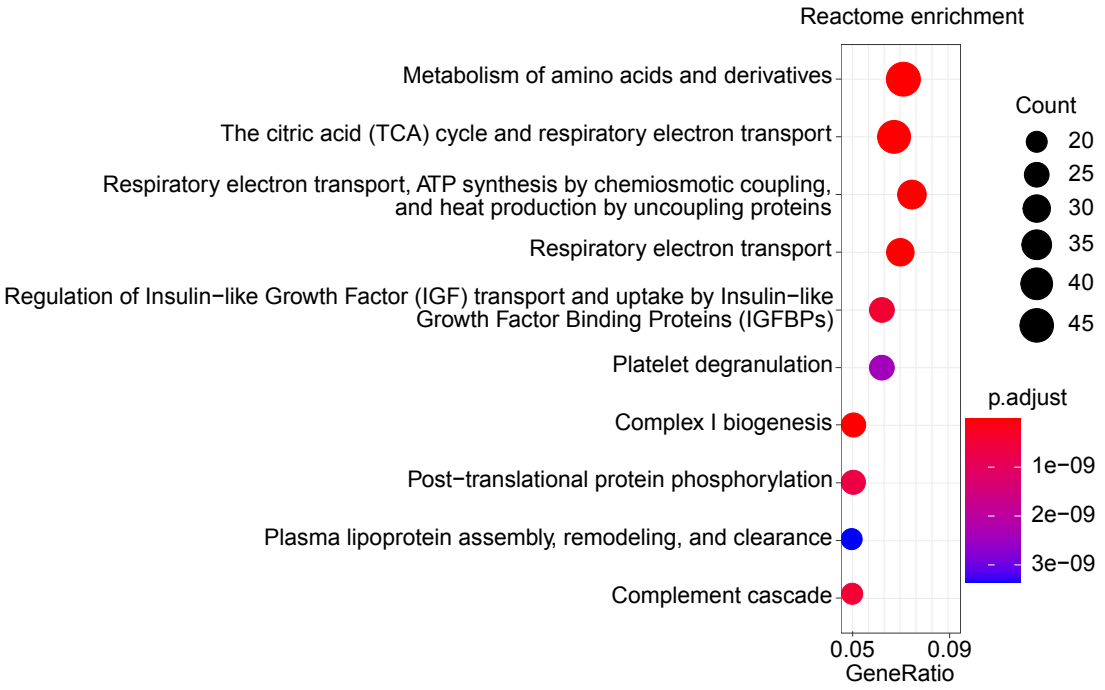

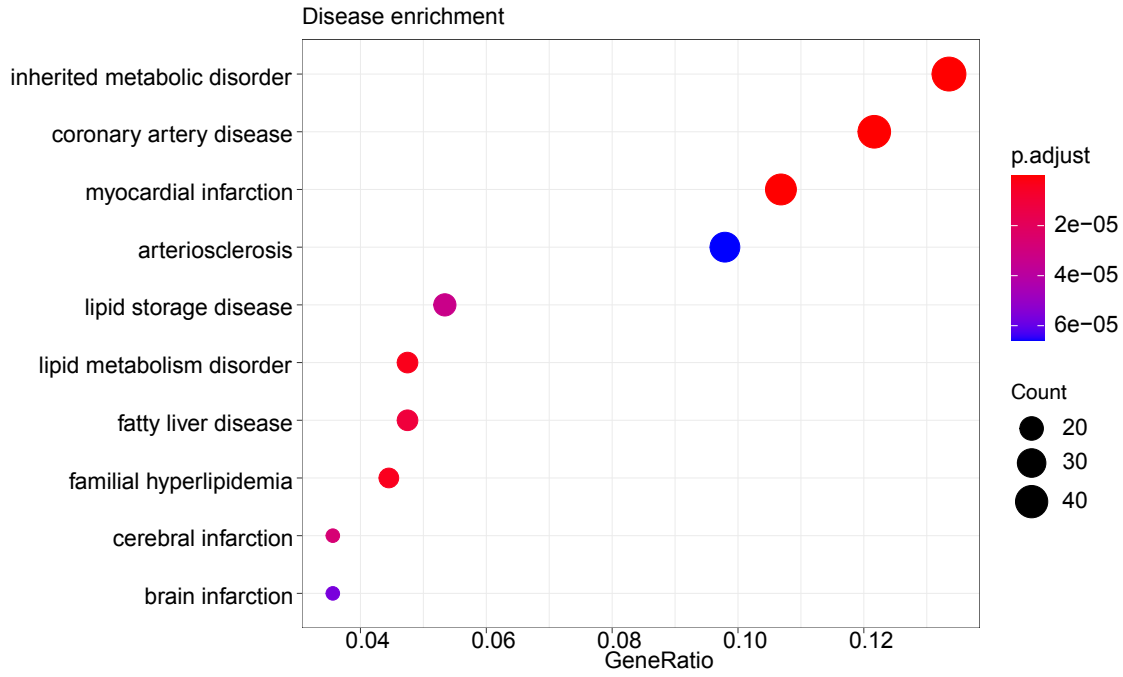

Appendix F: Gene set enrichment analysis of the CO-CENA orchid cluster
Automatized gene set enrichment analysis (GSEA) plots of the WT maternal obesity dataset, belonging to the CO-CENA clusters (Figure 5 and Figure 16). GSEA plots belong to cluster orchid and contains all significantly enriched mechanisms ($p<0.05$). GSEA was performed with the following datasets: Hallmark, KEGG, GO, Reactome, Disease. On every plot, Y axis indicates the significantly enriched mechanisms and X axis shows the gene-ratio (number of genes from the specific CO-CENA cluster, which were enriched to the indicated mechanism, divided by the number of genes classified to the mechanism according to the dataset). The size of the dots relate to the number of enriched genes (counts) and the color code is defined by the adjusted p-value (p-adjust).

Appendix G: WT GSEA Significantly enriched mechanisms - steelblue

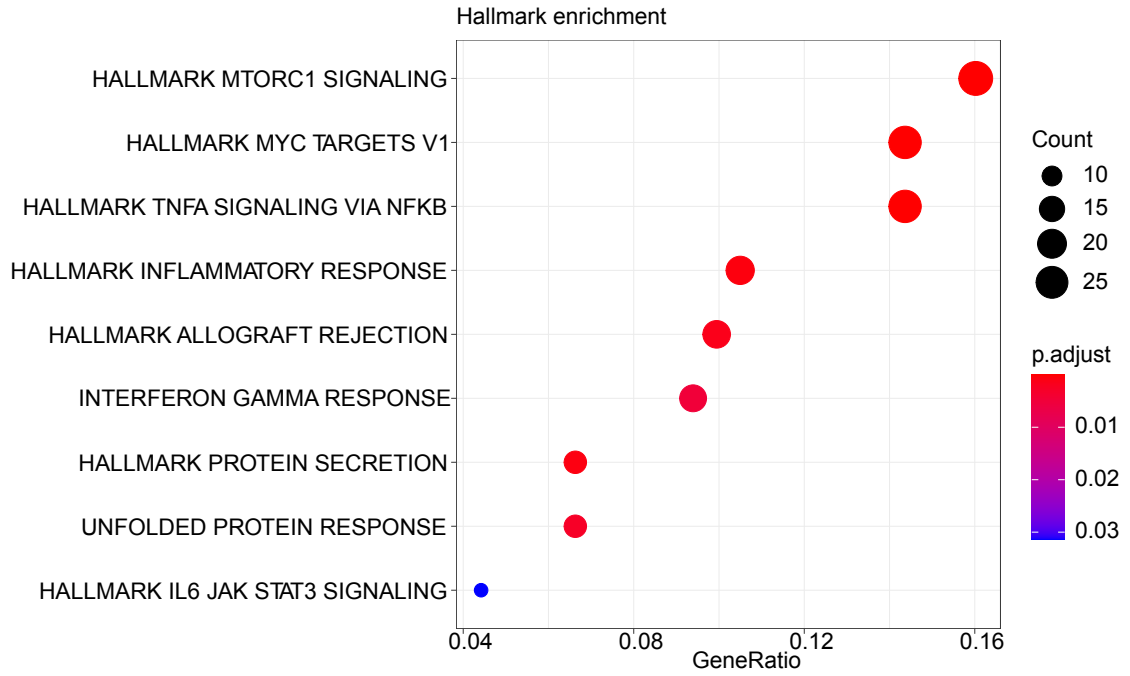

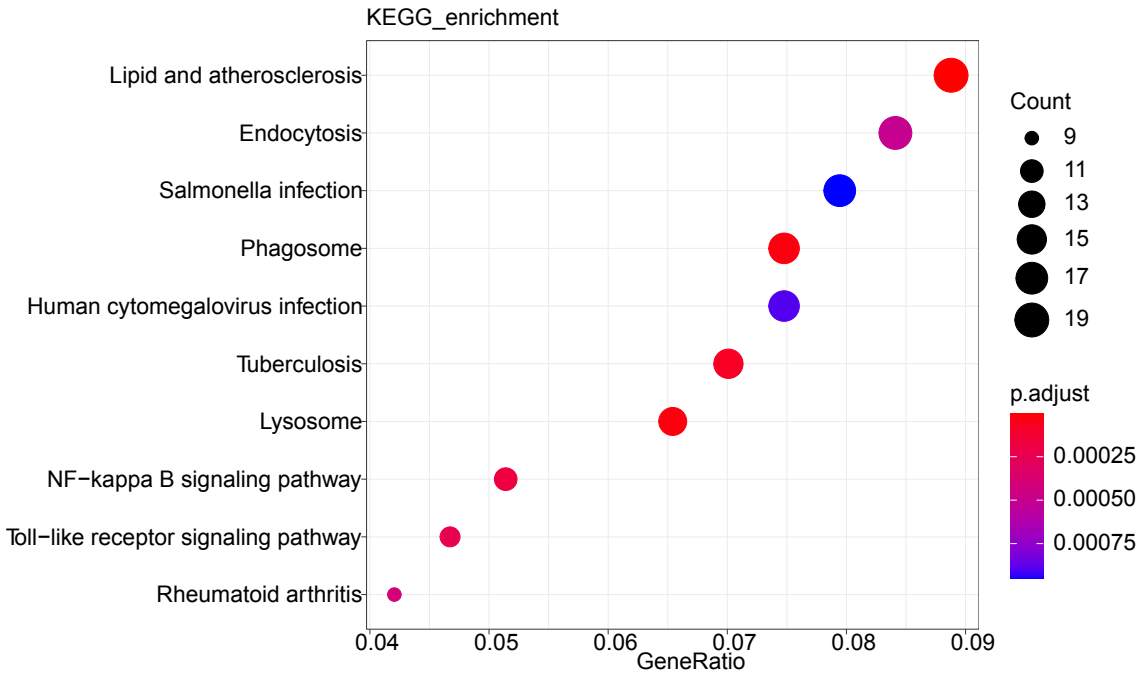

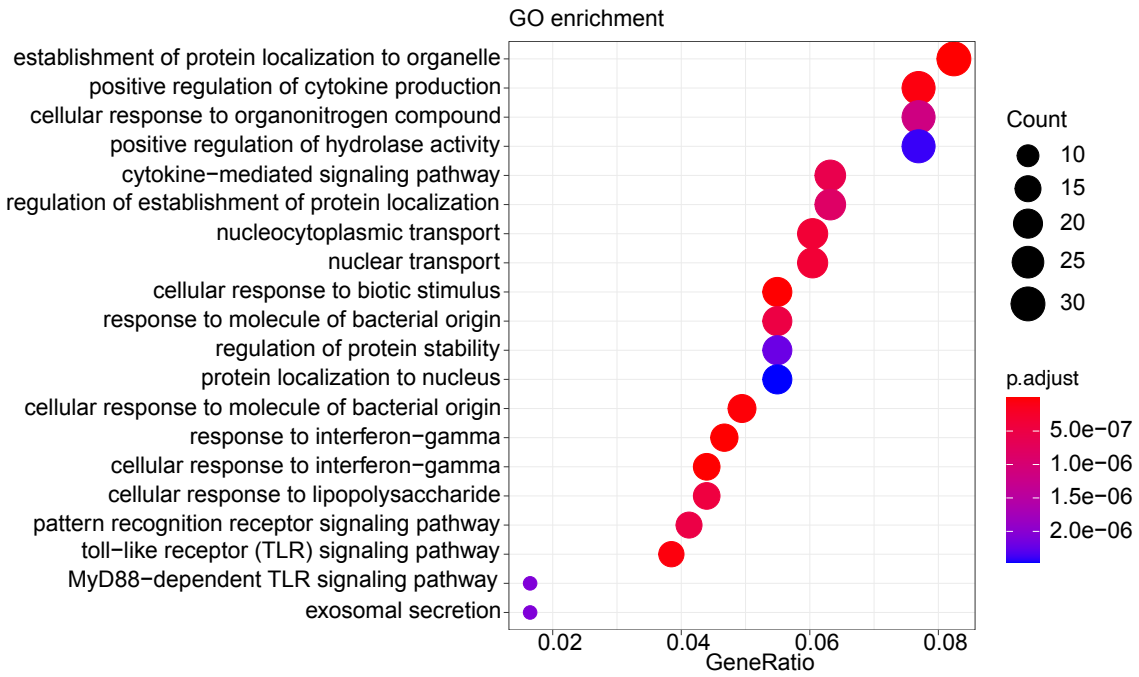
GO enrichment
establishment of protein localization to organelle
positive regulation of cytokine production
cellular response to organonitrogen compound
positive regulation of hydrolase activity
cytokine−mediated signaling pathway
regulation of establishment of protein localization
nucleocytoplasmic transport
nuclear transport
cellular response to biotic stimulus
response to molecule of bacterial origin
regulation of protein stability
protein localization to nucleus
cellular response to molecule of bacterial origin
response to interferon−gamma
cellular response to interferon−gamma
cellular response to lipopolysaccharide
pattern recognition receptor signaling pathway
toll−like receptor (TLR) signaling pathway
MyD88−dependent TLR signaling pathway
exosomal secretion
0.02
0.04
0.06
0.08
GeneRatio
Count
10
15
20
25
30
p.adjust
5.0e−07
1.0e−06
1.5e−06
2.0e−06

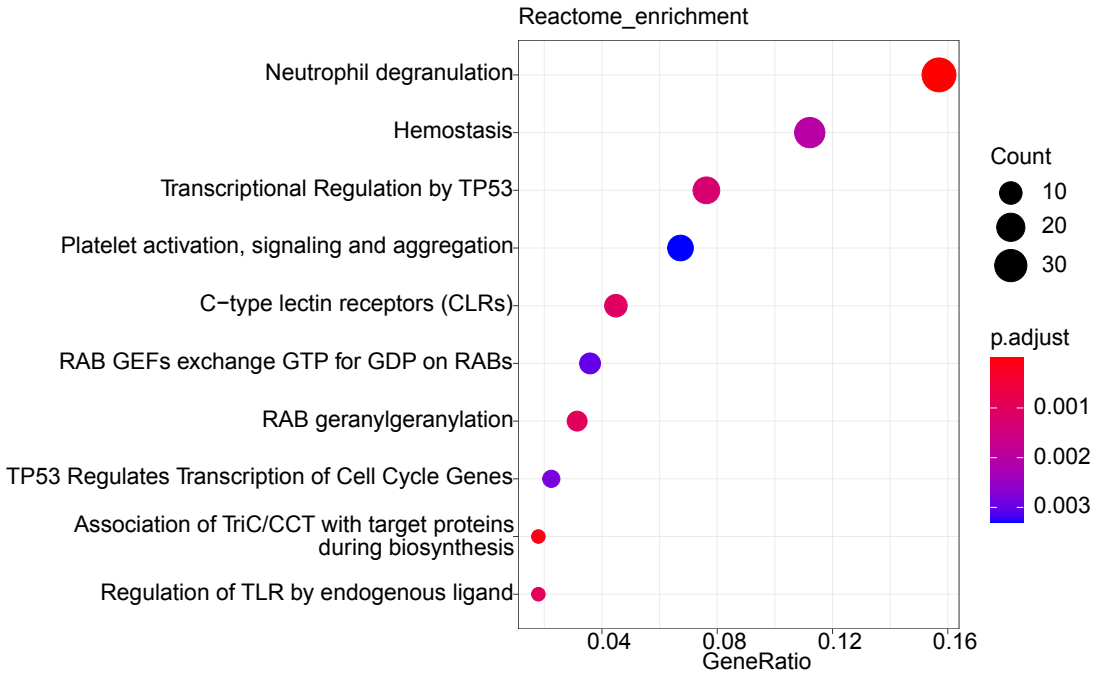

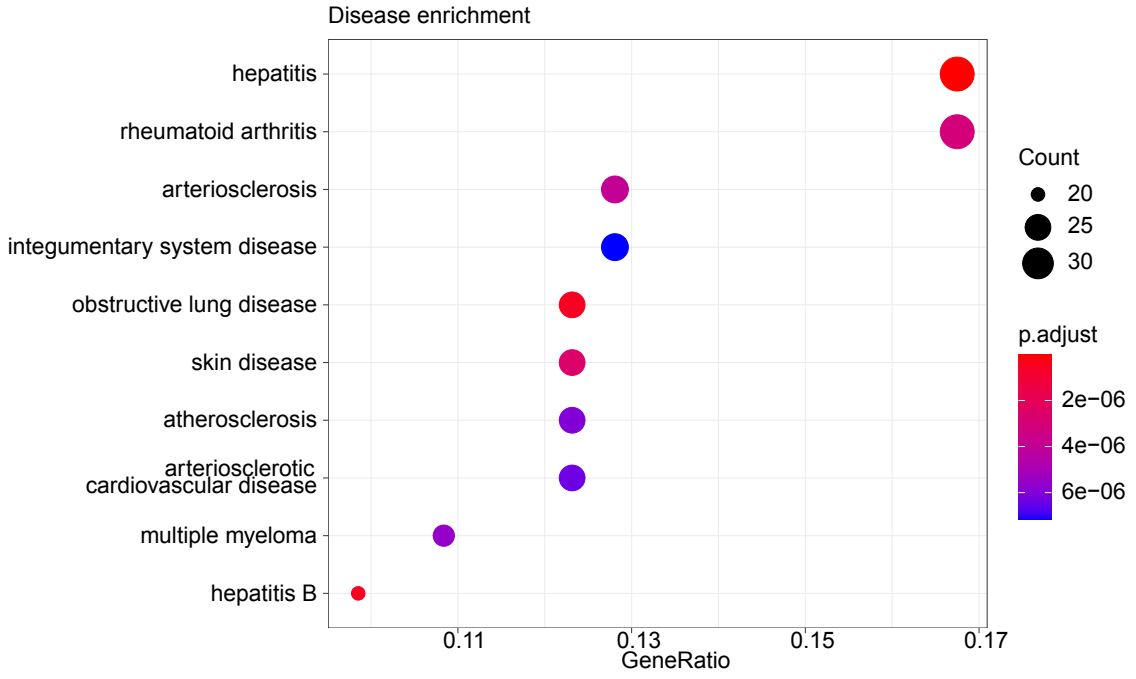

Appendix G: Gene set enrichment analysis of the CO-CENA steelblue cluster
Automatized gene set enrichment analysis (GSEA) plots of the WT maternal obesity dataset, belonging to the CO-CENA clusters (Figure 5 and Figure 16). GSEA plots belong to cluster steelblue and contains all significantly enriched mechanisms ($p<0.05$). GSEA was performed with the following datasets: Hallmark, KEGG, GO, Reactome, Disease. On every plot, Y axis indicates the significantly enriched mechanisms and X axis shows the gene-ratio (number of genes from the specific CO-CENA cluster, which were enriched to the indicated mechanism, divided by the number of genes classified to the mechanism according to the dataset). The size of the dots relate to the number of enriched genes (counts) and the color code is defined by the adjusted p-value (p-adjust).

Appendix H: Gating strategy for KC and Hepatocyte sorting

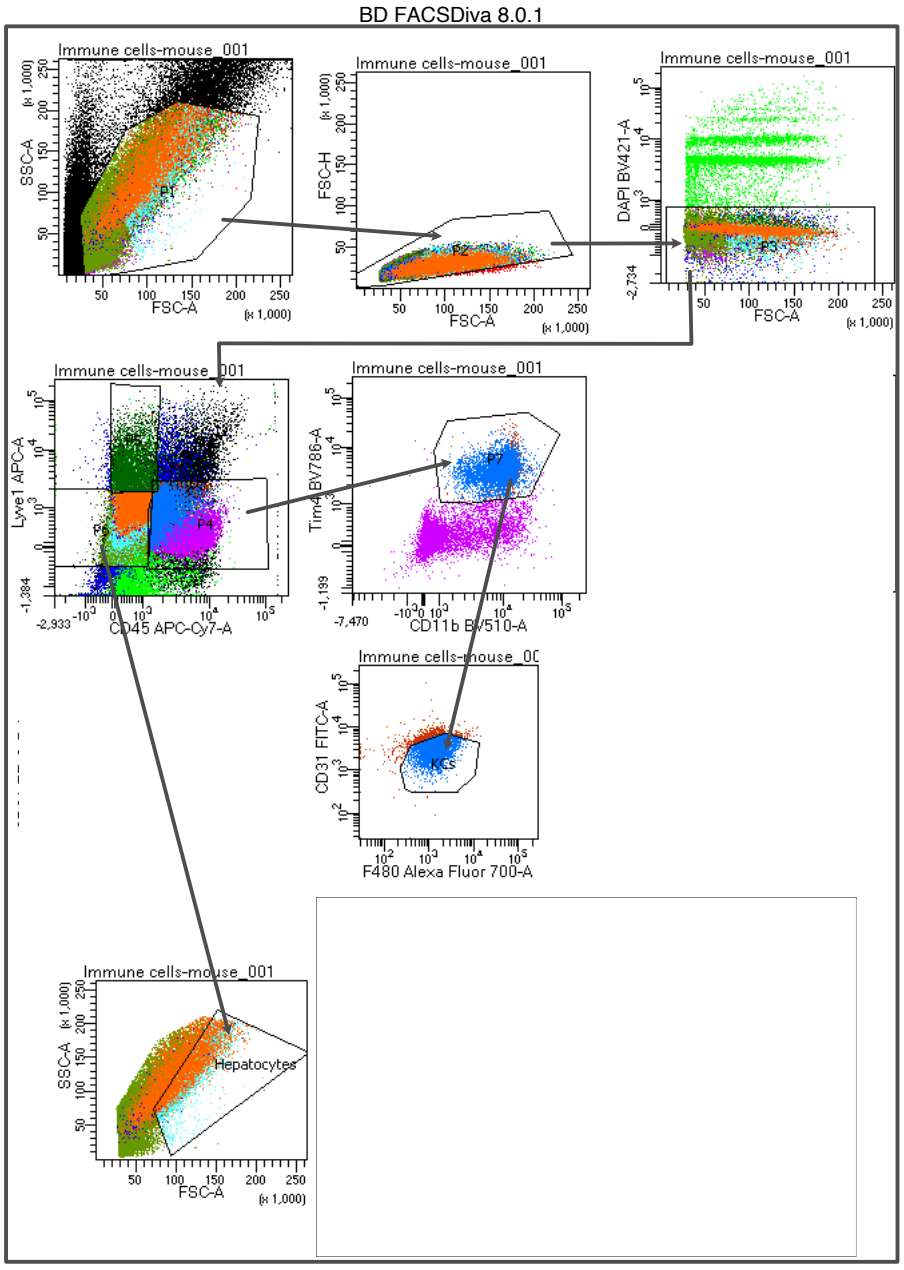

Appendix H: Gating strategy of KC and hepatocyte sorting for RNA-sequencing
Gating strategy was exported from BD FACS machine, directly after sorting. Liver single cells were centrifuged 50G 3 min, the supernatant was used to sort KC, and the pellet was used to sort hepatocytes. Cells were separated via two optical detectors, forward and side scatters (FSC-A and SSC-A), targeting size and granularity (P1). FSC-H gating allowed to exclude doublets, and keep only the singlets (P2). DAPI was used on the BV-421 channel to exclude deaths cells (P3). $CD45^{+}$ (p4) myeloid cells were further gated on $Tim4^{+}$ and $CD11b^{low}$ (P7). That population was further gated for $F4/80^{+}$ and $CD31^{-}$ Kupffer cells (KCs). Hepatocytes were gated as $CD45^{-}$ $Lyve1^{-}$ population with high intensity of FSC-A, as this measure is proportional to the diameter of the cell.

Appendix I: Gating strategy for myeloid cell analysis

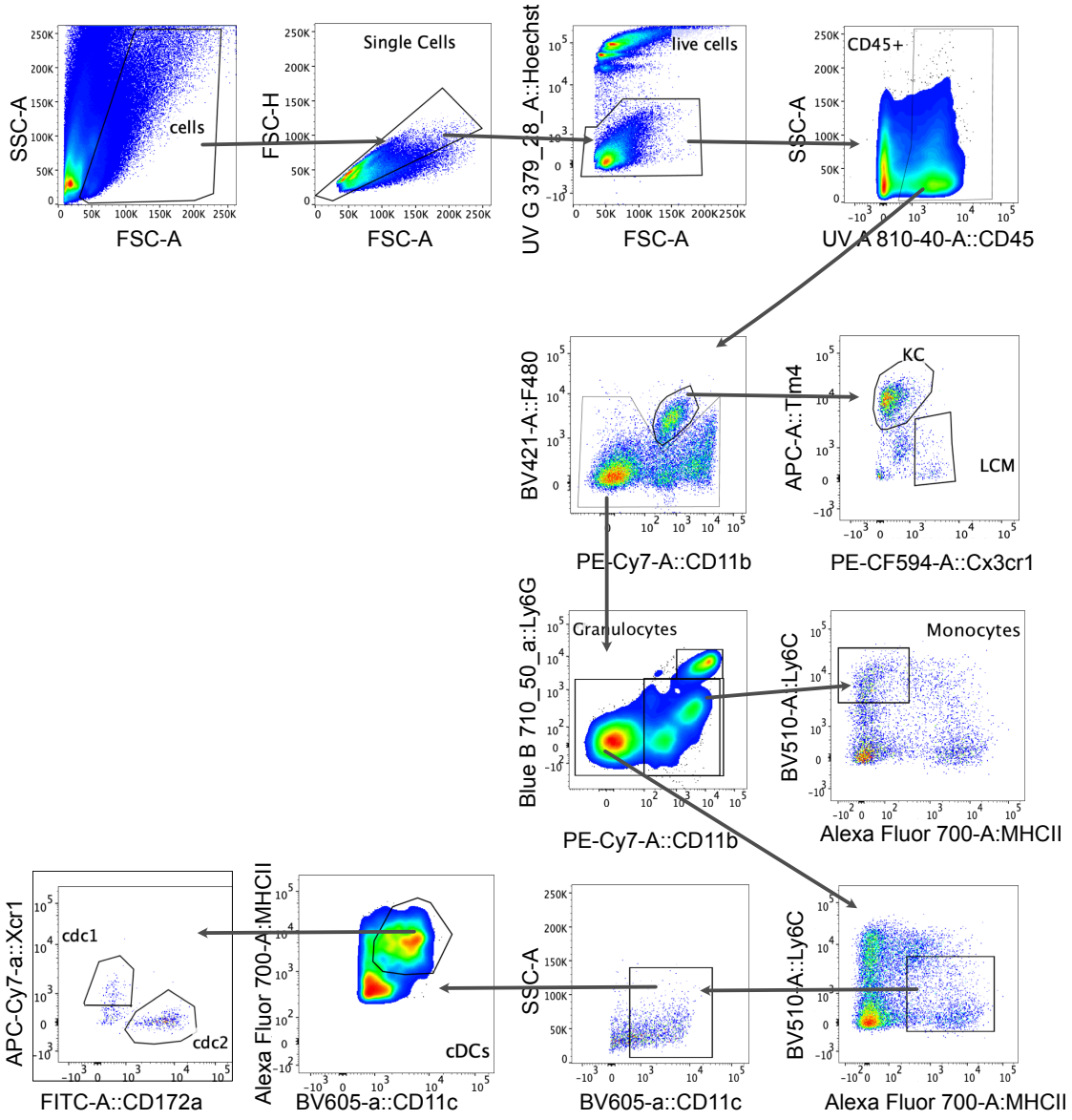

Appendix I: Gating strategy of myeloid cell analysis via Flow cytometry
Gating strategy was exported via the Flowjo Software, directly after analysis. Liver single cells were centrifuged 50G 3 min, the supernatant was used for further analysis of the myeloid cells. Cells were separated via two optical detectors, forward and side scatters (FSC-A and SSC-A), targeting size and granularity (cells). FSC-H gating allowed to exclude doublets, and keep only the singlets ("Single Cells"). Hoechst was used to exclude death cells ("live cells"). $CD45^+$ myeloid cells were further gated on $F4/80^+$ and $CD11b^{low}$, which population was further gated on Tim4+ and considered as KC and the $Tim4^-$ $Cx3cr1^+$ population as liver capsular macrophages (LCM). The non-macrophage population was further gated on granulocytes ($CD11b^+$ $Ly6G^+$), monocytes ($Ly6C^+$) and dendritic cells ($MHCII^+$ $CD11c^+$). Dendritic cells were further classified into cDC1 ($Xcr1^+$) and cDC2 ($CD172a^+$).

Appendix J: Gating strategy for HSC analysis in bone marrow

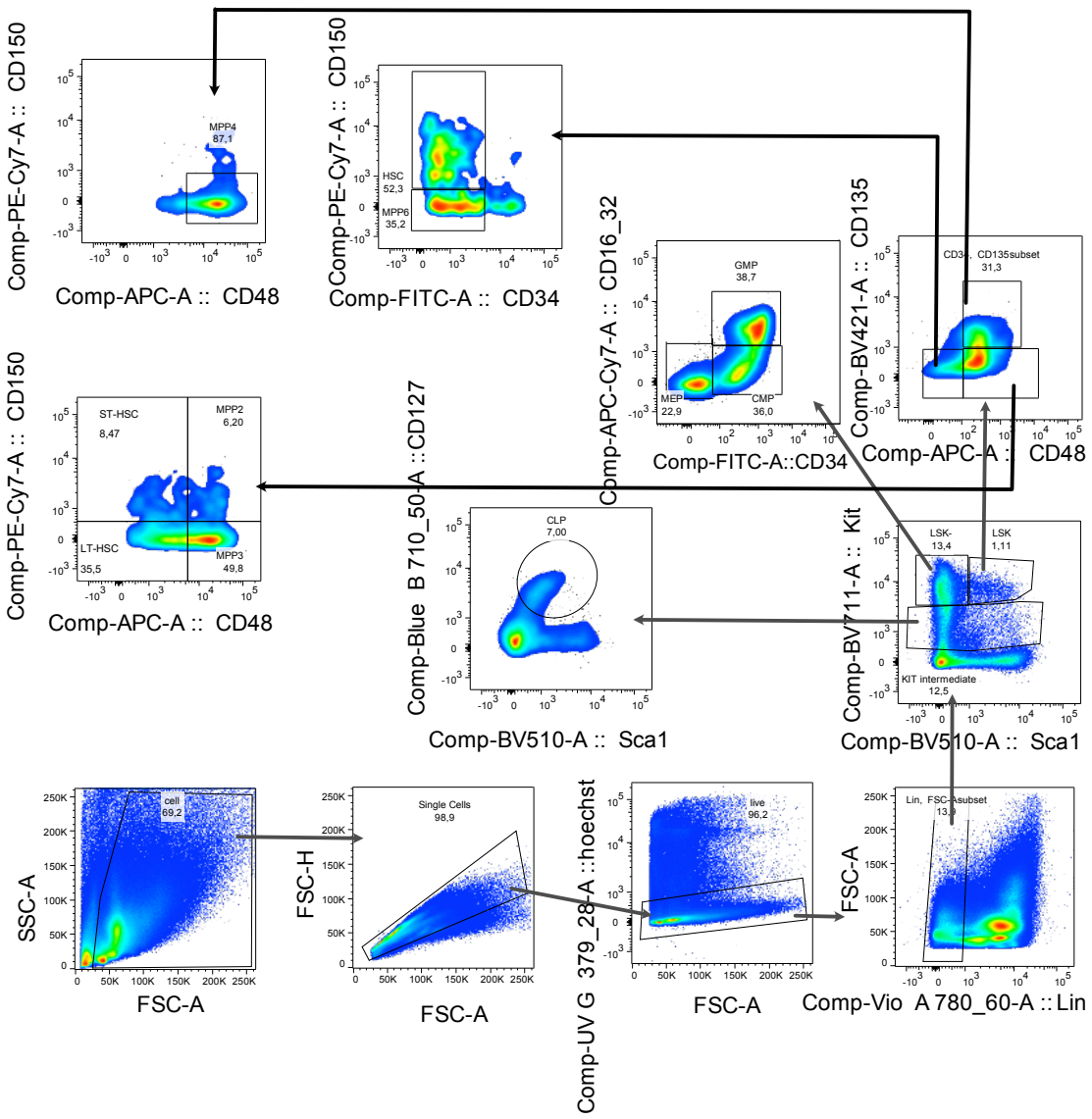

Appendix J: Gating strategy of hematopoietic stem cell analysis via Flow cytometry
Gating strategy was exported via the Flowjo Software, directly after analysis. Cells were separated via two optical detectors, forward and side scatters (FSC-A and SSC-A), targeting size and granularity (cell). FSC-H gating allowed to exclude doublets, and keep only the singlets ("Single Cells"). Hoechst was used to exclude death cells ("live cells"). Lin^- cells were further classified based on their Kit and Sca1 expression (LSK-, LSK, and KIT^{low}). Common lymphoid progenitors are further identified via their $CD127^+$ expression (CLP). LSK- population was used to identify granulocyte-monocyte progenitors (GMP) as CD34+ CD16/32+, common myeloid progenitors (CMP) as CD34+ CD16/32-, and megakaryocyte-erythrocyte progenitor (MEP) as CD34- CD16/32-. LSK population was further discriminated to identify the different Multipotent progenitors (MPP). All MPP are CD48+, MPP1/ST-HSC (CD150+, CD48low), MPP2(CD150+, CD48high), MPP3(CD150-, CD48high), MPP4(CD150-, CD48high), MPP5/LT-HSC(CD150-, CD48low).

Appendix K: Normalized expression of O2PLS target transcripts

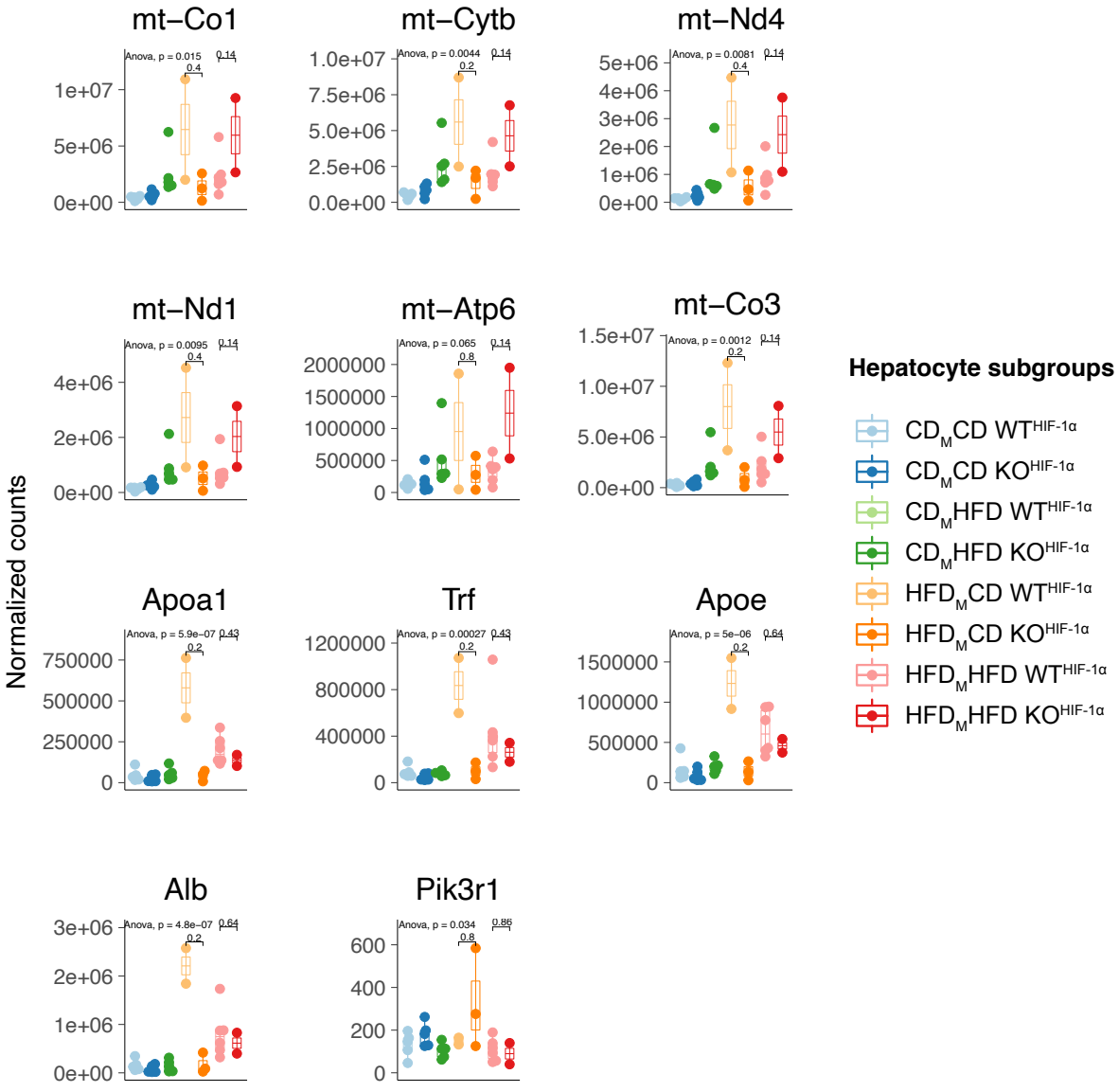

Appendix K: Normalized expression of O2PLS target transcripts
Normalized expression counts of O2PLS target genes (Figure 28) in sorted hepatocytes of the Hif-1α maternal obesity model. Those transcripts are the key regulators in the accumulation of CE and TAG species in hepatocytes. There is no genotype specific DE-gene between those candidates. However, condition specific analysis of variance (ANOVA) results in high significance p<0.005 for all transcripts, which gives positive feedback on signal quality.
Light-blue - $CD_MCD\ WT^{HIF\text{-}1\alpha}$ (n=5) - mother is on control diet before and during pregnancy (Control Diet $_{Maternal}$), and the offspring is on control diet after birth. Mouse is $HIF\text{-}1\alpha^{f/f}\ Lysm^{+/+}$ comparable genotype to wild-type (WT).
Dark-blue - $CD_MCD\ KO^{HIF\text{-}1\alpha}$ (n=5) - mother is on control diet before and during pregnancy (Control Diet $_{Maternal}$), and the offspring is on control diet after birth. Mouse is $HIF\text{-}1\alpha^{f/f}\ Lysm^{cre/+}$, macrophage-specific knock-out of hypoxia-inducible factor 1a (HIF-1α).
Light-green - $CD_MHFD\ WT^{HIF\text{-}1\alpha}$ (n=0) - mother is on control diet before and during pregnancy (Control Diet $_{Maternal}$), and the offspring is on a high-fat diet after birth. Mouse is $HIF\text{-}1\alpha^{f/f}\ Lysm^{+/+}$ comparable genotype to wild-type (WT).
Dark-green - $CD_MHFD\ KO^{HIF\text{-}1\alpha}$ (n=5) - mother is on control diet before and during pregnancy (Control Diet $_{Maternal}$), and the offspring is on a high-fat diet after birth. Mouse is $HIF\text{-}1\alpha^{f/f}\ Lysm^{cre/+}$, macrophage-specific knock-out of (HIF-1α).
Yellow - $HFD_MCD\ WT^{HIF\text{-}1\alpha}$ (n=2) - mother is on a high-fat diet before and during pregnancy (High-fat Diet $_{Maternal}$), and the offspring is on control diet after birth. Mouse is $HIF\text{-}1\alpha^{f/f}\ Lysm^{+/+}$ comparable genotype to wild-type (WT).
Orange - $HFD_MCD\ KO^{HIF\text{-}1\alpha}$ (n=3) - mother is on a high-fat diet before and during pregnancy (High-fat Diet $_{Maternal}$), and the offspring is on control diet after birth. Mouse is $HIF\text{-}1\alpha^{f/f}\ Lysm^{cre/+}$, macrophage-specific knock-out of HIF-1α.
Pink - $HFD_MHFD\ WT^{HIF\text{-}1\alpha}$ (n=6) - mother is on a high-fat diet before and during pregnancy (High-fat Diet $_{Maternal}$), and the offspring is on a high-fat diet after birth. Mouse is $HIF\text{-}1\alpha^{f/f}\ Lysm^{+/+}$ comparable genotype to wild-type (WT).
Red - $HFD_MHFD\ KO^{HIF\text{-}1\alpha}$ (n=2) - mother is on a high-fat diet before and during pregnancy (High-fat Diet $_{Maternal}$), and the offspring is on a high-fat diet after birth. Mouse is $HIF\text{-}1\alpha^{f/f}\ Lysm^{cre/+}$, macrophage-specific knock-out of HIF-1α.